Entanglement detection and fractional quantum Hall effect in optical lattices

Rebecca N. Palmer, Merton College

Thesis submitted for the degree of Doctor of Philosophy in Physics, Michaelmas Term, 2007

Abstract

Entanglement detection and fractional quantum Hall effect in optical lattices

R.N. Palmer, Merton College, D.Phil. Michaelmas 2007

We consider the purity-based entanglement detection scheme introduced in [C. Moura Alves and D. Jaksch, Phys. Rev. Lett. **93**, 110501 (2004)]. We describe how it could be implemented in an optical lattice using two-atom loss, and prove that in this form it detects all pure entangled states even without any spatial resolution. We then prove that correcting for certain reasonable types of experimental error is possible, and practical for error rates up to the order of one over the number of lattice sites considered. Limited spatial resolution similarly becomes a significant improvement over no spatial resolution only at nearly single site level. We also show how to use this process for state parameter estimation and collapse-revival evidence of entanglement, for which it remains useful even when the error rate is too high to permit unambiguous entanglement detection.

We also consider an optical lattice bosonic analogue of the fractional quantum Hall (FQH) effect. This system can reach high "magnetic fields" very difficult to attain in the solid state FQH system, where the discrete nature of the lattice becomes important. Near simple rational numbers l/n of flux quanta per lattice cell, we find that the single particle states become nearly periodic with period n lattice sites, and have an n fold degeneracy which leads to FQH states resembling those of n-internal-state particles. Standard time of flight expansion would reveal this periodicity and be able to distinguish FQH states from vortex lattice or Mott insulator states. Shot noise correlation would provide further information on the nature of the FQH states.

Contents

1 Introduction **8**

1.1 Purity-based entanglement detection 9

1.2 Fractional quantum Hall effect in optical lattices 12

1.3 Organization 14

2 Optical lattices **16**

2.1 Lattice potential 16

2.2 Bose Hubbard model 17

2.2.1 Superfluid-Mott insulator transition 19

2.3 Hamiltonian control: quantum simulation 21

2.4 Quantum computation 23

2.4.1 Spatial resolution limitations 24

3 Entanglement **26**

3.1 Density matrices 26

3.2 Entanglement theory 28

3.2.1 Definition of entanglement 28

3.2.2 Creation and examples 29

3.2.3 Communication uses and measures 31
3.2.4 Relation to quantum computation 35
3.2.5 Mathematical tests 37
3.2.6 Physical detection: introduction 39
3.3 Conventional detection methods: witness operators 42
3.3.1 Fidelity witness 44
3.3.2 Mixed state witnesses 45
3.3.3 Bell inequalities 46
3.3.4 Witness measurement 49
3.3.5 Easily measurable witnesses 50
3.4 Conventional detection methods: state tomography 52
3.4.1 Linear inversion 52
3.4.2 Maximum likelihood estimation 53

4 Purity-based entanglement detection 56
4.1 Ideal scheme 56
4.1.1 Purity inequalities 56
4.1.2 Pairwise beamsplitter 58
4.1.3 Examples 61
4.2 Realisation in optical lattices 64
4.2.1 The pairwise beam splitters 65
4.2.2 Measuring the lattice site occupation 67
4.3 Entanglement detection without spatial resolution 68
4.4 Effects of experimental error 71
4.4.1 Without spatial resolution 72

4.4.2 With spatial resolution 79
4.4.3 Imperfect spatial resolution 80
4.5 State parameter estimation 82
4.5.1 Macroscopic superposition states 83
4.5.2 Cluster states 84
4.5.3 Products of entangled subsystem states 85
4.6 Details of the beam splitter operation 86

5 Quantum Hall effect: review **89**
5.1 Physical realisations 90
5.1.1 Semiconductor system 90
5.1.2 Rotating gas system 91
5.2 Single particle states: Landau levels 92
5.3 Many-particle states 95
5.3.1 Laughlin states 96
5.3.2 Read-Rezayi states 97
5.3.3 Vortex lattice state 100
5.3.4 Two component states 100
5.4 Anyonic excitations and topological computation 101

6 Optical lattice quantum Hall effect **105**
6.1 The Hamiltonian 105
6.2 Small α limit: continuum approximation 106
6.2.1 Comparison to other realisations 110
6.3 Near simple rational α: multi-component wavefunctions 111
6.3.1 Single particle states 111

6.3.2 Interacting particles 113
6.4 Time of flight expansion 116
6.5 Correlation measurement 119
6.6 Hall current and disorder 122
6.7 Derivation of high α states 127

7 Conclusions **132**

7.1 Purity-based entanglement detection 132
7.2 Fractional quantum Hall effect 133

Acknowledgments

I thank my supervisor Dr Dieter Jaksch and my collaborator Carolina Moura Alves for many useful discussions.

This work was primarily funded by a Merton College Domus Scholarship, and was supported by EPSRC through the QIP IRC (www.qipirc.org) GR/S82176/01 and project EP/C51933/1, by the EU network OLAQUI, and by the Fundação para a Ciência e Tecnologia (Portugal).

Publications

Some of this work was previously published as:

Ch. 4: R.N. Palmer, C. Moura Alves, and D. Jaksch, Phys. Rev. A **72**, 042335 (2005).

Ch. 6: R.N. Palmer and D. Jaksch, Phys. Rev. Lett. **96**, 180407 (2006).

Secs. 4.1 and 4.2.1 were originally C. Moura Alves' work; the remainder of these chapters is primarily my own research.

Chapter 1

Introduction

Quantum information processing [1] is the manipulation of information stored in a quantum device, usually a collection of 2-level quantum systems (called qubits), which takes advantage of quantum laws such as superposition. Any unitary operation can be constructed from 1- and 2-qubit unitary operations (quantum logic gates). A sufficiently large network of such gates, called a *quantum computer*, could factorize integers [2] and simulate locally interacting many-body quantum systems [3] in polynomial time, both of which are believed to require exponential time on a classical computer.

A major barrier to the construction of quantum computers is decoherence, which is caused by interaction of the qubits with their environment. 2-qubit gates require the qubits to interact with each other, and it is difficult to make a system which will do this without also interacting too much with its environment. It is possible to correct decoherence and other errors using quantum error correction [4], but this only helps if the error rate is sufficiently small to begin with [5]; if the error rate is too high, more errors occur during

the correction process than are removed by it.

A wide variety of physical implementations of quantum computing have been proposed, and some, including ion traps [6] and liquid NMR [7], have been experimentally demonstrated with a few qubits. We here consider neutral atoms in optical lattices [8, 9]. The easiest operations in this implementation act identically on all atoms or nearest-neighbour pairs at the same time, and it is hence particularly suited to simulating translationally invariant many-body quantum systems, especially lattice systems such as condensed matter systems [10, 11], and preparing certain many-qubit entangled states such as cluster states [12]. Its main limitation is that the atoms are generally too close together to be individually addressed; several methods have been proposed to overcome this [13, 14, 15, 16] but it remains a difficult problem.

1.1 Purity-based entanglement detection

Entanglement [17] is a type of correlation between spatially separated subsystems allowed in quantum systems but forbidden in classical systems. It is essential for some quantum communication tasks such as teleportation [18], and is also important in quantum computing. Multi-particle entanglement is a resource required by many quantum information algorithms, for example the ancilla states used for fault tolerant quantum error correction [19, 20], and the cluster or graph state used for measurement-based (one-way) quantum computation [21].

Few particle entanglement has been created in a number of systems including photons [22, 23] and ion traps [6], and has been verified and charac-

terised by quantum state tomography [22, 24]. However, full state tomography requires at least $O(2^n)$ measurements for n qubits, making it completely impractical for states involving large numbers of qubits, such as cluster states in optical lattices [12, 25]. Entanglement witnesses can avoid this problem [26, 27], but any given witness detects only a limited range of entangled states [28]. Both entanglement witnesses (including Bell inequalities) and state tomography also require the ability to resolve individual qubits, which is very difficult in optical lattices.

We consider a third method introduced in [29], based on the purity inequalities [30] which roughly state that if the whole system is purer than one of its parts then it is entangled. To measure the purities of the reduced density matrices, it applies a pairwise beamsplitter between corresponding qubits of two copies of the state $\rho_{12\ldots n}$ being tested, then observes whether these qubits bunch (both go into the same site) or not. Since symmetric states bunch while antisymmetric states do not [29], and purity is the expectation of the swap operator, purity of subsystem $A = 1 - 2 \times$ (probability that an odd number of pairs in A remain unbunched).

We describe how this could be implemented in an optical lattice using a period 2 superlattice to perform the beamsplitters, then fast 2 atom loss from a Feshbach resonance to remove the bunched pairs, leaving the unbunched ones. We show that counting these unbunched pairs, without any spatial resolution, is sufficient to detect entanglement in all pure or sufficiently near-pure entangled states, and that in many cases including the cluster state, the number of experimental runs required is independent of the number of qubits in the state.

We also consider the effect of experimental error: in practice, the beamsplitter will be perturbed by the interaction between the atoms, the loss process will not perfectly discriminate between pairs and single atoms, and the detection will not be 100% efficient. We show that the effect of all these errors can be made arbitrarily small by applying an appropriate correction and increasing the number of experimental runs. There is no sharp limit to the amount of error that can be corrected, but the number of runs required is roughly exponential in the expected number of errors kq, where k is the size of the subsystem whose purity is being measured and q is the error probability at each site, so there is a practical limit $kq \lesssim 1$. This applies both with and without spatial resolution, but for some states such as the cluster state, spatial resolution allows entanglement detection with lower k values. We also apply a similar method to correcting limited spatial resolution to obtain full spatial resolution, and similarly find that this can be done but has a huge overhead unless it was already nearly single site resolution.

We also consider using this scheme for state parameter estimation, finding that it can be useful for this, and can also provide collapse-revival evidence of entanglement similar to the existing optical lattice method [12] but without the restriction to states with all their single particle density matrices equal, even when a high error rate limits it to k values too small for unambiguous entanglement detection of the state being considered.

1.2 Fractional quantum Hall effect in optical lattices

Anyons [31] are particles existing on a 2D surface which are neither bosons nor fermions under exchange, but have a more complicated braiding statistics where the sense (clockwise or anticlockwise) of the exchange matters. *Non-Abelian anyons* also have multiple topologically distinct states, on which non-trivial quantum operations can be performed by moving the anyons around each other, a process called *topological quantum computing* [32, 31]. Because these states are a global topological property, they cannot be disturbed by local noise, or by small errors in the anyons' paths; all that matters is the topology of the paths, which would allow extremely low error rates [33].

The most promising source of non-Abelian anyons is the fractional quantum Hall (FQH) effect. This occurs in a 2D system of interacting particles in an external vector potential, originally electrons of a semiconductor in a magnetic field, at certain simple rational ratios of particles to flux quanta [34, 35]. Its ground state is then strongly correlated and incompressible, and its conductance is entirely off-diagonal, and precisely quantised despite the inevitable presence of noise [34].

The elementary excitations of FQH states have fractional particle number [36] and are anyons [37, 38]. It is believed that in some cases [39, 40] they are non-Abelian anyons suitable for universal topological quantum computation [41].

We consider an optical lattice realisation of the FQH system. The 2-dimensionality and interaction are easy in an optical lattice, and there are

several possible ways to produce the required vector potential ("magnetic") term [42, 43, 44, 45]. This can be viewed as a quantum simulation [10] of the solid state FQH system, where the optical lattice represents the crystal lattice and the atoms represent electrons. However, the opposite particle statistics and different interaction potential ($\delta(r)$ rather than $1/r$) lead to a significantly different set of allowed FQH states, and it is also an interesting system in its own right.

The optical lattice can be used to study the high field regime $\alpha \sim 1$ (α is the number of magnetic flux quanta per lattice cell). The solid state FQH system is limited to $\alpha \lesssim 10^{-4}$ for its crystal lattice unit cell at experimentally attainable magnetic fields [46], while superlattice structures with $\alpha \sim 1$ are possible but difficult [47]. There the discreteness of the lattice becomes important, which in the absence of trapping produces a fractal single particle band structure called the Hofstadter butterfly [46, 44].

We find that near simple rationals, $\alpha \approx \alpha_c \equiv l/n$, in the presence of weak trapping, the single particle wavefunctions have an approximate n site periodicity and an n fold degeneracy. At long lengthscales, these cause them to behave as if they had n internal states and were in only the residual field $\alpha - \alpha_c$. The density and Hall current of each FQH state hence become proportional to $\alpha - \alpha_c$ rather than α. This can have the opposite sign to α, causing the Hall current to flow in the opposite direction to what low field theory would predict.

We also consider how to detect these states using existing measurement techniques. Under time of flight expansion we find that the resulting density profile is broadly similar to the in-trap density profile, giving stepped peaks

with each step corresponding to a different FQH state. The above n site near-periodicity also becomes visible as more than one peak per Brillouin zone. Under the shot noise correlation procedure of [48, 49], we find anticorrelation at small relative momenta in FQH states, which we relate to their real space correlation functions. This contrasts with little or no correlation in vortex lattices and positive correlation in Mott states.

1.3 Organization

This thesis is organised as follows. Chapter 2 reviews optical lattices: the optical potential, the Bose Hubbard model, and their possible quantum simulation and quantum computation uses.

Chapter 3 reviews entanglement, its importance in quantum communication and computation, and the existing methods of detecting it, witness operators (Sec. 3.3) and quantum state tomography (Sec. 3.4). Chapter 4 describes our method of detecting entanglement: Sec. 4.1 describes its principles of operation, and Sec. 4.2 possible methods for realising it in an optical lattice. Sec. 4.3 shows that it can detect entanglement even without spatial resolution, and Sec. 4.4 considers the effects of experimental errors. Sec. 4.5 considers using it for state parameter estimation. Sec. 4.6 is an appendix giving details of the beamsplitter operation and the possible errors in it.

Chapter 5 reviews the fractional quantum Hall effect in both electron and atomic gas systems, including the Laughlin and Read-Rezayi states and their multicomponent analogues, and their possible use for topological quantum

computation. Chapter 6 describes our work on the optical lattice quantum Hall system: Sec. 6.1 introduces it, and Sec. 6.2 reduces the low α limit to the ordinary (continuum) QH Hamiltonian, and compares it to other FQH systems. Sec. 6.3 considers the high α states, first for a single particle then for many particles. Secs. 6.4 and 6.5 consider time of flight expansion and shot noise correlation measurements of these states. Sec. 6.6 considers the Hall current and the effect of adding disorder to the system. Sec. 6.7 is an appendix giving a detailed derivation of the high α single particle states.

Chapter 7 gives conclusions for both parts.

Chapter 2

Optical lattices

An *optical lattice* is a standing light wave acting as a periodic potential for ultracold neutral atoms. In this chapter we review their properties and potential uses for quantum simulation and computation. More detailed reviews of this subject can be found at [8, 9, 50], and focusing on the quantum simulation aspects, [10].

2.1 Lattice potential

In this section we describe how an optical lattice creates a periodic potential, and how its unwanted side effects such as spontaneous emission can be minimised.

The energy levels of an atom in an oscillating electric field, such as a light wave, are shifted by an amount proportional to the square of the field strength; this is called the AC Stark effect. For two counterpropagating laser beams forming a standing wave $E(x,t) = E_0 \cos(\omega t - kx) + E_0 \cos(\omega t + kx) =$

$2E_0 \cos kx \cos \omega t$, the energy shift is $V_{\text{lat}}(x) = A(\omega)(2E_0 \cos kx)^2 \equiv V_0 \cos^2 kx$ [8]; because of the square the distance between lattice minima is half the laser wavelength. If the laser frequency ω is sufficiently close to a transition frequency ω_e that this transition dominates over all others, $A(\omega) \propto 1/(\omega - \omega_e)$, so red detuning ($\omega < \omega_e$) places the lattice potential minima at light intensity maxima, while blue detuning places them at light intensity minima.

The proportion of atoms in the higher energy state under these conditions is approximately $V_{\text{lat}}(x)/(\omega - \omega_e)$ [8]. Since this population can spontaneously emit photons, which is undesirable as it destroys coherence and the recoil heats the atom, large detunings are used to minimise it [9]. These detunings are much larger than the Doppler shifts from the motion of the atoms, so the atoms see $V_{\text{lat}}(x)$ as a conservative potential, depending on position but not velocity.

This can be extended to a 3-dimensional lattice by using more beams; a number of geometries are possible, but we consider only the cubic one, which has 3 pairs of beams along $\pm x, \pm y, \pm z$, of orthogonal polarizations and/or slightly different frequencies to avoid interference. Their potentials hence add to give $V_{\text{lat}}(\mathbf{x}) = V_x \cos^2 kx + V_y \cos^2 ky + V_z \cos^2 kz$.

2.2 Bose Hubbard model

In this section we derive the Bose Hubbard approximate Hamiltonian for the basic lattice setup, and review its superfluid and Mott insulator ground states.

As the lattice potential is periodic, the single particle eigenstates are

Bloch functions $\psi_{\mathbf{K},n}(\mathbf{x}) = e^{i\mathbf{K}\cdot\mathbf{x}}\tilde{\psi}_{\mathbf{K},n}(\mathbf{x})$ where $\tilde{\psi}$ is periodic with the lattice period $d = \pi/k$, labelled by a quasimomentum $\mathbf{K}$ within the first Brillouin zone $-k < K_x, K_y, K_z \leq k$ and a band index n, analogous to single electron eigenstates in a crystal lattice.

An alternative basis is given by the Wannier functions $w_n(\mathbf{x} - \mathbf{x}_i$ [8], labelled by a band index n and a lattice site i centred at $\mathbf{x}_i$, where w_n is the "most localised" state in band n. For suitable relative phases of the Bloch functions it is given by $w_n(\mathbf{x} - \mathbf{x}_i) = \int d^3\mathbf{K} e^{-i\mathbf{K}\cdot\mathbf{x}_i}\psi_{\mathbf{K},n}(\mathbf{x})$.

Typically the lattice is deep enough and the atoms cold enough that only the lowest band is significantly occupied and its Wannier function $w_1(\mathbf{x} - \mathbf{x}_i) \equiv w(\mathbf{x} - \mathbf{x}_i)$ has most of its probability within lattice cell i (the tight binding regime). Under these conditions the lattice Hamiltonian can be approximated by nearest neighbour hopping,

$$\begin{aligned} H_{\text{hop}} = &\sum_{p,q,r} J_x a^\dagger_{p,q,r} a_{p-1,q,r} + J_x a^\dagger_{p,q,r} a_{p+1,q,r} + J_y a^\dagger_{p,q,r} a_{p,q-1,r} \\ &+ J_y a^\dagger_{p,q,r} a_{p,q+1,r} + J_z a^\dagger_{p,q,r} a_{p,q,r-1} + J_z a^\dagger_{p,q,r} a_{p,q,r+1}, \qquad (2.1) \\ J_x = &- \int d^3x w^*(\mathbf{x}) \left(-\frac{1}{2m_0}\nabla^2 + V_{\text{lattice}} \right) w(\mathbf{x} - (d, 0, 0)), \qquad (2.2) \end{aligned}$$

and similarly for the other hopping rates J_y, J_z, where d is the lattice spacing and $a_{p,q,r}$ is the annihilation operator for a particle in the lattice site labelled by the integer coordinates (p, q, r). The advantage of using the Wannier basis rather than the Bloch basis is that trapping and contact interaction can then

be included as the purely on-site terms

$$H_{\text{int}} = \frac{U}{2}\sum_{p,q,r} a^{\dagger}_{p,q,r}a^{\dagger}_{p,q,r}a_{p,q,r}a_{p,q,r}, \tag{2.3}$$

$$U = g_0 \int d^3x |w(\mathbf{x})|^4, \tag{2.4}$$

$$H_{BH} = H_{\text{hop}} + H_{\text{int}} + V_{\text{trap}}(p,q,r)a^{\dagger}_{p,q,r}a_{p,q,r}, \tag{2.5}$$

where g_0 is the contact interaction strength [8]. The Hamiltonian H_{BH} is called the *Bose Hubbard* Hamiltonian [51].

2.2.1 Superfluid-Mott insulator transition

The nature of the ground state depends on the ratios U/J of interaction to hopping (where J is any of J_x, J_y, J_z). For bosonic atoms, in the $U/J \to 0$ limit the ground state is a Bose-Einstein condensate, called a *superfluid* state, with all the particles in one single particle orbital given by a discrete space version of the Gross-Pitaevskii equation [52]. In the absence of trapping this is the zero quasimomentum orbital,

$$|\,\psi_{SF}\rangle = \left(\sum_{p,q,r} a^{\dagger}_{p,q,r}\right)^{N} |\,\text{vac}\rangle\,, \tag{2.6}$$

where N is the number of particles and $|\,\text{vac}\rangle$ is the vacuum state. In the presence of a weak trap its density takes the shape of the trapping potential, analogous to the Thomas-Fermi approximation for continuum BECs [52]. The low-lying excitations of this state are long wavelength phonons, which are gapless in the thermodynamic (infinitely large system) limit [9].

The ground state in the $U/J \to \infty$ limit is the state with exactly one particle in each of the lowest (in trapping potential) N lattice sites, called a *Mott insulator* state.

$$|\,\psi_{MI}\rangle = \prod_{p,q,r} a^{\dagger}_{p,q,r}\,|\,\mathrm{vac}\rangle\,. \tag{2.7}$$

The low-lying excitations of this are particle-hole pairs, which have a nonzero energy gap U even in the thermodynamic limit. There are also Mott insulator states with $2, 3, \ldots$ particles per site; in a trap these can coexist with each other and the superfluid state, forming a stepped density profile [53]. A trapping potential is essential to induce this phase separation; a uniform system with a noninteger number of particles per lattice site remains superfluid for all U/J.

Away from these limits both superfluid and Mott insulator states change gradually as U/J varies, but in the thermodynamic limit there is a sharply defined boundary between gapless (superfluid) and gapped (Mott insulator) excitations [54, 55]. This is an example of a phase transition at zero temperature (between ground states), which is called a quantum phase transition. Since H_{BH} cannot be solved exactly, the exact location of this transition is not known; a mean field calculation [51, 54] gives the estimate $U/J \approx 35$ for a 3D isotropic ($J_x = J_y = J_z$) lattice, but this simple description cannot accurately describe the transition and a more sophisticated variational model gives $U/J \approx 18$ [55]. Experimental measurements of the momentum distribution [56] and excitation spectrum [57] show the transition but cannot yet measure the transition point accurately enough to conclusively distinguish these, partly because the transition is only sharp in the infinite system limit.

2.3 Hamiltonian control: quantum simulation

In this section we consider the unusually large amount of control available over the optical lattice Hamiltonian, and how this can be used to simulate other quantum systems.

The basic lattice described by the Bose-Hubbard model already allows easy control of all its dimensionless parameters. Increasing the laser intensity along one axis increases the lattice depth, making the Wannier function more tightly confined, which decreases J along that axis, over a practical range of a few orders of magnitude [8], and increases U. While U is not independent of the Js, only the ratios U/J are dimensionless. This can be done much faster than the dynamical timescales, allowing observation of the coherent response to such a parameter change. The trap strength, and the number of atoms initially loaded into the lattice, can also be controlled.

The independent control of J on each axis allows effectively 2D or 1D systems to be created, by using a very strong lattice on the dimensions to be frozen out, reducing their J to negligible levels, and a weak lattice (or no lattice at all) along the dimensions to be retained. Each plane or line of the lattice then behaves as an independent 2D or 1D system.

Other controllable terms can be added to the Hamiltonian by going beyond the basic 6 beam lattice setup. For example, magnetic-like phase terms can be created in a variety of ways: rotating the lattice [58, 42], an EIT laser carrying orbital angular momentum [43], laser-induced hopping [44, 59], or an oscillating quadrupole potential [45]. The methods of Sec. 2.4 can also be used. The sum of a set of individually implementable Hamiltonians can

be simulated by switching between them on a timescale short compared to their dynamical timescales [11].

Optical lattices do not contain the impurities and lattice defects that real crystals inevitably have, giving them much lower disorder than typical solid state systems. However should disorder be desired, for example for studying localization [60], it can be added in a controlled way [10]. Pseudorandom disorder can be added using additional lasers angled to create a superlattice of period incommensurate with the main lattice [61, 60]. Truly random disorder can be added using a speckle laser [61] for long (at least a few sites) correlation length, or a second species of atoms held in a deep lattice to act as impurities [62] for short (single site) correlation length.

This high level of control allows the optical lattice Hamiltonian to be made to match that of other physically different quantum systems, and in particular strongly correlated condensed matter systems, the optical lattice representing the crystal lattice. Experiments on the optical lattice can then be used to study the other system; this is called *quantum simulation* [10]. It can be seen as a form of analogue quantum computation, but unlike full (digital) quantum computation it is experimentally feasible now, because it requires only global control of the Hamiltonian parameters (not single site addressing) and a noisy simulator corresponds to a noisy original rather than being unusable for more than a few qubits above a low error-correction threshold. Such a simulation may be preferable to experimenting directly on the original system because it allows different types of measurements, control of parameters that are fixed in the original, or access to otherwise inaccessible parameter regimes.

2.4 Quantum computation

In this section we describe how quantum gates can be implemented in an optical lattice, and how their inability to resolve individual qubits might potentially be overcome.

Optical lattices can trap multiple hyperfine states, allowing the one atom per site Mott insulator state to be used as a quantum register, with two orthogonal hyperfine states acting as the qubit states $|\,0\rangle$ and $|\,1\rangle$. Single qubit operations can be performed using microwave or Raman laser pulses [63].

The lattices felt by different hyperfine states can be moved relative to each other by changing the polarisation of the laser beams. Moving them by one lattice spacing so the $|\,0\rangle$ state of one qubit sits on top of the $|\,1\rangle$ state of the next, waiting for a time ϕ/U and moving them back creates a phase shift ϕ on $|\,0\rangle\,|\,1\rangle$ neighbouring pairs only [63]. If all the qubits start in $|+\rangle \equiv (|\,0\rangle + |\,1\rangle)/\sqrt{2}$, the resulting state is

$$|\,\phi_n\rangle = \frac{1}{\sqrt{2^n}} \prod_{j=1}^{n} (|\,0\rangle_j \, e^{i\phi\sigma_{z,j+1}} + |\,1\rangle_j) = \frac{1}{\sqrt{2^n}} \sum_{x=0}^{2^n-1} e^{i\phi c(x)} \,|\,x\rangle\,, \tag{2.8}$$

where $c(x)$ is the number of occurrences of the sequence 01 in the n-bit binary number x. Taking $\phi = \pi$ then applying another $\pi/2$ single qubit rotation gives a 1D cluster state [12], and repeating the process for the other dimension(s) creates a 2D or 3D cluster state, which would then require only single qubit measurements to perform universal measurement-based (one-way) quantum computation [21].

2.4.1 Spatial resolution limitations

However, these single qubit measurements would have to address individual qubits, which is very difficult as they are half a lattice laser wavelength apart and diffraction limits the focusing of the Raman and readout lasers to the order of a wavelength. In this section we describe a number of methods which aim to get around this problem.

One option is to have the atoms further apart. Increasing the lattice spacing is possible by either using long wavelength lattice lasers such as CO_2 lasers [13] or by forming each standing wave from two beams crossing at an angle instead of counterpropagating [14]. However, at given laser power this decreases J, U and the band gap, making operations slow and vulnerable to excitation of higher Bloch bands, and the above state dependent shift gate does not work if the laser wavelength is too far detuned [13]. These problems can be avoided by using the long wavelength lattice to pattern load a normal lattice [13, 64], giving atoms at the long lattice spacing with the normal tight confinement.

Another possibility is to use a beam focused as tightly as possible along with additional beams or microwave fields so arranged that their effects cancel out on the target qubit's neighbours but not the target itself [15]. A variant of this is to "hide" the target's neighbours in additional internal states, using fields that cancel out at the target [16].

One can also use the lattice as a quantum cellular automaton, which uses global operations, along with a pointer state (either a special internal state, or a normal qubit on a different row) whose position identifies the qubit

being acted on [65]. While it is necessary to initially create the pointer, this process does not need to be coherent, so may be easier than single qubit addressing during the computation. A disadvantage of this method is that parallel operations are limited. This makes quantum error correction more difficult, but it is possible using multiple regularly spaced additional pointers that are activated for error correction then deactivated for computation [66].

Chapter 3

Entanglement

Entanglement may be qualitatively understood as correlations between quantum systems that are stronger than would be allowed classically; we give a precise definition in Sec. 3.2.1. In this chapter we review its properties and potential uses, and the main existing methods of detecting it, entanglement witnesses (including Bell inequalities) and quantum state tomography.

3.1 Density matrices

In this section we review the density matrix description of quantum states and decoherence.

A *density matrix* (density operator) ρ is a positive (all eigenvalues non-negative) Hermitian matrix with $\mathrm{Tr}\,\rho = 1$, of size $d \times d$ where d is the dimension of the system's state vector (Hilbert) space. For a pure state (one with a state vector $|\,\psi\rangle$), $\rho = |\,\psi\rangle\langle\psi\,|$. The action of a quantum operation (gate) $|\,\psi\rangle \to U\,|\,\psi\rangle$ becomes $\rho \to U\rho U^\dagger$.

The expectation of an observable O is $\mathrm{Tr}\,\rho O$, and the probability of the outcome $O = o_i$ is the expectation $\mathrm{Tr}\,\rho P_i$ of the projector P_i onto that eigenspace, $P_i = \sum_j |\, i,j\rangle \langle i,j\,|$ where the $|\, i,j\rangle$ are a basis of eigenstates of O, $O\,|\, i,j\rangle = o_i\,|\, i,j\rangle$. Such measurements are called *projective measurements*. We also sometimes consider a more general type of measurement (the most general possible on a single copy of the state) called a *positive operator valued measure (POVM)*. This still has probability $\mathrm{Tr}\,\rho P_i$ of outcome i, but the P_i do not have to be projectors but can be any set of positive Hermitian operators satisfying $\sum_i P_i = \mathbb{I}$, the minimum conditions necessary for $\mathrm{Tr}\,\rho P_i$ to be a valid set of probabilities (ie. positive reals summing to 1) for any density matrix ρ.

Unlike state vectors, density matrices allow *mixed states*, which can be used to describe systems subject to decoherence (interaction with their environment), which all real experimental systems are to some extent, without the need to explicitly write the states of the environment. The density operator ρ_A of the system only is obtained from the density matrix ρ_{AE} of the system and environment using the *partial trace* $\rho_A = \mathrm{Tr}_E \rho_{AE}$, defined in terms of matrix elements as

$$\rho_{A(i,j)} = \sum_k \rho_{AE(ik,jk)}, \tag{3.1}$$

where the indices i, j run over states of the system A and k over states of the environment E. If O is any observable acting on the system A only,

$$\mathrm{Tr}\,\rho_A O = \sum_{i,j} \rho_{A(i,j)} O_{j,i} = \sum_{i,j,k} \rho_{AE(ik,jk)} O_{j,i} = \mathrm{Tr}\,\rho_{AE}(O \otimes \mathbb{I}_E), \tag{3.2}$$

so the *reduced density matrix* ρ_A completely describes the observable state of the system if (as is usually the case in practice) the state of the environment is not measurable. Similarly $U_A \rho_A U_A^\dagger = \mathrm{Tr}_E (U_A \otimes U_E) \rho_{AE} (U_A \otimes U_E)^\dagger$, where U_A and U_E are any unitary operations on the system and environment respectively, so if the system does not further interact with the same environment then ρ_A evolves in the normal way. The density matrix of such a decohered system is hence defined to be ρ_A.

For example, a state $|\,\psi\rangle = \sum_i a_i \,|\,\psi_i\rangle\,|\,e_i\rangle$, where the $|\,e_i\rangle$ are orthogonal states of the environment, becomes $\rho = \sum_i |a_i|^2 \,|\,\psi_i\rangle\,\langle\psi_i\,|$. Such a state can also arise from or be interpreted as classical randomness (state $|\,\psi_i\rangle$ with probability $|a_i|^2$); the two interpretations are equivalent if we define the environment to include the source of the randomness.

3.2 Entanglement theory

In this section we review the properties of quantum entanglement and its potential uses. More detailed reviews of this subject can be found at [17, 67].

3.2.1 Definition of entanglement

A density matrix $\rho_{12\ldots n}$ of $n \geq 2$ subsystems is called *separable* if it can be written as a classical mixture of product states, that is

$$\rho_{12\ldots n} = \sum_i p_i \prod_{j=1}^{n} |\,\psi_{ij}\rangle_j\,\langle\psi_{ij}\,|_j \tag{3.3}$$

where the p_i are probabilities ($0 \leq p_i \leq 1$, $\sum_i p_i = 1$) and the $|\psi_{ij}\rangle_j$ are arbitrary states of subsystem j, and *entangled* if it cannot [68]. Eq. (3.3) is allowed to be a convergent infinite series, but for finite dimensional systems this is never necessary [69].

Unlike the pure state case, separable states are not necessarily product states $\rho = \bigotimes_j \rho_j$, but can contain classical correlations, for example $\rho = (|00\rangle\langle 00| + |11\rangle\langle 11|)/2$ (where $|00\rangle \equiv |0\rangle \otimes |0\rangle$). The separable states, unlike the product states, make up a non-zero volume fraction of all states; however, it is a superexponentially small one, for n qubits

$$(c_1 3^{-3n/8})^{4^n-1} \leq \frac{\text{Vol(separable states)}}{\text{Vol(all states)}} \leq (c_2\sqrt{2n\ln n}3^{-3n/8})^{4^n-1}, \qquad (3.4)$$

for some constants c_1, c_2 [70].

Note that Eq. (3.3) is in general *not* the eigenvalue decomposition of ρ, since there are no orthogonality conditions on the $|\psi_{ij}\rangle_j$: a mixture of entangled states can be separable. For example, $(|00\rangle\langle 00| + |{+}{+}\rangle\langle {+}{+}|)/2$ (where $|+\rangle \equiv (|0\rangle + |1\rangle)/\sqrt{2}$) is separable, but its eigenstates are the entangled $|00\rangle \pm |{+}{+}\rangle$.

3.2.2 Creation and examples

In this section we give some simple examples of entangled states and how they are created.

Almost any interaction between quantum systems can create entanglement; the main difficulty is that systems which interact with each other tend also to interact with their environment, and entanglement with the environ-

ment appears as decoherence rather than usable entanglement because it is not possible to measure or control the complete state of the environment.

The *Bell states* are the maximally entangled 2 qubit states,

$$|\,01\rangle - |\,10\rangle \quad \text{(singlet)}, \tag{3.5}$$

$$|\,00\rangle + |\,11\rangle\,, \quad |\,00\rangle - |\,11\rangle\,, \quad |\,01\rangle + |\,10\rangle \ \text{(triplet)}. \tag{3.6}$$

Like any entangled state, these can be built up using one and two qubit gates, in this case starting from $|\,11\rangle\,, |\,00\rangle\,, |\,10\rangle\,, |\,01\rangle$ respectively and applying a Hadamard gate on the first qubit followed by a CNOT gate, which has been done in ion traps [71]. They can also be created by parametric downconversion of photons [72]. They are used in many quantum communication tasks, including teleportation [18].

The *cat* (GHZ) *state* of n qubits is

$$|\,0\rangle^{\otimes n} + |\,1\rangle^{\otimes n} \equiv |\,000\ldots0\rangle + |\,111\ldots1\rangle\,, \tag{3.7}$$

which can be created by extending the above gate sequence to $n-1$ CNOTs with one control qubit and different target qubits, and can be used for fault tolerant measurement in quantum error correction [19].

The 1D *cluster state* is

$$\prod_j (|\,0\rangle_j + |\,1\rangle_j\,\sigma_{z,j+1}), \tag{3.8}$$

where $\sigma_{z,j}$ is a phase flip acting on qubit j. It can be created using controlled-

phase gates between nearest neighbours, starting with all qubits in the $|+\rangle = (|0\rangle + |1\rangle)/\sqrt{2}$ state. This is equivalent to a nearest neighbour Ising interaction [21], which allows this state to be created using only collective operations, for example state selective movement in an optical lattice [12]. It can also be built up from Bell pairs using two qubit measurements [73]. Its 2D and 3D extensions, created in the same way, are universal resource states for measurement-based (one-way) quantum computation [21], which after the initial creation of this state uses only single qubit measurements. This form of quantum computation is hence suited to systems where this type of collective operation is easier than individual 2-qubit operations (optical lattices), or where 2-qubit operations require postselection (linear optics [73]).

We will now consider how entanglement could be useful in quantum communication and computation, which provide a motivation for studying it.

3.2.3 Communication uses and measures

In this section we consider the importance of entanglement as a resource for quantum communication, limitations on the local manipulation of entanglement, and ways of quantifying entanglement based on this.

Consider n distant parties, each having their own quantum system on which they can perform arbitrary quantum operations, including multi-qubit operations if they hold all the qubits involved, but only able to communicate classically with each other. This is called LOCC (local operations and classical communication). Any separable state can be prepared under these conditions, for example by choosing i according to the probability distribu-

tion $\{p_i\}$ of the definition Eq. (3.3) and communicating it to all the parties j, who then each prepare the state $|\psi_{ij}\rangle_j$ by local operations. However, entangled states cannot be prepared by LOCC without prior entanglement, as applying any local operation to a separable state gives another separable state, and mixtures of separable states (as created by random choices and/or measurement result feedforward) are separable.

Since entanglement cannot be created by LOCC, prior entanglement becomes a resource, and the question arises of how much of it is needed for a given task. It is reasonable to require that a quantity intended to measure amount of entanglement not increase, at least on average, under LOCC. However this does not uniquely define amount of entanglement, as there exist pairs of states neither of which can be converted into the other by LOCC [74].

The natural unit of bipartite entanglement is the maximally entangled pair of qubits, called an *ebit*, EPR pair, or singlet. (The use here of the singlet state $(|10\rangle - |01\rangle)/\sqrt{2}$ rather than a triplet state such as $(|00\rangle + |11\rangle)/\sqrt{2}$ is a convention; any Bell basis state has 1 ebit of entanglement, as they can all be interconverted by local operations.) One ebit plus LOCC is equivalent to the transfer (in either direction) of one qubit plus LOCC, as locally creating a singlet then sending one of its qubits to the other party creates one ebit, and conversely one ebit can be used to teleport one qubit [18, 71].

Any n-qubit entangled state can be prepared from $n-1$ ebits by LOCC, by first one party preparing it in n of their own qubits, then using the ebits to teleport these qubits to the other parties. Some states can be prepared from fewer ebits using quantum data compression [75]. The *entanglement of*

formation $E_f(\rho)$ of a state ρ is defined as the minimum over LOCC protocols of the (expected) number of ebits required to prepare a *single* copy of ρ, while the *entanglement cost* $E_c(\rho)$ is defined as the minimum over LOCC protocols of the (expected) number of ebits per copy required to prepare multiple copies of ρ. It is conjectured that E_f is additive, which would imply $E_c(\rho) = E_f(\rho)$, but it has only been proved that $E_f(\rho) \geq E_c(\rho) = \lim_{m\to\infty} E_f(\rho^{\otimes m})/m$ [76]. E_c is strictly positive for all 2 party entangled states [77].

Entanglement distillation is the reverse process of preparing maximally entangled qubit pairs from copies of some other entangled state by LOCC. The *distillable entanglement* $E_d(\rho)$ is defined as the maximum expected number of ebits per copy that can be prepared by LOCC from copies of ρ. Not all entangled states can be distilled; those which cannot ($E_d = 0$) are called *bound entangled* states. This creates irreversibility: preparing a bound entangled state requires $E_c > 0$ ebits, but no ebits can be recovered from it.

Entanglement distillation is potentially useful as it allows high fidelity quantum communication (arbitrarily high fidelity if the local operations are perfect) over a noisy quantum channel, by sending halves of singlets through the channel, then distilling the resulting mixed entangled pairs into high fidelity singlets. The amount of noise this can handle is limited by the need for the channel output to be a distillable state, but can be quite large: any 2 qubit state with $> 50\%$ fidelity with a singlet is distillable by the procedure of [78]. The total distance can be increased further by adding additional devices (quantum repeaters) between the two parties that wish to share entanglement, and first creating imperfect entangled pairs between neighbouring repeaters, then alternately distilling them to increase fidelity and combining

them by entanglement swapping (teleporting half of one pair through an adjacent pair) to increase distance. This in principle allows a high fidelity ebit to be created over a noisy quantum channel of arbitrarily large total distance in polynomial time [79].

2 party distillation protocols involving only one-way communication are equivalent to quantum error correction [80], with the two halves of the initial entangled state being equivalent to the states of a single system before and after the error process. Classical error correction and privacy amplification in quantum key distribution (including prepare and measure protocols without actual entanglement) are also equivalent to distillation followed by measurement, which is used to prove that they are secure against coherent attacks [81]. However, the class of private states (encoding a perfectly secure classical bit) is larger than the class of maximally entangled states, which for some states allows more than E_d bits of secure key to be obtained [17].

For 2 party pure states (of any Hilbert space dimension, or equivalently any number of qubits per party) these entanglement measures are all equal to the entropy of the reduced density matrix of either party [75],

$$E_f(|\,\psi\rangle) = E_c(|\,\psi\rangle) = E_d(|\,\psi\rangle) = -\mathrm{Tr}\,\rho_A \log_2 \rho_A, \quad \rho_A = \mathrm{Tr}_{\,B}\,|\,\psi\rangle\,\langle\psi\,|\,, \tag{3.9}$$

and are hence written as just $E(|\,\psi\rangle)$. This makes LOCC manipulation of 2 party pure entanglement asymptotically (in the limit of many copies) reversible.

However, mixed states or states of more than 2 parties generally have $E_c > E_d$. This makes their preparation from ebits irreversible, as not all

the entanglement used can be recovered by distillation. We may then ask whether there is some larger set of resource states, and associated vector measure of entanglement $\mathbf{E}$ giving a quantity of each resource, from which preparation of a general state is reversible $\mathbf{E}_c = \mathbf{E}_d$. For multiparty pure states, such a set is called a minimal reversible entanglement generating set (MREGS), but it is not known whether a finite MREGS exists, even for 3 parties [74, 82]. It is known that the number of states in an MREGS must be strictly larger than the number $n(n-1)/2$ of pairs of parties [74].

The entanglement measures E_c, E_f and E_d are in general difficult to evaluate, because of the optimization in their definitions. For 2 party mixed states

$$E_f(\rho) = \min_{\{|\psi_i\rangle\}} \sum_i p_i E(|\psi_i\rangle), \quad \rho = \sum_i p_i |\psi_i\rangle\langle\psi_i|, \tag{3.10}$$

because one way to prepare ρ from this number of ebits is to choose i with probability distribution $\{p_i\}$ and prepare $|\psi_i\rangle$, while it is impossible to prepare ρ from fewer ebits because the expectation of this expression is nonincreasing under LOCC [80]. However, this formula does not provide an easy way to evaluate E_f because the minimum is hard to take. There are a number of other entanglement measures which are easier to calculate but less directly related to a state's value for communication [17].

3.2.4 Relation to quantum computation

Entanglement is essential for measurement-based quantum computation, as local measurements on a separable initial state of known decomposition Eq. (3.3) can be efficiently simulated classically: choose i with probability

distribution $\{p_i\}$, then choose each measurement result with the probabilities appropriate to the single qubit state $|\psi_{ij}\rangle_j$. This is related to the above in that the measurements are a LOCC process with each physical qubit being a party, so logical qubits can only move by teleportation, requiring prior entanglement.

The status of entanglement in circuit model quantum computation is less clear: it is known that exponential advantage over classical computation requires gates that *can* create entanglement from some separable inputs [83], but it is not known whether it is necessary that entanglement *actually* be created during the quantum computation.

It has been proved that *pure* state quantum computation can be classically simulated in polynomial time if its entanglement is limited to a fixed number of qubits per entangled block [84] or a polynomial Schmidt rank (number of terms when written as a superposition of products) [85]. However, applying the same methods to mixed states only proves that this amount of *correlation* is essential if a quantum computation is to be exponentially faster than classical computation [86], as they do not distinguish quantum correlation (entanglement) from classical correlation. They also do not rule out a polynomial advantage with unentangled pure states; this is possible at least in the oracle (black box) setting, the Bernstein-Vazirani algorithm being an $O(n)$ example [87].

Computation with highly mixed states is possible, and standard in liquid NMR as preparing a pure state in that system is impractical [7], but there is no known way to obtain exponential advantage over classical computation without entanglement. Pseudopure states $\rho = \epsilon |\psi\rangle \langle\psi| + (1-\epsilon)\mathbb{I}/d_{\text{tot}}$

can run any quantum algorithm on $|\psi\rangle$ [88] and are always separable for $\epsilon < \sqrt{54/17} \times 6^{-n/2}$ [89]. However, they require $O(1/\epsilon^2)$ copies to distinguish the answer from the random noise, so such a small ϵ makes them slower than classical computation; for $\epsilon > 2^{1-n}$ they are entangled for $|\psi\rangle = |0\rangle^{\otimes n-2}(|11\rangle + |00\rangle)/\sqrt{2}$, a 2 qubit Bell state [90]. It remains unproven whether DQC1, which starts with all but one of its qubits in the maximally mixed state [91] and can run a limited [92] but nontrivial [91, 93] range of quantum algorithms, always requires entanglement [94].

3.2.5 Mathematical tests

In this subsection we consider algorithms for proving that a known density matrix ρ is entangled, including the purity test which our method is based on.

The *partial transpose* is defined in terms of matrix elements as

$$\rho^{T_A}_{ik,jl} = \rho_{jk,il}, \tag{3.11}$$

where the indices i, j label states of subsystem A and k, l states of subsystem B. The resulting operator is basis-dependent, but its eigenvalues are not. For states of more than two subsystems, the partial transpose can be taken with respect to any bipartition into two subsets $A, B \subset \{1, \ldots, n\}, A \cup B = \{1, \ldots, n\}$. If ρ is separable then it has positive partial transpose (that is, all eigenvalues of ρ^{T_A} are non-negative) with respect to any bipartition, so finding a negative eigenvalue of ρ^{T_A} proves that ρ is entangled [95].

The converse is not true: positive partial transpose (PPT) states can be

entangled [96, 69, 97], and for large n nearly all of them are [70]. However, PPT states always remain PPT under LOCC [98] and under tensor product [95], and hence cannot be distilled, as pure entangled states are non-PPT [98]. It is not known whether, conversely, all non-distillable 2 party states are PPT [17]. The 4 qubit Smolin state [99] is non-distillable as a 4 party state, and is PPT for $2+2$ but not $1+3$ qubit bipartitions. However, if this state is considered as a 2 party state along any of its non-PPT bipartitions, it becomes distillable.

The *purity* of a state ρ is defined to be $\mathrm{Tr}\,\rho^2$. Since the eigenvalues of a density matrix are non-negative,

$$0 < \mathrm{Tr}\,\rho^2 \leq (\mathrm{Tr}\,\rho)^2 = 1, \tag{3.12}$$

with equality ($\mathrm{Tr}\,\rho^2 = 1$) for pure states. A *reduced purity* $\mathrm{Tr}\,\{\rho_A^2\}$ is the purity of the reduced density matrix $\rho_A = \mathrm{Tr}_B\rho$ ($A, B \subset \{1,\ldots,n\}, A \cup B = \{1,\ldots,n\}$) of a subset A of the subsystems. The reduced purities of separable states satisfy the inequalities [30, 29]

$$\mathrm{Tr}\left\{\rho_A^2\right\} > \mathrm{Tr}\left\{\rho_C^2\right\}, A \subset C, \tag{3.13}$$

qualitatively that the whole of a separable state cannot be purer than its parts, while an entangled state can be.

Other mathematical entanglement tests include the range test [69] and the majorization test [100]. However, none of the above tests detects *all* entangled states. It is in general NP-hard to mathematically determine whether a

given ρ is entangled [101]; general algorithms are known [102, 103], but their run time is exponential in n.

3.2.6 Physical detection: introduction

We however are concerned with the *physical* detection of entanglement, where we have physical copies of ρ that we can perform measurements on but do not know what ρ is.

Physical entanglement detection is always a statistical process: for any fixed finite number of copies of the state, there is always some nonzero probability of erroneously detecting entanglement in at least some separable states. For any fixed finite number of copies N of a state ρ, the total state is $\rho^{\otimes N} \equiv \rho \otimes \ldots \otimes \rho$ (N factors). Any measurement process on these N copies (including measurements where the copies interact with each other and/or ancillas, with arbitrary classical post-processing) is equivalent to some POVM measurement, that is a positive operator for each possible outcome, on the total state $\rho^{\otimes N}$. Let E_N be the operator for the outcome "state is entangled", which hence has probability $\mathrm{Tr}\,(\rho^{\otimes N} E_N)$, so if this outcome can ever occur then $E_N \neq \mathbf{0}$. In the maximally mixed state $\rho_I \equiv \mathbb{I}/d_{\mathrm{tot}}$, which is separable ($= \bigotimes_j \mathbb{I}_j/d_j$), where d_j and d_{tot} are the state space dimensions of the jth subsystem and the whole system respectively,

$$\mathrm{Tr}\,(\rho_I^{\otimes N} E_N) = d_{\mathrm{tot}}^{-N} \mathrm{Tr}\, E_N > 0, \tag{3.14}$$

where the inequality follows from E_N having non-negative eigenvalues and is strict because $E_N \neq \mathbf{0}$; hence any physical measurement that ever detects

entanglement in anything will sometimes erroneously detect entanglement in the maximally mixed state.

We hence define a valid entanglement detection method to be one whose probability of error tends to 0 as $N \to \infty$, that is

$$\max_{\rho \text{ separable}} \mathrm{Tr}\left(\rho^{\otimes N} E_N\right) \to 0 \tag{3.15}$$

$$\mathrm{Tr}\left(\rho_t^{\otimes N} E_N\right) \to 1, \text{ some entangled } \rho_t \tag{3.16}$$

as $N \to \infty$; the states ρ_t are the states this method detects. Relevant considerations for choosing a method include speed of the above convergence (and hence the number N of state copies required for an acceptably low probability of error), which states ρ_t are detected, and how easy it is to carry out the measurement described by E_N.

One approach is to measure the whole density matrix ρ, a process called *state tomography* [24] (Sec. 3.4), then apply a mathematical entanglement test. This can detect everything and requires only single qubit measurements, but requires exponentially many state copies, making it unusably slow for more than a few qubits.

Another option is to use an observable whose expectation is positive in all separable states and negative in the state we want to detect; these are called *entanglement witnesses* [104] (Sec. 3.3). These can be suitable for larger numbers of qubits (the number of copies required is often independent of the number of qubits in the state), but each witness only detects a limited range of states, making this method most appropriate when we have some prior knowledge of what ρ is likely to be. Their ease of measurement varies.

Our method is based on the purity test and the fact that, while purity is not a linear function of ρ and hence not the expectation of any observable on a single copy of ρ, it *is* a linear function of $\rho \otimes \rho$ and the expectation of an observable on *two* copies $\rho \otimes \rho$ [29], namely the swap operator $V \,|\, \psi\rangle \,|\, \phi\rangle = |\, \phi\rangle \,|\, \psi\rangle$ between corresponding subsystems of the two copies:

$$\mathrm{Tr}\, V(\rho \otimes \rho) = \mathrm{Tr}\, \rho^2. \tag{3.17}$$

Reduced purities Tr $\{\rho_A^2\}$ are obtained similarly by swapping only those subsystems in the set A.

This detects all pure or sufficiently near-pure entangled states, in many cases with a number of state copies independent of the number of qubits in the state. The implementation we consider requires the ability to perform a beamsplitter between identical bosonic qubits (which, while a two qubit operation, does not require interaction between the qubits) and observe whether they come out the same way or opposite ways; this is feasible for photons, and we describe how it could also be done for atoms in an optical lattice.

Other mathematical tests using polynomials of degree k in the state ρ similarly correspond to physical observables on k copies of ρ, and hence are in principle physically realisable [105, 106]. However, the complexity of a single measurement of such an observable, whether by expansion and local measurement (Sec. 3.3.4), by controlled shifts [105], or by full quantum computation [106], is in general exponential in k. The partial transpose test has $k = 2^n$ [105, 106] and hence complexity double exponential in n, making this method even slower than full state tomography for large numbers of

qubits.

We next describe entanglement witnesses and state tomography in more detail.

3.3 Conventional detection methods: witness operators

An *entanglement witness* is defined to be an observable (Hermitian operator) W with non-negative expectation on all separable states and negative expectation on some entangled states,

$$\langle W \rangle_\rho \equiv \mathrm{Tr}\,(W\rho) \geq 0, \text{ all separable } \rho \tag{3.18}$$

$$< 0, \text{ some entangled } \rho. \tag{3.19}$$

W then *detects* entanglement in those states ρ for which $\langle W \rangle_\rho < 0$. (Some definitions add a normalisation condition $\mathrm{Tr}\, W = 1$; we do not.)

Like all entanglement detection methods, such witnesses are statistical in nature: it is the *expectation* (average) of a witness that is non-negative in separable states, not every single measurement of it. To detect entanglement using a witness W it is hence necessary to measure it many times, using a new copy of the state ρ each time, and take the average $\langle W \rangle_\rho$. The maximum uncertainty (standard deviation) ΔW of a given witness W in any state is half the difference between the largest and smallest eigenvalues of W, attained in states which are equal combinations (superposition or mixture) of the corresponding eigenstates. To make the entanglement of a state ρ visible

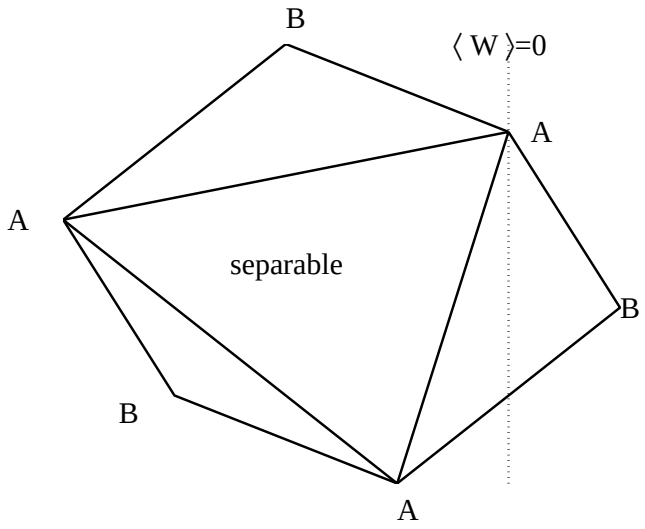


Figure 3.1: The possible density matrices of n d level subsystems form a convex set in the $(2d)^n - 1$ dimensional (over $\mathbb{R}$) space of $d^n \times d^n$ trace-1 Hermitian matrices, and the separable states a convex subset of it. An entanglement witness W detects the states on one side of the hyperplane $\langle W \rangle = 0$, here the states to the right of the dotted line. A are product (pure separable) states, B pure entangled states; their appearance as isolated points is an artifact of the 2D diagram, they are in fact connected sets of dimension $2n(d-1)$ and $2(d^n - 1)$ respectively. Note that unlike the one-qubit Bloch sphere, the pure states do not cover the entire surface, so not every witness can be written as $c - |\,\psi\rangle\,\langle\psi\,|$.

above the statistical noise, $\alpha(\Delta W/|\langle W \rangle_\rho|)^2$ measurements of W are hence sufficient, where $\alpha \sim 10$ depends on the statistical confidence level desired.

Entanglement witnesses have a geometrical interpretation as hyperplanes $\langle W \rangle = 0$ in density matrix space, with all the separable states on one side and the detected states being those on the other side (Fig. 3.1). Since the set of separable states is convex (that is, any mixture of separable states is itself separable), for any given entangled state there exists a witness that will detect it [96]. However, no one witness detects all (or even all pure) entangled states: if W detects ρ_1 and ρ_2, it will also detect any mixture $(1-\lambda)\rho_1 + \lambda\rho_2$

by linearity, so any set of states which can form a separable mixture (for example, any two of the Bell basis states) cannot all be detected by the same witness [28]. Hence one needs to know in advance roughly what the state is likely to be to choose an appropriate witness to use; if one finds $\langle W \rangle < 0$ then the state is entangled, but if $\langle W \rangle > 0$ then this only means that the state is not what one thought it was, not necessarily that it is separable. This makes witnesses appropriate for verifying the success of experiments which aim to prepare a specific entangled state, such as [23], but inappropriate for analyzing unknown processes.

3.3.1 Fidelity witness

A conceptually simple way to construct an entanglement witness that detects a given pure entangled state $|\,\psi\rangle$ is [23]

$$W_f = c\mathbb{I} - |\,\psi\rangle\langle\psi\,|\,, \qquad c = \max_{\phi \text{ separable}} |\langle\phi\,|\,\psi\rangle|^2\,. \tag{3.20}$$

We call this the fidelity witness because $\langle W_f \rangle_\rho = c - F(\rho, |\,\psi\rangle\langle\psi\,|)$ where F is the fidelity. It measures how close the actual state is to the target state $|\,\psi\rangle$, detecting entanglement if ρ is "too close" to $|\,\psi\rangle$ to be separable. This works because the entangled states are an open set (that is, every entangled state has a nonzero distance from it within which there are no separable states). This witness can be modified to verify other properties, such as the presence of genuine multipartite (rather than any) entanglement, by instead maximising c over the states without the desired property.

Since its eigenvalues have a range of 1 (one is $c - 1$, all the others are c),

$\Delta W_f = 1/2$, so $O(1/2(1-c))^2$ copies are sufficient to detect the entanglement of $|\psi\rangle$. For the GHZ and cluster states, $c = 1/2$ detects only genuine multipartite entanglement for any n [26], so their entanglement can in principle be detected using a number of state copies independent of n. However, this uncertainty assumes the *direct* measurement of W_f, which requires nonlocal measurements; we will consider in Sec. 3.3.4 how to measure W_f using local measurements.

3.3.2 Mixed state witnesses

For mixed target states ρ_t the fidelity cannot be used directly, as it is not $\operatorname{Tr}\rho_t\rho$ but $[\operatorname{Tr}(\rho_t^{1/2}\rho\rho_t^{1/2})^{1/2}]^2$, which is not linear in ρ and hence not the expectation of an observable. $W = c\mathbb{I} - \rho_t$ works for some states but not all, as $\operatorname{Tr}\rho_t\rho$ is not maximised by $\rho = \rho_t$ but may be higher for some separable ρ. A general method of finding a witness that detects a given ρ_t is given in [103], but its calculation time is exponential in n; since it is in general NP-hard to determine whether a given state is entangled [101], it is also NP-hard to find a witness that detects it [107].

Faster methods do exist for some classes of mixed states. If ρ_t has non-positive partial transpose, that is $\langle\psi|\rho_t^{T_A}|\psi\rangle < 0$ for some $|\psi\rangle$ and some subset $A \subset \{1,\ldots,n\}$, a suitable witness is $W = (|\psi\rangle\langle\psi|)^{T_A}$ [108]. A method for edge states (positive partial transpose states that cannot be written as mixtures of other such states) is given in [109], but while any positive partial transpose state can be written as a mixture of an edge state and a separable state and any witness for the original state will also detect the edge state

[109], the converse is not true. Another method is described in [107].

3.3.3 Bell inequalities

Bell inequalities test whether a state is compatible with local realism. They were originally designed and used for testing quantum mechanics itself [72], but can also be used to test for entanglement as only entangled states can violate local realism.

Ordinary Bell inequalities are linear inequalities of expectations of observables, and hence can be rearranged to $\langle W_B \rangle > 0$ form; as this is satisfied by all separable states, W_B is an entanglement witness. The converse is not true: not all entanglement witnesses are Bell inequalities. The distinction is important when testing quantum mechanics itself, but less important when testing for entanglement of a given state assuming the validity of quantum mechanics.

Local realism means that a state's correlations can be reproduced by a *local hidden variable model*, that is a probability distribution of the form

$$P(O_1 = o_1, \ldots, O_n = o_n) = \sum_i p_i \prod_j P(O_j = o_j | i), \tag{3.21}$$

where O_j is an observable acting only on subsystem j, the probability distribution p_i of the hidden variable i depends only on the state and not on the choice of observables O_j to be measured, and the probability distribution $P(O_j = o_j|i)$ of the observable O_j depends on the state, O_j and i but not on the choices O_k or results o_k of measurements on other subsystems $k \neq j$.

Every separable quantum state has a local hidden variable model; one

way to construct it is to write the state in the form (3.3), then take the p_i to be the same and the $P(O_j = o_j|i)$ to be the quantum probabilities in the state $|\,\psi_{ij}\rangle_j$. Hence every linear Bell inequality that can be violated by quantum states is an entanglement witness. However, not every quantum state with a local hidden variable model for projective measurements (the type allowed in a linear Bell inequality) is separable. An explicit local hidden variable model for projective measurements on the state $(|\,10\rangle - |\,01\rangle)(\langle 10\,| - \langle 01\,|)/4 + \mathbb{I}/8$, which is entangled as it has non-positive partial transpose, is constructed in [68]. It is conjectured that all positive partial transpose states, including the entangled ones, also have local hidden variable models [110]. Hence not every entangled state can be detected using Bell inequalities, and not every entanglement witness is a Bell inequality. Bell inequalities can however detect some multipartite bound (but non-PPT) entangled states, and even be maximally violated by them as in the case of the 4 qubit Smolin state [99].

The complete set of full correlation Bell inequalities for n subsystems each with two 2-outcome measurements is [111]

$$W_B = 1 - 2^{-n} \sum_{s\in\{0,1\}^n} \left(\sum_{r\in\{0,1\}^n} \pm_r (-1)^{r\cdot s} \right) \prod_{j=1}^{n} O_j^{(s_j)}, \qquad (3.22)$$

$$\langle W_B \rangle_\rho \geq 0 \text{ if } \rho \text{ has a local hidden variable model,} \qquad (3.23)$$

where $O_j^{(0)}, O_j^{(1)}$ are any two measurements acting on subsystem j with outcomes ± 1. There are 2^{2^n} such inequalities for any given set of O_j (though some of them are trivial and never violated by quantum states, and are hence not witnesses) each labelled by a set of 2^n signs $\pm_r$.

Useful members of this set include the ordinary 2-subsystem Bell (or CHSH) inequality [72],

$$W_B = 1 - \frac{1}{2}\left(O_1^{(0)}O_2^{(0)} + O_1^{(0)}O_2^{(1)} + O_1^{(1)}O_2^{(0)} - O_1^{(1)}O_2^{(1)}\right), \tag{3.24}$$

and Mermin's inequality for detecting cat states [112],

$$W_B = 2^{n/2} - \mathrm{Im}\prod_{j=1}^{n}(O_j^{(0)} + iO_j^{(1)}). \tag{3.25}$$

The choice $O_j^{(0)} = \sigma_{x,j}, O_j^{(1)} = \sigma_{y,j}$ gives maximal violation of Mermin's inequality for the state $(i\,|\,0\rangle^n + |\,1\rangle^n)/\sqrt{2}$. It can be made to detect other locally equivalent states, such as the standard cat state, by applying the appropriate local operation to the O_j.

Bell inequalities, unlike other entanglement witnesses, remain valid for *any* local 2-outcome measurements O_j. Hence Bell inequality violation is entanglement even if one does not trust the measuring apparatus to measure the same observables as it is supposed to, as long as there is no communication between different subsystems. However, the usefulness of this is limited as which entangled states are detected does depend on the choice of O_j, and some settings (such as $O_j^{(0)} = O_j^{(1)}$) detect nothing at all; while a faulty measurement will not detect "entanglement" that is not there, it may well miss entanglement that is there.

There are also generalisations of Bell inequalities to collective measurements on multiple copies of the state at a time, and to more than one round of POVM measurements with classical communication; these are nonlinear

and hence not entanglement witnesses. The local hidden variable model of [68] breaks down when these are allowed, and all 2-party distillable entangled states become detectable [113]. It is conjectured that 2-party bound entangled states remain undetectable, but only the restriction to multi-copy LOCC preprocessing followed by a 2-setting, 2-outcome full correlation ([111] type) Bell inequality has been proven [113].

3.3.4 Witness measurement

While every witness is an observable and hence in principle directly measurable, in practice only local (single subsystem) measurements are usually available. In this subsection, we find that while it is possible to measure any witness under these conditions, some witnesses are exponentially slow to measure.

Any witness can be written as a sum of locally measurable observables [108, 23, 26],

$$W = \sum_{i=1}^{k} f_i(O_{i1}, \ldots, O_{in}) \tag{3.26}$$

where the O_{ij} are observables acting on subsystem j only and the f_i are functions of n real variables. A single measurement of W can then be made using k copies of the state, by measuring each O_{ij} on subsystem j of copy i, and the results are substituted into Eq. (3.26).

This works because the operators $O_{i1}, \ldots, O_{in}$, since they act on different subsystems, must commute and hence have a full set of simultaneous eigenstates $\bigotimes_{j=1}^{n} |\, O_{ij} = o_{ij}\rangle_j$, which are then also the eigenstates of $f_i(O_{i1}, \ldots, O_{in})$ with eigenvalues $f_i(o_{i1}, \ldots, o_{in})$.

The Bell inequalities have $k = 2^n$, and known expansions of the fidelity witness W_f for many target states also have exponentially growing k [26, 108] (an exception is the W state, for which $k = n^2 - n + 1$ [27]), making this procedure require impracticably huge numbers of state copies for more than a few qubits. Attempts have hence been made to find witnesses with lower k, which we describe in the next subsection.

3.3.5 Easily measurable witnesses

One approach [26, 114] starts from a locally measurable set of commuting stabilizer operators $S_1, \ldots, S_l$ with eigenvalues ± 1 which uniquely define the target state $|\psi\rangle$ as the only state stabilized ($S_i |\psi\rangle = |\psi\rangle$, ie eigenvalue $+1$) by all of them. Possible target states with $l = 2$ (the minimum, as an $l = 1$ state would be separable) include the GHZ state

$$S_1 = \prod_{j=1}^{n} \sigma_{x,j}, \quad S_2 = -1 + 2^{1-n} \prod_{j=2}^{n} (\sigma_{z,j-1}\sigma_{z,j} + 1), \tag{3.27}$$

and the cluster state

$$S_1 = -1 + 2 \prod_{j \text{ odd}} \frac{1}{2}(1 + \sigma_{z,j-1}\sigma_{x,j}\sigma_{z,j+1}), \tag{3.28}$$

with $\sigma_{z,i} \equiv \mathbb{I}$ when $i \notin \{1, \ldots, n\}$ and S_2 the same except over even j. This can be extended to graph states, including multidimensional cluster states, by including σ_z factors for all nearest neighbours of j [26]. For the S_i to be locally measurable neighbouring vertices j must not be in the same S_i, but this allows $k = 2$ for cluster states of any size and dimensionality.

Defining W_s by

$$W_s \equiv c + \frac{1}{2}\left(l - 2 - \sum_{i=1}^{l} S_i\right), c = \max_{\phi \text{ separable}} |\langle\phi\,|\,\psi\rangle|^2, \tag{3.29}$$

W_s is diagonal in the basis of common eigenstates of the S_i, with eigenvalue $c-1$ in $|\,\psi\rangle$ and all other eigenvalues $\geq c$. W_f is also diagonal in this basis with eigenvalues $c-1, c$, so $W_s \geq W_f$ with equality in the state $|\,\psi\rangle$. Hence W_s is also an entanglement witness ($\langle W_s\rangle \geq \langle W_f\rangle \geq 0$ in separable states) that detects $|\,\psi\rangle$, and $c - \langle W_s\rangle_\rho$ is a lower bound for the fidelity $F(\rho, |\,\psi\rangle\langle\psi\,|) = c - \langle W_f\rangle_\rho$. Since the S_i were assumed locally measurable, $k = l$ copies of the state are sufficient for one measurement of W_s, and since they have eigenvalues ± 1, $\Delta W_s \leq l$. Hence $O(l^3/(c-1)^2)$ state copies are sufficient to detect the entanglement of $|\,\psi\rangle$ using only local measurements; for the GHZ and cluster states this is independent of n.

Note that if W_s could be directly projectively measured, it could be used to sort individual copies into good ($W_s = c-1$) and bad ($W_s > c-1$) copies of $|\,\psi\rangle$, as the result $W_s = c-1$ would project the state onto $|\,\psi\rangle$, the only eigenstate of this eigenvalue. This is used as the ancilla verification step of quantum error correction [5, 115], but requires 2 qubit gates, making it more difficult to carry out.

Another method [27] uses the W state's fidelity witness, which unlike most fidelity witnesses has a $k = O(n^2)$ expansion, and stochastic local operations, which can convert any given genuine multipartite entangled pure state into one detected by this witness (though not always into the W state itself) with nonzero success probability, so verifying its entanglement as local operations

cannot create entanglement. Since applying an operation to the state is equivalent to applying the inverse operation to the witness, it is not necessary to physically perform these local operations. This gives a witness for any such state requiring only $k = n^2 - n + 1$ state copies per witness measurement, but its ΔW and hence the number of state copies required to actually detect entanglement using it are not given.

3.4 Conventional detection methods: state tomography

Quantum state tomography is the process of measuring the complete density matrix ρ of a quantum system; one can then attempt to determine mathematically whether ρ is entangled.

3.4.1 Linear inversion

The simplest way to carry out state tomography is to invert the linear expectation equations

$$\langle O_k \rangle_\rho = \mathrm{Tr}\,(O_k \rho) = \sum_{i,j=1}^{d^n} O_k^{(ij)} \rho_{ij}, 1 \leq k \leq (2d)^n, \tag{3.30}$$

where the O_k are any linearly independent observables. Treating ij as a single index, ρ as a vector and O as a $(2d)^n \times (2d)^n$ matrix [24], we can invert this to get

$$\rho_{ij} = \sum_{k=1}^{(2d)^n} O_{ij}^{-1(k)} \langle O_k \rangle_\rho. \tag{3.31}$$

Since a complete projective measurement has d^n outcomes, whose probabilities are observables with one constraint (adding up to 1), and one of the O_k can be taken to be 1 (enforcing $\mathrm{Tr}\,\rho = 1$), this process requires at least $((2d)^n - 1)/(d^n - 1) \approx d^n$ different measurement settings.

A simple choice of O_k for qubits are the multi-qubit Pauli operators

$$O_k = \bigotimes_{j=1}^{n} \sigma_{k_j,j}, \quad k_j = 0, x, y, z, \sigma_0 = \mathbb{I}. \tag{3.32}$$

These are orthonormal when treated as vectors ($\mathrm{Tr}\,O_i O_j = \delta_{ij}$), so $O^{-1} = O^T$ preserves vector lengths, and in particular does not turn small statistical errors in the measured $\langle O_k \rangle_\rho$ into large errors in the estimate of ρ [116]. They are also locally measurable, requiring a total of 3^n measurement settings (all possible combinations of Pauli x, y and z).

A disadvantage of the linear method is that the inevitable statistical errors in the measured $\langle O_k \rangle_\rho$ can cause its estimate of ρ to have negative eigenvalues, and hence not be an allowed density matrix. This happens with high probability (around 75% in 2 qubit experiments [24]) if the true ρ is pure or nearly pure, because of the large number of zero or small eigenvalues that can be made negative by a small error. The maximum likelihood method avoids this problem.

3.4.2 Maximum likelihood estimation

Likelihood is a statistical term for the probability of obtaining the same measurement results as were actually obtained, considered as a function of the unknown parameters (in the context of tomography, the quantum state ρ of

the system) of the probability distribution. *Maximum likelihood estimation* means using the parameter value (quantum state) that maximises the likelihood as an estimate of the true parameter value (state). This maximisation is done over allowed density matrices only, so cannot produce unphysical negative eigenvalues.

Considering a series $i = 1, \ldots, N$ of measurements given by the POVM operators P_{ij}, with results $j(i)$, the likelihood is [117]

$$L(\rho) = \prod_{i=1}^{N} \operatorname{Tr} \rho P_{i,j(i)}, \tag{3.33}$$

and the maximum likelihood estimate of ρ is the density matrix (positive, Hermitian, trace 1 matrix) that maximises $L(\rho)$.

Since Eq. (3.33) uses the POVM description of measurement, it can handle imperfect measurements; for example, a computational basis measurement of a qubit with probability p of an error giving the result 0 when the true state is $|\,1\rangle$ would be $P_{i0} = |\,0\rangle\langle 0\,| + p\,|\,1\rangle\langle 1\,|$, $P_{i1} = (1-p)\,|\,1\rangle\langle 1\,|$. This allows maximum likelihood tomography to use imperfect detectors, as long as the error probability is known and errors in different measurements are independent, and still converge to the true ρ (though typically more slowly) as the number of measurements $N \to \infty$.

The maximisation can be done by writing ρ in a form that forces it to be a physical density matrix, usually $\rho = T^\dagger T / \operatorname{Tr} T^\dagger T$ where T is a triangular complex matrix, and maximising $L(\rho(T))$ using a generic maximisation algorithm [24]. There are also tomography-specific maximisation algorithms, including the EMU algorithm [118], and the $R\rho R$ algorithm [119, 120, 121],

which is the iteration

$$\rho_{k+1} = \frac{R(\rho_k)\rho_k R(\rho_k)}{\mathrm{Tr}\, R(\rho_k)\rho_k R(\rho_k)}, \quad R(\rho_k) = \frac{1}{N}\sum_{i=1}^{N} \frac{P_{i,j(i)}}{\mathrm{Tr}\, \rho_k P_{i,j(i)}}, \tag{3.34}$$

normally started from the maximally mixed state $\rho_0 = \mathbb{I}/d^n$. The $R\rho R$ iteration is not guaranteed to converge [121], but in practice often converges faster than alternatives which are [121].

The advantage of state tomography is that it tells one everything about the state: not only whether it is entangled, but in exactly what way. The disadvantage is the exponentially large number of state copies needed (at least 2^n for n qubits), which makes it completely impractical to use for more than a few qubits.

Chapter 4

Purity-based entanglement detection

4.1 Ideal scheme

In this section we describe the ideal (error-free) operation of the entanglement detection scheme we will study, as introduced in [29].

4.1.1 Purity inequalities

Our network uses the purity inequalities of [30] for multipartite entanglement detection, as introduced in Sec. 3.2.5. These inequalities provide a set of necessary conditions for separability in multipartite states. Consider a state $\rho_{123\ldots n}$ of n subsystems. If $\rho_{123\ldots n}$ is separable, then the purities Tr $\{\rho_B^2\}$ of the reduced density operators ρ_B of subsets $B \subseteq \{1, 2, \ldots, n\}$ (which we call

the *reduced purities*) are non-increasing:

$$\mathrm{Tr}\left\{\rho_A^2\right\} \geq \mathrm{Tr}\left\{\rho_B^2\right\} \text{ for all } A \subseteq B. \tag{4.1}$$

We can use these inequalities to give a relation between the average purities of all reduced density operators of a given number k of subsystems defined by

$$\overline{\mathrm{Tr}\left\{\rho_{(k)}^2\right\}} = \left[\binom{n}{k}\right]^{-1} \sum_{|B|=k} \mathrm{Tr}\left\{\rho_B^2\right\}, \tag{4.2}$$

where B is summed over all combinations of k subsystems. For completeness we define $\overline{\mathrm{Tr}\left\{\rho_{(0)}^2\right\}} \equiv 1$. From Eq. (4.1) we find that for any separable state

$$\overline{\mathrm{Tr}\left\{\rho_{(k)}^2\right\}} \geq \overline{\mathrm{Tr}\left\{\rho_{(k')}^2\right\}} \text{ for all } k \leq k'. \tag{4.3}$$

Eq. (4.3) is weaker than Eq. (4.1), but we will see in Sec. 4.3 that $\overline{\mathrm{Tr}\left\{\rho_{(k)}^2\right\}}$ can be measured without spatial resolution, making it useful where this is not available.

Any state ρ that violates any of the inequalities Eqs. (4.1, 4.3) is entangled. If $\rho_{123\ldots n}$ is separable and pure, $\mathrm{Tr}\{\rho_{123\ldots n}^2\} = 1$ and all the above inequalities become equalities; since a state with all $\mathrm{Tr}\{\rho_B^2\} = 1$ is necessarily a product state, all pure entangled states violate Eqs. (4.1, 4.3). All pure entangled states can hence be detected by comparing $\mathrm{Tr}\{\rho_{123\ldots n}^2\}$ with any other $\mathrm{Tr}\{\rho_B^2\}$ or $\overline{\mathrm{Tr}\left\{\rho_{(k)}^2\right\}}$. This can be compared with (linear) entanglement witnesses, where different states often require different witnesses. From the Schmidt decomposition of any pure state into two disjunct subsystems A and B with $A \cup B = \{1, 2 \ldots n\}$, we find $\mathrm{Tr}\{\rho_A^2\} = \mathrm{Tr}\{\rho_B^2\}$ and hence

$\overline{\text{Tr}\left\{\rho_{(k)}^2\right\}} = \overline{\text{Tr}\left\{\rho_{(n-k)}^2\right\}}$ for all pure ρ.

Mixed entangled states do not always violate Eqs. (4.1, 4.3), but since Tr $\{\rho_B^2\}$ is continuous in ρ a sufficiently small amount of noise added to a pure entangled state will leave it still violating the inequalities. In the examples studied in this paper the noise level at which the inequalities no longer detect entanglement is a large fraction of the level at which entanglement ceases to be present. The permissible range of values for the purities of any state ρ is

$$2^{-k} \leq \text{Tr}\left\{\rho_B^2\right\} \leq 1 \quad \text{or} \quad 2^{-k} \leq \overline{\text{Tr}\left\{\rho_{(k)}^2\right\}} \leq 1, \tag{4.4}$$

where $k = |B|$. The minimum is attained by the maximally mixed state $\rho = 2^{-n}\mathbb{I}$ (with $\mathbb{I}$ the identity operator) and the maximum by any pure product state.

States which are locally equivalent have the same purities, which makes sense for an entanglement test as local unitaries cannot create or destroy entanglement.

This can be used to test for entanglement across a given partition as well as for any entanglement, because Tr $\{\rho_B^2\} <$ Tr $\{\rho_{A\cup B}^2\}$ always indicates that B is entangled with A, whatever other entanglement might also be present.

4.1.2 Pairwise beamsplitter

The reduced purities Tr $\{\rho_A^2\}$ are nonlinear functions of the density matrix ρ and hence not the expectation of any single copy observables. However, as noted in Sec. 3.2.6, they are linear functions of the two-copy density matrix $\rho \otimes \rho$ and hence the expectation of an observable on two copies, namely the

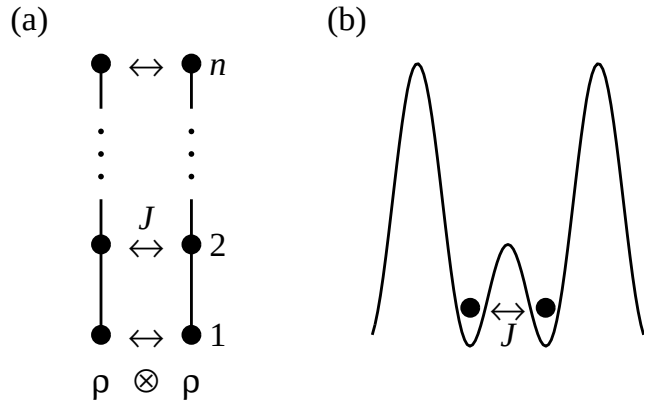


Figure 4.1: (a) Layout of qubits. The two rows I and II are prepared in two copies $\rho_{12...n} \otimes \rho_{12...n}$ of the state to be tested, then a beamsplitter is performed between corresponding pairs. (b) Superlattice potential.

swap operator V_A which swaps subsystems in the set A between the two copies:

$$\mathrm{Tr}\,(V_A \rho \otimes \rho) = \mathrm{Tr}\,(\rho_A^2). \tag{4.5}$$

V_A is the difference of the symmetric and antisymmetric projectors, $V_A = (\mathbb{I} + V_A)/2 - (\mathbb{I} - V_A)/2$. If the subsystems are identical bosonic qubits, these can be measured with a 50:50 beamsplitter between corresponding sites in the two copies (Fig. 4.1a). Consider first the case where A is a single qubit $\{j\}$. On applying the beamsplitter, symmetric states bunch, that is both qubits go into the same site, while antisymmetric states do not [29] (for details see Sec. 4.6). In photons this is called Hong-Ou-Mandel interference [122]. Two qubits in column j and in state $\rho_j \otimes \rho_j$ will thus end up in the same site (which we denote by +) or in different sites (-) with probabilities

$$P_{\pm}^{(j)} = \frac{1}{2}\mathrm{Tr}\,\{(\mathbb{I} \pm V_j)\rho_j \otimes \rho_j\} = \frac{1}{2} \pm \frac{1}{2}\mathrm{Tr}\,\left\{\rho_j^2\right\}. \tag{4.6}$$

Here $S_\pm = (\mathbb{I} \pm V_j)/2$ are the symmetric and antisymmetric projectors for site j. By distinguishing doubly occupied sites from singly occupied ones we can thus determine the purity of ρ_j. This has been used to measure the purity of photons [123].

For n qubits, the probability of a given combination of symmetric and antisymmetric projections is given by [29]

$$P_{\pm_1\pm_2\cdots\pm_n} = \mathrm{Tr}\left\{\prod_{i=1}^{n}\frac{\mathbb{I}\pm_i V_i}{2}\rho_{12\ldots n}\otimes\rho_{12\ldots n}\right\} \tag{4.7}$$

$$= \sum_{B\subset\{1,\ldots,n\}}\left(\prod_{i\in B}\pm_i\right)\mathrm{Tr}\left\{\rho_B^2\right\}, \tag{4.8}$$

where the second equality follows from expanding the product and using $V_B = \prod_{i\in B} V_i$ and Eq. (4.5). Inverting the linear equation Eq. (4.8), we find that

$$\mathrm{Tr}\left\{\rho_B^2\right\} = P(j_B \text{ even}) - P(j_B \text{ odd}) = 1 - 2P(j_B \text{ odd}), \tag{4.9}$$

which makes sense as a product of symmetric and/or antisymmetric states is symmetric overall if it contains an even number of antisymmetric states and antisymmetric if it contains an odd number.

Since this scheme does not require any interaction between the qubits, it will probably be easier to implement than the scheme of [124], which would require controlled-swap gates. It has been successfully implemented in photons for $n = 2$ [125].

4.1.3 Examples

We now apply the above method to two families of states, macroscopic superposition states and cluster-like states.

Macroscopic superposition states

Macroscopic superposition states $|\,\gamma_n\rangle$ defined by

$$|\,\gamma_n\rangle = \frac{|\,0\rangle^n + (\gamma\,|\,0\rangle + \sqrt{1-|\gamma|^2}\,|\,1\rangle)^n}{\sqrt{2+\gamma^n+\bar{\gamma}^n}}, \tag{4.10}$$

with a single complex parameter γ satisfying $|\gamma| \leq 1$ arise naturally in several systems such as BECs [126] and superconductors [127]. The quantity $n(1-|\gamma|^2)$ has been suggested as a measure of the effective size of the state, as in some respects $|\,\gamma_n\rangle$ is equivalent to a cat state of $n(1-|\gamma|^2)$ particles [128]. The purities of $|\,\gamma_n\rangle$ are given by

$$\text{Tr}\left\{\rho_B^2\right\} = \frac{2+2\gamma^k\bar{\gamma}^k+2\gamma^{n-k}\bar{\gamma}^{n-k}+4\gamma^n+4\bar{\gamma}^n+\gamma^{2n}+\bar{\gamma}^{2n}}{(2+\gamma^n+\bar{\gamma}^n)^2}, \tag{4.11}$$

where $k = |B|$. These purities violate Eq. (4.1), showing that $|\,\gamma_n\rangle$ is entangled, for all $|\gamma| < 1$ and measuring the purities allows determining γ. For $\gamma = 0$ the state $|\,\gamma_n\rangle$ is a cat state, which is pure ($\text{Tr}\left\{\rho^2\right\} = 1$) while all its subsets have purity $\text{Tr}\left\{\rho_B^2\right\} = 1/2$. Up to local unitaries it is the only state with these purities, so can be unequivocally identified by our test.

We demonstrate the effect of noise on our method by considering dephasing noise which is one of the dominant noise mechanisms in optical lattices. Other forms of noise, such as bit flip noise or depolarising noise, can be

treated similarly. We assume the dephasing noise to act independently on each qubit ρ_j mapping its state according to $\rho_j \to (1-d/2)\rho_j + (d/2)\sigma_z\rho_j\sigma_z$, where $0 \leq d \leq 1$ is the strength of the decoherence and $\sigma_{z,j}$ is a phase flip applied to qubit j. Thus a state ρ is transformed by the dephasing map according to

$$\rho \to \sum_A \left(1-\frac{d}{2}\right)^{n-|A|} \left(\frac{d}{2}\right)^{|A|} \left(\prod_{j\in A} \sigma_{z,j}\right) \rho \left(\prod_{j\in A} \sigma_{z,j}\right), \tag{4.12}$$

where A is the set of qubits which undergo a phase flip. Applying the map Eq. (4.12) to the cat state $|\,(\gamma=0)_n\rangle$ we find for the resulting density operator

$$\begin{aligned} \rho &= \frac{1}{2}\left(|\,0\rangle^n \langle 0\,|^n + |\,1\rangle^n \langle 1\,|^n\right) \\ &\quad + \frac{(1-d)^n}{2}\left(|\,0\rangle^n \langle 1\,|^n + |\,1\rangle^n \langle 0\,|^n\right), \end{aligned} \tag{4.13}$$

and thus $\mathrm{Tr}\,\{\rho^2\} = (1+(1-d)^{2n})/2$ while $\mathrm{Tr}\,\{\rho_B^2\} = 1/2$ for all subsets B. Therefore entanglement is detected whenever it is present. This is not generally the case as can easily be seen by looking at a Werner state $\rho = (1-d)\,|\,(\gamma=0)_n\rangle\,\langle(\gamma=0)_n\,| + 2^{-n}d\,\mathbb{I}$ for which entanglement is detected if $d < 1-(2^{n-1}+1)^{-1/2}$. However, e.g. in the case $n=2$ this state is entangled iff $d < 2/3$ [68], while our test works only for $d < 1-1/\sqrt{3}$.

Cluster-like states

Cluster and graph states are multipartite entangled states which form the basic building blocks of the one-way quantum computer [21]. We consider

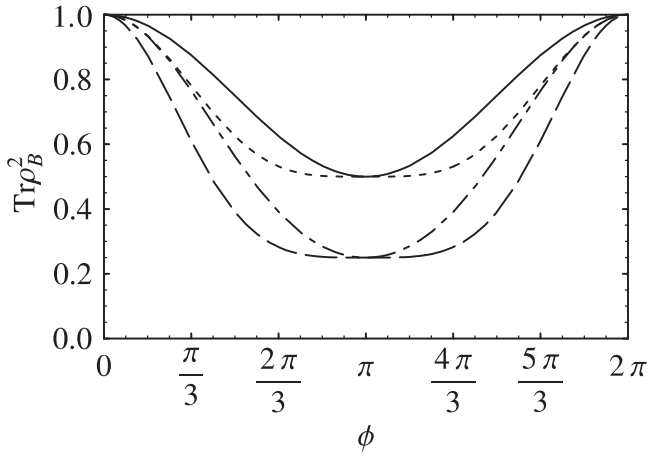


Figure 4.2: Effect of varying ϕ on Tr $\{\rho_B^2\}$ where B is any one atom not at an end (dotted), any two atoms not at ends and with at least two others between them (dashed), any two or more consecutive atoms not including an end (dash-dotted), any one or more consecutive atoms including one end (solid). These purities are independent of n. Examples of such subsets (for $n \geq 6$) are $B = \{2\}, \{2,5\}, \{2,3,4,5\}, \{1,2,3,4,5\}$ respectively. Since these are in increasing order, the state is entangled if the purities are not in decreasing order, that is for all ϕ except integer multiples of 2π.

cluster-like states $|\,\phi_n\rangle$ defined by

$$|\,\phi_n\rangle = \frac{1}{\sqrt{2^n}} \prod_{j=1}^{n} (|\,0\rangle_j \, e^{i\phi\sigma_{z,j+1}} + |\,1\rangle_j) = \frac{1}{\sqrt{2^n}} \sum_{x=0}^{2^n-1} e^{i\phi c(x)} \,|\,x\rangle\,, \qquad (4.14)$$

where $c(x)$ is the number of occurrences of the sequence 01 in the n-bit binary number x. These states have already been created in optical lattices [12] and represent a cluster state for $\phi = \pi$. Current methods for detecting them essentially perform a tomographic measurement of the average single particle density matrix, which goes from pure $(|\,0\rangle + |\,1\rangle)(\langle 0\,| + \langle 1\,|)/2$ at $\phi = 0$ to maximally mixed $\mathbb{I}/2$ at $\phi = \pi$ and back again at $\phi = 2\pi$. This method thus yields one measurement $\overline{\mathrm{Tr}\left\{\rho_{(1)}^2\right\}}$ relating to entanglement and two measurements relating to local unitaries.

Our network permits the measurement of further correlations and it does not need the assumption that all atoms have the same single particle density matrix. It therefore allows a better characterization of $|\phi_n\rangle$. For any ϕ which is not an integer multiple of 2π, $|\phi_n\rangle$ is a pure state with no separable subsystems, and hence for any subset B we have Tr $\{\rho_B^2\} < 1 =$ Tr $\{\rho^2\}$ as can be seen from Fig. 4.2. For creating the states $|\phi_n\rangle$ each qubit only needs to interact with their two nearest neighbours except for the two extremal atoms 1 and n which will interact with only their one neighbour [21, 12]. Because of this the reduced purity of a subset B is determined by the boundary between it and the rest of the system. Subsets of different sizes but with the same boundary structure have the same purity. Several examples of these purities are shown in Fig. 4.2 as a function of ϕ. For example, all sets of two or more adjacent atoms, located anywhere in the row that do not include either extremal atom have the same purity $(1 + \cos^2(\phi/2))^2/4$ (dash dotted curve in Fig. 4.2) which is independent of n. The degree of violation of Eq. (4.1) varies smoothly with ϕ and measuring the various different purities allows to determine ϕ (up to its sign).

4.2 Realisation in optical lattices

In this section we describe a possible realisation of the above scheme in an optical lattice.

We use the usual quantum computing lattice (Sec. 2.4), that is a 3D lattice sufficiently deep to be in the one atom per site Mott insulator state with negligible hopping, and using two hyperfine internal states of the atoms

as the qubit states [63]. We then create copies of the state $\rho_{12\ldots n}$ to be tested in adjacent rows (or planes) of the lattice (Fig. 4.1a), by any method that does not create correlations between different copies, for example cold controlled collisions for a 1D or 2D cluster state [12]. We denote the two copies between which we are to perform a beamsplitter by I and II, and denote the qubits within a state by 1 to n. We denote the creation operators by $(a_l^{(j)})^\dagger|\text{vac}\rangle \equiv |\,0\rangle_l^j$ and $(b_l^{(j)})^\dagger|\text{vac}\rangle \equiv |\,1\rangle_l^j$, where $l \in \{I, II\}$ labels the copy (x coordinate) and $j \in \{1, \ldots, n\}$ labels the qubit (y and/or z coordinate).

4.2.1 The pairwise beam splitters

The hopping term $-J_x(a_i^\dagger a_{i+1} + b_i^\dagger b_{i+1} + \text{h.c.})$ of the Bose Hubbard Hamiltonian is equivalent to a beamsplitter when applied for an appropriate time, and can easily be turned on by reducing the laser intensity and hence lattice depth in the x direction. However, this would produce a beamsplitter between every pair of adjacent rows: not only between our two copies I and II, but between them and the copies (or lack thereof) in the rows on either side.

To obtain the pairwise beamsplitter we need, we can use a period 2 superlattice [64], which lowers the barrier between rows I and II to permit hopping, while retaining the high barriers around the sides (Fig. 4.1b). This then gives the required hopping term H_{BS} with each site coupled to only one of its neighbours, corresponding to a pairwise beamsplitter. Some on-site repulsion U will remain, and the total Hamiltonian is hence $H = H_{\text{BS}} + H_U$,

where

$$
\begin{aligned}
H_{\mathrm{BS}} &= -J\sum_{j=1}^{n}(a_I^{(j)\dagger}a_{II}^{(j)} + b_I^{(j)\dagger}b_{II}^{(j)} + \mathrm{h.c.}), \qquad (4.15)\\
H_U &= \sum_{l=I,II}\sum_{j=1}^{N}\frac{U}{2}a_l^{(j)\dagger}a_l^{(j)\dagger}a_l^{(j)}a_l^{(j)} + \\
&\quad \frac{U}{2}b_l^{(j)\dagger}b_l^{(j)\dagger}b_l^{(j)}b_l^{(j)} + Ub_l^{(j)\dagger}b_l^{(j)}a_l^{(j)\dagger}a_l^{(j)},
\end{aligned}
$$

where J is the hopping matrix element and U is the onsite interaction energy. The ratio U/J can be varied by changing the intensity of the main lattice and/or superlattice lasers, which can be done much faster than the dynamical timescales $1/J,\ 1/U$.

The 50:50 pairwise beamsplitter is perfectly realised in the noninteracting limit $U = 0$ by applying H_{BS} for a time $t_{bs} = \pi/(4J)$ (for details see Appendix 4.6). However, in practice it is impossible either to control J perfectly accurately or to completely turn off the interaction U. The antisymmetric component never bunches as long as the potential remains symmetric, as bosonic symmetry forbids this, but the symmetric component can fail to bunch. The probability q_{bs} of this is given by

$$
q_{bs} \approx \frac{\pi^2}{8}\left(\frac{\delta J}{J}\right)^2 + \frac{1}{16}\left(\frac{U}{J}\right)^2, \qquad (4.16)
$$

where δJ is the error in J (for details see Appendix 4.6). If the fluctuations δJ occur from run to run rather than from site to site q_{bs} can be interpreted as a statistical random variable. We will discuss how to correct this error in Sec. 4.4.

4.2.2 Measuring the lattice site occupation

One way to distinguish singly from doubly occupied sites is to induce rapid two-atom loss using a Feshbach resonance [129], wait long enough for this to empty the doubly occupied sites, then count the remaining atoms.

A single Feshbach resonance will cause the loss of either $|\,aa\rangle$, $|\,ab\rangle + |\,ba\rangle$, or $|\,bb\rangle$. ($|\,ab\rangle - |\,ba\rangle$ is forbidden by bosonic symmetry.) Hence, in order to empty doubly-occupied sites in all three states, we can either turn on consecutively three separate Feshbach resonances, or change the internal state of the pairs of atoms during the loss process using an appropriate sequence of microwave or Raman laser pulses. Even if three resonances are experimentally accessible, the latter might yield better results as we can choose the resonance with the best ratio of two-atom to single-atom loss. To ensure equal loss probabilities for all initial doubly occupied states (which will be important when we later come to correcting for incomplete loss), and avoid the need for precise control, we can use a large number of pulses of random relative phase and approximate area $\pi/2$ each, at equal intervals.

Each initial state then spends 1/3 of the time in the resonant state, and the probability of failing to lose a pair of atoms occupying the same site is hence $q_l = \exp(-t_l/3\tau_d)$, where t_l is the total duration of the sequence and τ_d the two-atom loss time constant. This method will not be perfect since single particles are also lost from the system with some time constant τ_s and hence t_l cannot be chosen arbitrarily large. The probability of losing a single particle is $p_l = 1 - \exp(-t_l/\tau_s)$ where $\tau_s \gg \tau_d$. Both p_l and q_l are error probabilities, so the choice of t_l is a compromise between the two; their

sum $p_l + q_l$ is minimized by choosing $t_l = \ln(\tau_s/(3\tau_d))/(1/3\tau_d - 1/\tau_s)$. An experiment performed by Widera *et. al* [129] measured $\tau_d = 1.3$ms and no detectable loss of single atoms for resonance times up to 100ms. If we take $\tau_s = 500$ms the above gives $t_l = 19$ms and error probabilities of $q_l = 0.8\%$ and $p_l = 3.7\%$.

The interaction-difference phase that formed the main experiment of [129] is another possibility, but was designed for measuring interaction parameters and for our purpose would appear to add unnecessary complication.

Having done this, we then need to count the remaining atoms. Unambiguous entanglement detection requires single atom counting, using for example cavity enhanced emission [130], though we will see in the next section that it does not require any spatial resolution of the lattice sites. Rough estimates such as from a simple image are however sufficient for state parameter estimation (Sec. 4.5).

4.3 Entanglement detection without spatial resolution

We assume in this section that we can accurately count the total numbers of singly/doubly occupied sites but that we cannot know their locations. We show that this information is sufficient to measure $\overline{\text{Tr}\left\{\rho_{(k)}^2\right\}}$, and hence detect entanglement via violation of Eq. (4.3).

The probabilities $P(j)$ of measuring j singly occupied sites in one row ($2j$

single atoms in total) are given by

$$\begin{aligned} P(j) &= \sum_{|A|=j} \frac{1}{2^n} \sum_B (-1)^{|A\cap B|} \mathrm{Tr}\,\{\rho_B^2\} \\ &= \frac{1}{2^n} \sum_{k=0}^{n} \binom{n}{k} \overline{\mathrm{Tr}\,\left\{\rho_{(k)}^2\right\}} \sum_l \binom{k}{l} \binom{n-k}{j-l} (-1)^l, \end{aligned} \tag{4.17}$$

where the summation indices are $k = |B|$, $l = |A \cap B|$, $j = |A|$, and A is the set of singly occupied (antisymmetric) sites. We form the generating function

$$\begin{aligned} \sum_{j=0}^{n} x^j P(j) &= \frac{1}{2^n} \sum_{k=0}^{n} \binom{n}{k} \overline{\mathrm{Tr}\,\left\{\rho_{(k)}^2\right\}} (1-x)^k (1+x)^{n-k} \\ &= \left(\frac{1+x}{2}\right)^n \sum_{k=0}^{n} \binom{n}{k} \overline{\mathrm{Tr}\,\left\{\rho_{(k)}^2\right\}} \left(\frac{1-x}{1+x}\right)^k \end{aligned}$$

and let $y = (1-x)/(1+x)$, to obtain

$$\sum_{j=0}^{n} (1-y)^j (1+y)^{n-j} P(j) = \sum_{k=0}^{n} y^k \binom{n}{k} \overline{\mathrm{Tr}\,\left\{\rho_{(k)}^2\right\}}, \tag{4.18}$$

from which we find

$$\overline{\mathrm{Tr}\,\left\{\rho_{(k)}^2\right\}} = \left[\binom{n}{k}\right]^{-1} \sum_{j=0}^{n} P(j) \sum_l \binom{j}{l} \binom{n-j}{k-l} (-1)^l. \tag{4.19}$$

Therefore, although we cannot determine the purity of a given subset of the row of atoms, we can still determine average purities associated with subsets of atoms of a given size by measuring $P(j)$. We will prove later (see Eq. (4.26)) that the accuracy in finding $P(j)$ (and hence number of experimental runs) required for obtaining a given accuracy of $\overline{\mathrm{Tr}\,\left\{\rho_{(k)}^2\right\}}$ has

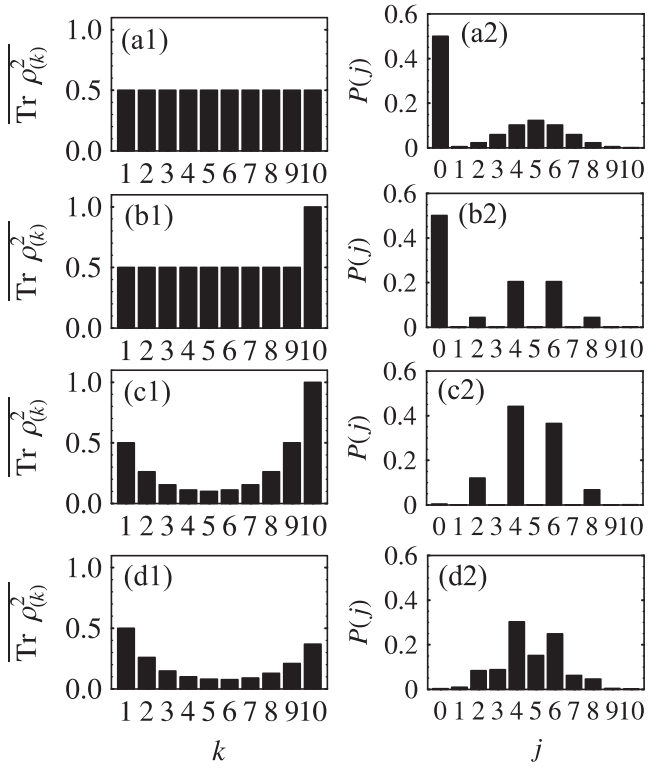


Figure 4.3: $\overline{\mathrm{Tr}\left\{\rho^2_{(k)}\right\}}$ against k (left) and $P(j)$ against j (right) for $n = 10$. (a) Classically correlated state $\rho = (|\,0\rangle^n \langle 0\,|^n + |\,1\rangle^n \langle 1\,|^n)/2$. (b) Cat state $|\,(\gamma = 0)_{10}\rangle$. (c) Cluster state $|\,(\phi = \pi)_{10}\rangle$. (d) Same as (c) with 10% dephasing decoherence.

an upper bound independent of n and k if no errors are present. The network is thus efficient in detecting the presence of entanglement in all pure (and some mixed) entangled states via the violation of Eq. (4.3). In comparison, state tomography and most entanglement witnesses do not work without spatial resolution.

In Fig. 4.3 we show the probabilities $P(j)$ and the resulting average purities for a variety of different states. For a classically correlated state shown in Fig. 4.3a the values of $\overline{\mathrm{Tr}\left\{\rho^2_{(k)}\right\}}$ are monotonically decreasing with k showing that Eq. (4.3) is not violated. The maximally entangled state shown in

Fig. 4.3b has the characteristic that $\overline{\text{Tr}\left\{\rho^2_{(k)}\right\}} = 1/2$ for $0 < k < n$ while $\overline{\text{Tr}\left\{\rho^2_{(n)}\right\}} = 1$ and thus the inequalities are violated in this case. The cluster state shown in Fig. 4.3c violates the inequalities for all $j > n/2$ and therefore its entanglement is detected. Finally, in Fig. 4.3d we show a noisy cluster state which was affected by phase noise acting independently on each atom [131]. It can clearly be seen that decoherence reduces the violation of the inequalities but that entanglement is detectable for small amounts of noise.

We will now study how the working of the network is affected by experimental errors. In particular we will estimate how many runs are necessary to obtain the probabilities $P(j)$ with sufficient accuracy in the presence of errors.

4.4 Effects of experimental error

The errors introduced in Sec. 4.2 affect the ability to find the purities $\text{Tr}\{\rho_B^2\}$ as well as the average purities $\overline{\text{Tr}\left\{\rho^2_{(k)}\right\}}$ associated with $\rho_{12\ldots n}$. All of these errors are of one of two mathematical kinds: extra *pairs* of atoms and missing *single* atoms. We call these two errors "beam-splitter" and "detector" error respectively. Their respective probabilities $q = q_{bs} + q_l$ and $p = p_d + p_l$ are understood to include also errors occurring while particles are lost from doubly occupied sites. The relationship Eq. (4.9) between the purities of ρ_B and the probabilities of an even/odd number j_B of singly occupied sites in B indicates that an experimental error, occurring with probability p per site, changes the result $\text{Tr}\{\rho_B^2\}$ by $O(|B|p)$ if we do not attempt to correct for it. This renders the measured results totally meaningless as soon as

$|B|p \sim 1$, because the purity of any given state ρ_B is smaller or equal to one. However certain types of error, including the BS and detector errors, can be corrected by a suitable modification of the formulas Eqs. (4.9, 4.19) yielding $\mathrm{Tr}\,\{\rho_B^2\}$ and $\overline{\mathrm{Tr}\left\{\rho_{(k)}^2\right\}}$. This correction eliminates systematic errors, making $\mathrm{Tr}\,\{\rho_B^2\}$ and $\overline{\mathrm{Tr}\left\{\rho_{(k)}^2\right\}}$ correct on average, but tends to amplify the random errors that are inevitable in measuring probabilities using a finite number of experimental runs. These random errors can in principle be made arbitrarily small for any $p, q < 1$ by increasing the number of runs, but in practice there is a limit because, as we will show, the number of runs required scales approximately exponentially in $|B|p$. We will now investigate the effects of these errors on the performance of the entanglement detection network both without and with spatial resolution.

4.4.1 Without spatial resolution

We assume the probabilities p and q to be the same for all $2n$ lattice sites and in the case of q for all symmetric atom pair states $|\,aa\rangle$, $|\,bb\rangle$ and $|\,ab\rangle + |\,ba\rangle$. Errors at different lattice sites are assumed to be uncorrelated as they are caused by random processes occurring at the level of individual atoms or same-site pairs.

Beam splitter error

Let $P_{\rm exp}(i)$ be the probability of detecting i atoms in an experimental run. If only BS errors are present this probability is given by

$$P_{\rm exp}(2i) = \sum_{j=0}^{i} P(j) \binom{n-j}{n-i} q^{i-j} (1-q)^{n-i}, \tag{4.20}$$

where the factor two in $P_{\rm exp}(2i)$ accounts for $P(j)$ being the probability of having j antisymmetric pairs. We can use generating functions to invert Eq. (4.20)

$$\sum_{i=0}^{n} x^i P_{\rm exp}(2i) = \sum_{j=0}^{n} P(j) x^j (1-q+xq)^{n-j}, \tag{4.21}$$

leading to

$$P(j) = \sum_{i=0}^{j} \binom{n-i}{n-j} \frac{(-q)^{j-i}}{(1-q)^{n-i}} P_{\rm exp}(2i). \tag{4.22}$$

We now apply Eq. (4.22) to a subsystem B and substitute this into Eq. (4.9), giving

$$\text{Tr}\left\{\rho_B^2\right\} = \sum_{i_B=0}^{k} \left(\frac{1+q}{1-q}\right)^{k-i_B} (-1)^{i_B} P_{\rm exp}(2i_B), \tag{4.23}$$

where i_B refers to the number of atoms detected in B. This expression is then averaged over all B of size $|B| = k$ to give

$$\overline{\text{Tr}\left\{\rho_{(k)}^2\right\}} = \sum_{i=0}^{n} A_{ki} P_{\rm exp}(2i), \tag{4.24}$$

with

$$A_{ki} = \left[\binom{n}{k}\right]^{-1} \sum_{l=0}^{k} (-1)^l \left(\frac{1+q}{1-q}\right)^{k-l} \binom{i}{l} \binom{n-i}{k-l}. \tag{4.25}$$

Hence, using Eq. (4.25) instead of Eq. (4.19) corrects all the *systematic*

error caused by an imperfect BS. We are still left with the inherent *random* error associated with the measurement of the probabilities $P_{\exp}(2i)$, which is reduced by increasing the number of experimental runs.

Because of this random error the estimate of $\overline{\mathrm{Tr}\left\{\rho_{(k)}^2\right\}}$ obtained from N experimental runs (each using one pair $\rho \otimes \rho$) has the correct mean but a nonzero standard deviation $\sqrt{V_k/N}$, where this defines $V_k(p,q,\rho)$; hence $O(V_k)$ runs are necessary for meaningful results. Note that in general $V_k > 0$ even when $p = q = 0$, as it includes the inherent quantum uncertainty as well as that added by experimental error. In the case of BS error

$$\begin{aligned} V_k &= \sum_i P_{\exp}(i) A_{ki}^2 - \left(\overline{\mathrm{Tr}\left\{\rho_{(k)}^2\right\}}\right)^2 < \max_i \left(A_{ki}^2\right) \\ &\leq \left(\frac{1+q}{1-q}\right)^{2k} \approx e^{4kq}, \end{aligned} \tag{4.26}$$

where the approximation is valid for $k \gg 1$, $q \ll 1$. The bound Eq. (4.26) proves that the number of runs required to obtain meaningful estimates of $\overline{\mathrm{Tr}\left\{\rho_{(k)}^2\right\}}$ is reasonable for $k \lesssim 1/q$, however large n is.

We numerically computed the worst case by maximizing V_k with respect to $\overline{\mathrm{Tr}\left\{\rho_{(k)}^2\right\}}$ subject only to Eq. (4.4) and compare it to cluster states $|\,(\phi = \pi)_n\rangle$ in Fig. 4.4. The results confirm the analytically found exponential increase of V_k with q in the worst case. For the cluster state V_k increases only slowly with q for small $k \leq 1/q$ while for $k \gtrsim 1/q$ we find approximately exponential growth of V_k with q. We also computed the variances for cat states and found that they are quite close to the worst case shown in Fig. 4.5a. Therefore one may in an experiment generally not expect the

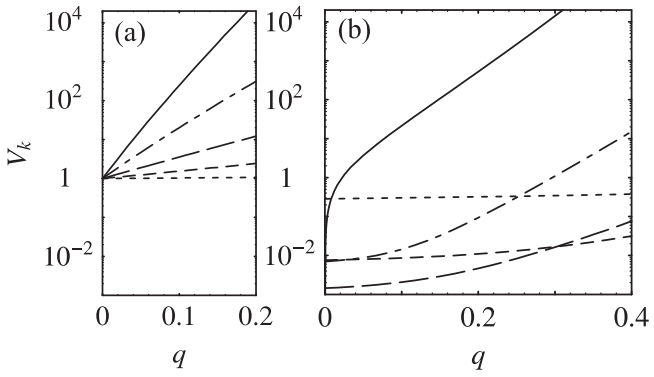


Figure 4.4: Variance V_k against BS error, for $k = 1$ (dotted), $k = 4$ (short dashed), $k = 7$ (long dashed), $k = 11$ (dash-dotted), $k = 15$ (solid) curve, and $n = 15$. (a) shows the result for the worst case and (b) for a cluster state.

variances V_k to be much smaller than our worst case results. Thus only BS errors up to $q = 1/k$ are acceptable and yield reliable results in a reasonable number of runs for all $0 \leq k \leq n$. However, as shown in Fig. 4.5 for $q = 1/k$, the average purities with $k \ll n$ will be determined much more accurately than those with $k \approx n$ and should thus be preferentially used for determining parameters characterizing the measured state.

We finally note that if J is fluctuating from run to run and q_{bs} hence becomes a random variable error correction is still possible. In this case we have to replace Eq. (4.20) by

$$P_{\exp}(2i) = \sum_{j=0}^{i} P(j) \binom{n-j}{n-i} \times \int \mathrm{d}J f(J) q(J)^{i-j} (1-q(J))^{n-i}, \tag{4.27}$$

where $f(J)$ is the probability density function of J and $q(J)$ denotes the BS error as a function of J. The resulting system of linear equations Eq. (4.27)

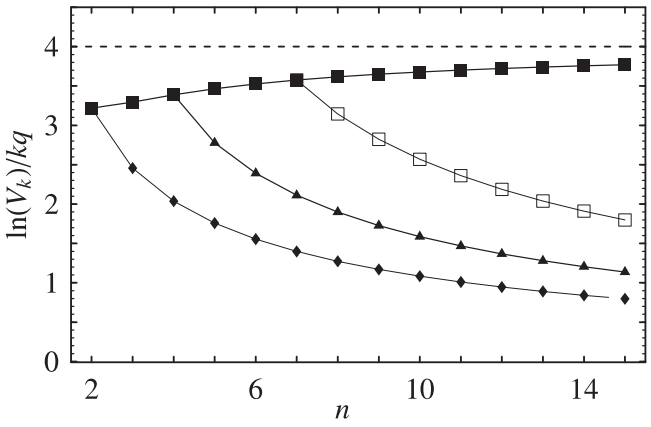


Figure 4.5: Worst case variance against n with BS error $q = 1/k$, for $k = 2$ (diamonds), $k = 4$ (triangles), $k = 7$ (hollow squares), $k = n$ (solid squares). The dotted horizontal line is the analytic bound $V_k \leq \exp(4kq)$. The solid curves are drawn to guide the eye.

can be treated using the methods introduced above.

Detector error

We now assume that only detector errors are present and each atom has a probability p of failing to be detected. In this case $P_{\text{exp}}(i)$ is related to $P(j)$ via

$$P_{\text{exp}}(i) = \sum_{j=i/2}^{n} P(j) \binom{2j}{i} p^{2j-i}(1-p)^{i}. \tag{4.28}$$

We can again solve this equation by methods similar to those used in Sec. 4.4.1, but this time it is not a true inverse because the system is over-determined: the observed number of atoms i can be either odd or even, but the true number $2j$ is always even. We obtain

$$P(j) = \sum_{i=2j}^{n} \binom{i}{2j} \frac{(-p)^{i-2j}}{(1-p)^{i}} P_{\text{exp}}(i), \tag{4.29}$$

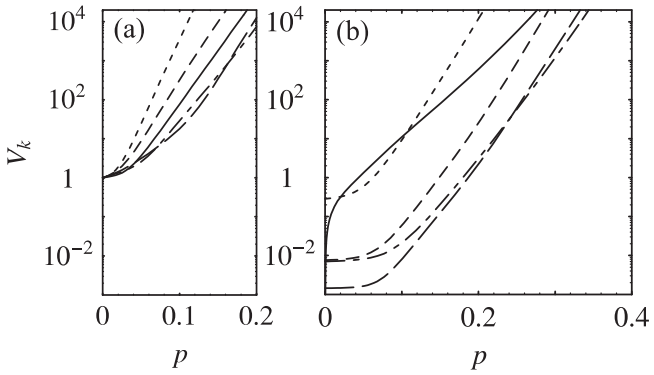


Figure 4.6: Variance against detection error without spatial resolution using Eq. (4.29), for $k = 1$ (dotted), $k = 4$ (short dashed), $k = 7$ (long dashed), $k = 11$ (dash-dotted), $k = 15$ (solid), and $n = 15$. (a) shows the result for the worst case and (b) for a cluster state.

where non-integer values of j are discarded. By combining Eqs. (4.19, 4.29) we obtain $\overline{\mathrm{Tr}\left\{\rho_{(k)}^2\right\}}$ in terms of $P_{\mathrm{exp}}(i)$. For the remaining random error measured by V_k we obtain the upper bound

$$V_k \leq \left(\frac{1+p}{1-p}\right)^{4n} \approx e^{8np}. \tag{4.30}$$

Numerical calculations for $n \leq 15$ confirm this exponential growth of V_k with np at $np \sim 1$. The results are shown in Fig. 4.6. This time, however, V_k is typically much smaller than the analytic bound, e.g. for the $n = 15$ cluster state, fitting $V_k \propto \exp(\beta np)$ gives $\beta \approx 2$. However, the exponential growth with n implies a practical limit of $n \sim 1/p$ for any k contrary to the case of BS errors.

This scaling can be improved by using the least squares method to handle the over-determined linear system of equations Eq. (4.28). We do not have an analytic bound analogous to Eq. (4.30) for the least squares method,

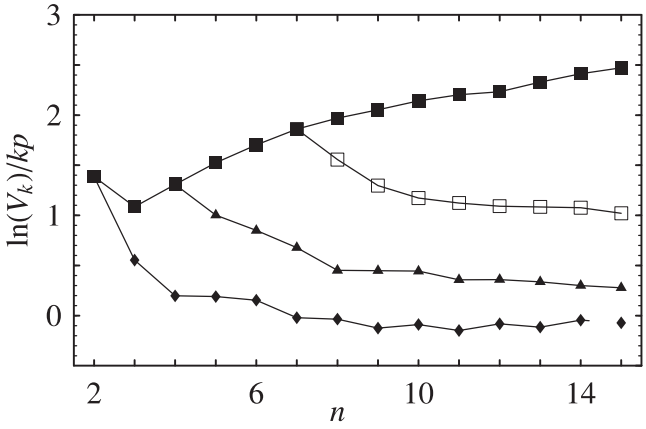


Figure 4.7: Worst case variance against n with detection error $p = 1/(2k)$ using least squares, for $k = 2$ (diamonds), $k = 4$ (triangles), $k = 7$ (hollow squares), $k = n$ (solid squares). The solid curves are drawn to guide the eye.

but numerical calculations for the cluster state and the worst case result in significantly lower values for V_k than those obtained from Eq. (4.29). Most importantly, as shown in Fig. 4.7, it appears that the scaling of V_k becomes exponential in kp, as in the case of BS errors, rather than np. This implies that an error of $p \lesssim 1/k$ is acceptable for obtaining meaningful estimates of $\overline{\mathrm{Tr}\left\{\rho_{(k)}^2\right\}}$ in a reasonable number of experimental runs.

In an actual experiment both BS and detector errors will be present, and first correcting for the detector error p using Eq. (4.29), then substituting the resulting $P(j)$ for $P_{\mathrm{exp}}(2j)$ in Eq. (4.25) to correct for the BS error q yields a combined analytical error bound of

$$V_k \leq \left(\frac{1+p}{1-p}\right)^{4n} \left(\frac{1+q}{1-q}\right)^{2k} \approx e^{8np+4kq}. \tag{4.31}$$

According to our numerical results using the least squares method this bound can be improved requiring only $p, q \lesssim 1/k$ for obtaining sufficiently small

errors.

4.4.2 With spatial resolution

If spatial resolution is available then Tr $\{\rho_B^2\}$, not just its average $\overline{\text{Tr}\left\{\rho_{(k)}^2\right\}}$ over all subsets B of size k, becomes accessible to measurement. This allows us to do some state characterizations which would otherwise be impossible and also introduces extra redundancy. As we will show below this does not affect the tolerance to BS errors but we will find that the detector error tolerance improves to $p^2 \sim 1/|B|$. Imperfections in the spatial resolution, however, will lead to additional errors in determining Tr $\{\rho_B^2\}$.

Beam splitter error

The variance of Tr $\{\rho_B^2\}$ due to BS errors can be directly inferred from Eq. (4.23), where only the atoms in B are counted. Using the same methods as in Sec. 4.4.1 we find an upper bound for V_B (defined analogously to V_k) given by $V_B \leq ((1+q)/(1-q))^{2|B|} \approx \exp(4|B|q)$. The BS error tolerance (for fixed $k = |B|$) is thus independent of whether spatial resolution is available or not.

Detector error

The situation is different for the detector error. Each antisymmetric pair contains two atoms only one of which needs to be detected to know that it was antisymmetric. Therefore the effective error probability becomes p^2.

The resulting formula is

$$\mathrm{Tr}\,\left\{\rho_B^2\right\} = \sum_{i=0}^{|B|}(-1)^i \left(\frac{1+p^2}{1-p^2}\right)^i P_{\mathrm{exp}}^B(i), \tag{4.32}$$

where $P_{\mathrm{exp}}^B(i)$ is the probability of measuring i antisymmetric sites in subset B. The variance bound is given by $V_B \leq ((1+p^2)/(1-p^2))^{2|B|} \approx \exp(4|B|p^2)$.

4.4.3 Imperfect spatial resolution

There is a new type of error to consider as the spatial resolution itself will not in practice be perfect. If we let $f(x, y)$ be the probability of finding at position x a particle which is actually at position y, then

$$P_{\mathrm{exp}}(A) = \sum_{i\in B}\sum_{\varsigma}\frac{1}{s(A)}\prod_{i=0}^{k} f(A_{\varsigma(i+k)}, B_i) f(A_{\varsigma(i)}, B_i) P(B), \tag{4.33}$$

where A is the "set" (its elements are not necessarily distinct) of observed atom positions, and $P_{\mathrm{exp}}(A)$ is the experimental probability of observing atoms exactly at these positions A. The set B denotes the antisymmetric sites and the probability of having antisymmetric sites at positions B is $P(B)$, $k = |B| = |A|/2$, and ς runs over all $(2k)!$ permutations of the $2k$ atoms in A. The i-th element of B and A are written as B_i and A_i, respectively. The symmetry factor $s(A)$ stands for the number of permutations ς which leave the ordered lists of atoms $\{A_i\}$ invariant (e.g., $s(\{1,1\}) = 2$, $s(\{1,2\}) = 1$), and is needed because our summation runs over different ordered lists $\{A_i\}$ of the same set A. This is an over-determined linear system, and just as in the case of detector error, we can either explicitly solve it by discarding some

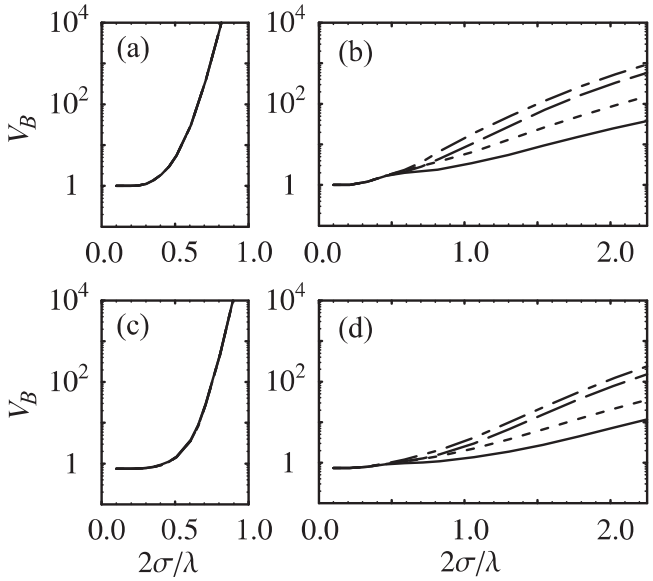


Figure 4.8: Variance of Tr $\{\rho_B^2\}$ as a function of the standard deviation σ, for $B = \{2\}$ (dotted), $B = \{2,3\}$ (dashed), $B = \{1,3\}$ (dash-dotted), $B = \{1,2,3\}$ (solid), and $n = 4$. (a) and (b) are worst case variances while (c) and (d) are for a cat state. (a) and (c) each show four almost coincident curves obtained from Eq. (4.34) while (b) and (d) are found by the least squares method.

of the equations or apply the least squares method. As an explicit solution we can e.g. use

$$P(B) = \sum_{\{A_i\}} \frac{s(A)}{2^k} \left(\prod_{i=1}^{2k} f^{-1}(B_i, A_i) \right) P_{\exp}(A), \tag{4.34}$$

where we define $B_{k+i} \equiv B_i$. The sum runs over all ordered lists $\{A_i\}$ and f^{-1} is the matrix inverse of f, that is $f^{-1}(y,x)f(x,z) = \delta_{xz}$.

As before by performing numerical calculations using the least squares method we find much lower variances than with Eq. (4.34). An example is shown in Fig. 4.8 where we plot the variance of Tr $\{\rho_B^2\}$ due to a Gaussian

position error of the form

$$f(x,y) = \frac{1}{\sqrt{2\pi}\sigma} \int_{x-\lambda/4}^{x+\lambda/4} \mathrm{d}z \exp[-(z-y)^2/(2\sigma^2)] \tag{4.35}$$

where σ is the standard deviation and λ is the wave length of the laser creating the optical lattice. The corresponding lattice spacing is $\lambda/2$. The results obtained from Eq. (4.34) shown in Fig. 4.8a, c require a resolution of $\sigma \lesssim \lambda/2$ whereas the least squares method shown in Fig. 4.8b, d yields reasonable variances V_B for spatial resolutions up to $\sigma \lesssim 3\lambda/2$. However, due to the exponentially large number of possibilities for A the least squares calculation becomes intractable for large n.

4.5 State parameter estimation

Because of the large number of particles typically present in an optical lattice, and the lack of spatial resolution to allow them to be divided into smaller groups, achieving the $1/p, 1/q \gtrsim k \sim n$ typically required for entanglement detection will probably be difficult. In this section we consider what can still be done with our scheme if this is not possible.

The n measurable quantities $\overline{\mathrm{Tr}\left\{\rho_{(k)}^2\right\}}$, $k = 1, \ldots, n$ do not provide us with enough information to determine an arbitrary state ρ. However, if it may be assumed that the state ρ is of a known form with less than n unknown parameters, it is often possible to determine these parameters from $\overline{\mathrm{Tr}\left\{\rho_{(k)}^2\right\}}$. In general this requires only as many $\overline{\mathrm{Tr}\left\{\rho_{(k)}^2\right\}}$ as there are parameters to be determined, making state parameter estimation possible when the noise

level is too high to reach the $k \sim n$ often required for entanglement detection without spatial resolution.

Even just $\overline{\mathrm{Tr}\left\{\rho_{(1)}^2\right\}}$, which requires only a crude atom number measurement with perhaps far from single atom resolution, is enough to estimate a single state parameter. Furthermore, if a collapse and revival of it is seen this is strong evidence of entanglement, though not an unambiguous detection as it assumes the decoherence is of a form that cannot increase purity (for example, dephasing or depolarising, but not spontaneous emission). This is similar to the tomographic measurement of $\overline{\rho_{(1)}}$ used in [12], but not equivalent to it: purity is nonlinear, so $\overline{\mathrm{Tr}\left\{\rho_{(1)}^2\right\}}$ and $\mathrm{Tr}\left\{\left(\overline{\rho_{(1)}}\right)^2\right\}$ are not the same thing. $\overline{\mathrm{Tr}\left\{\rho_{(1)}^2\right\}}$ works for any reversibly prepared entangled state, while $\mathrm{Tr}\left\{\left(\overline{\rho_{(1)}}\right)^2\right\}$ works only for states where each qubit has the same single qubit density matrix.

We demonstrate state parameter estimation by considering macroscopic superposition states $|\,\gamma_n\rangle$ and cluster-like states $|\,\phi_j\rangle$ introduced in Sec. 4.1.3. Finally, we will also look at product states of states of subsystems containing several atoms.

4.5.1 Macroscopic superposition states

Because the state $|\,\gamma_n\rangle$ is totally symmetric the individual purities given in Eq. (4.11) only depend on the size of the subsystem $k = |B|$ and thus $\overline{\mathrm{Tr}\left\{\rho_{(k)}^2\right\}} = \mathrm{Tr}\,\{\rho_B^2\}$. Hence, from the knowledge of $\overline{\mathrm{Tr}\left\{\rho_{(k)}^2\right\}}$ we can determine the value of γ which in principle only requires two of the purities. The remaining equations allow a partial check of the assumption that the

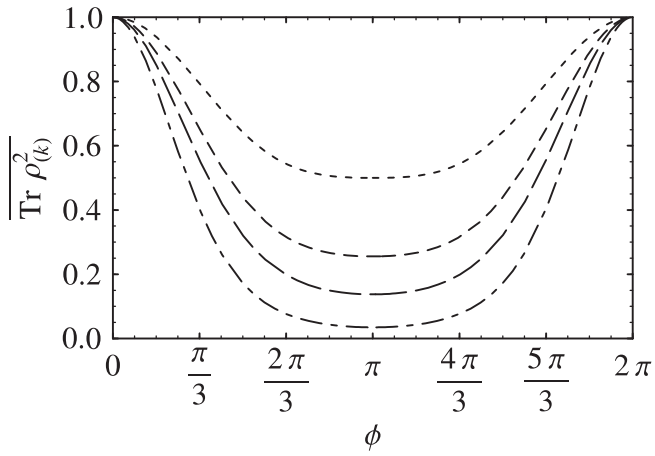


Figure 4.9: Average purities $\overline{\mathrm{Tr}\left\{\rho^2_{(k)}\right\}}$ ($k = 1$ dotted curve, $k = 2$ dashed curve, $k = 3$ dash-dotted curve, $k = 7$ solid curve) for the state $|\,\phi_{n=15}\rangle$. Since all states are pure we have $\overline{\mathrm{Tr}\left\{\rho^2_{(k)}\right\}} = \overline{\mathrm{Tr}\left\{\rho^2_{(n-k)}\right\}}$.

measured state indeed has the form $|\,\gamma_n\rangle$.

4.5.2 Cluster states

The states $|\,\phi_n\rangle$ are parameterized by the entangling phase ϕ. The average purities as a function of ϕ are depicted in Fig. 4.9. For any value of $0 < \phi < 2\pi$ the states violate the inequalities Eq. (4.3). The degree of violation increases with ϕ until $\phi = \pi$ where the state is a cluster state and the degree of violation is a maximum. If ϕ is increased further the state again approaches a product state and the degree of violation of the inequalities correspondingly decreases. Hence, from experimentally measured $\overline{\mathrm{Tr}\left\{\rho^2_{(k)}\right\}}$ one can determine the phase ϕ up to its sign. Again the over determined system (n equations for one unknown ϕ) provides a check on how well the state fits the assumed form $|\,\phi_n\rangle$.

The effect of dephasing according to the map Eq. (4.12) on a cluster

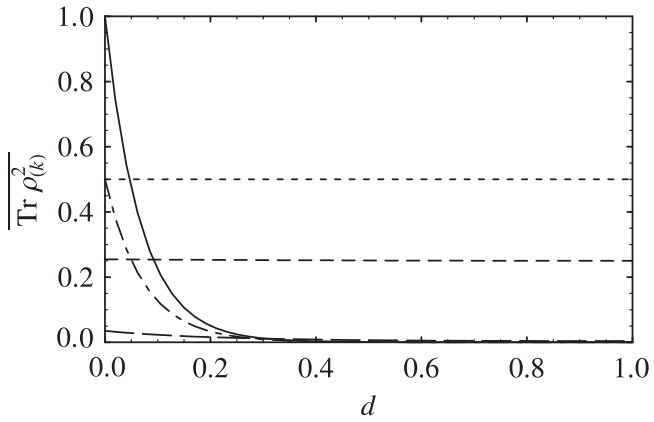


Figure 4.10: Effect of dephasing noise on the $n = 15$ cluster state, $k = 1$ (dotted), $k = 2$ (short dashed), $k = 8$ (long dashed), $k = 14$ (dash-dotted), $k = 15$ (solid).

state is shown in Fig. 4.10. The average purities decrease with increasing noise level d. Entanglement is certainly present and in principle detectable by our method as long as the $\overline{\mathrm{Tr}\left\{\rho^2_{(k)}\right\}}$ are not in descending order, in the case shown in Fig. 4.10 up to $d \approx 0.45$. Again, the parameter d can in principle be determined from measuring the average purities.

4.5.3 Products of entangled subsystem states

Finally we give an example of a class of states where even though ρ is characterized by more than n parameters, the associated average purities $\overline{\mathrm{Tr}\left\{\rho^2_{(k)}\right\}}$ only depend on n parameters. Consider the case where ρ is a product state of L subsystems, $\rho = \otimes_{i=1}^{L}\rho_i$, with each subsystem ρ_i composed of a known number n_i of atoms. In this case we have

$$\overline{\mathrm{Tr}\left\{\rho^2_{(k)}\right\}} = \sum_{\substack{\{k_1,\ldots,k_j\} \\ \sum_i k_i = k}} \prod_i \binom{n_i}{k_i} \overline{\mathrm{Tr}\left\{\rho^2_{i(k_i)}\right\}}. \tag{4.36}$$

Since there are $\sum_i n_i = n$ different $\overline{\mathrm{Tr}\left\{\rho^2_{i(k_i)}\right\}}$ in total, $\overline{\mathrm{Tr}\left\{\rho^2_{(k)}\right\}}$ provides us with enough information to determine the average purities $\overline{\mathrm{Tr}\left\{\rho^2_{i(k_i)}\right\}}$ of every subsystem.

If any of the $\overline{\mathrm{Tr}\left\{\rho^2_{i(k_i)}\right\}}$ so calculated are outside the allowed range $2^{-k_i} \leq \overline{\mathrm{Tr}\left\{\rho^2_{i(k_i)}\right\}} \leq 1$ then we can conclude that the state is not of the assumed form. In particular, with $L = n/2$ and all $n_i = 2$ this is a test for multi-particle as opposed to two-particle correlations in a given state. However, this test cannot distinguish multi-particle entanglement from multi-particle classical correlation plus two-particle entanglement, and hence is only an entanglement test if the state is pure.

4.6 Details of the beam splitter operation

Since the BS only couples two lattice sites in rows I and II of each column (see Fig. 4.1) we consider a single such pair and omit the column superscript j in this section. For $U = 0$, we obtain from the Heisenberg equations for the operators $\alpha = a, b$

$$\begin{aligned} \alpha_I(t) &= \cos(Jt)\alpha_I - i\sin(Jt)\alpha_{II}, \\ \alpha_{II}(t) &= \cos(Jt)\alpha_{II} - i\sin(Jt)\alpha_I. \end{aligned} \tag{4.37}$$

Hence, applying H_{BS} for a time $t_{bs} = \pi/(4J)$ implements a perfect pairwise BS.

Initially the atom pair is in a state of the form $\rho \otimes \rho$, where ρ is a single qubit state and hence has a spectral decomposition of the form $\rho =$

$\lambda_1 |\, c\rangle \langle c\,| + \lambda_2 |\, d\rangle \langle d\,|$, with $\lambda_1 + \lambda_2 = 1$, $|\, c\rangle = c^\dagger |\, \mathrm{vac}\rangle$, and $|\, d\rangle = d^\dagger |\, \mathrm{vac}\rangle$. Here $c^\dagger$, $d^\dagger$ are linear superpositions of $a^\dagger$, $b^\dagger$ with coefficients depending on ρ. Therefore we can write

$$\begin{aligned} \rho \otimes \rho &= \lambda_1^2 |\, c_I c_{II}\rangle \langle c_I c_{II}\,| + \lambda_2^2 |\, d_I d_{II}\rangle \langle d_I d_{II}\,| \\ &+ \frac{\lambda_1\lambda_2}{2}(|\, c_I d_{II}\rangle + |\, d_I c_{II}\rangle)(\langle c_I d_{II}\,| + \langle d_I c_{II}\,|) \\ &+ \frac{\lambda_1\lambda_2}{2}(|\, c_I d_{II}\rangle - |\, d_I c_{II}\rangle)(\langle c_I d_{II}\,| - \langle d_I c_{II}\,|), \end{aligned} \tag{4.38}$$

which is a classical mixture of a symmetric state with probability $P_+ = 1 - \lambda_1\lambda_2$ and an antisymmetric state with probability $P_- = \lambda_1\lambda_2$. After the BS the resulting state $\rho' = \exp(iH_{BS}t)\rho \otimes \rho \exp(-iH_{BS}t)$ is given by

$$\begin{aligned} \rho' &= \lambda_1^2 |\, \Phi_1\rangle \langle \Phi_1\,| + \lambda_2^2 |\, \Phi_2\rangle \langle \Phi_2\,| \\ &+ \lambda_1\lambda_2 |\, \Phi_3\rangle \langle \Phi_3\,| + \lambda_1\lambda_2 |\, \Phi_4\rangle \langle \Phi_4\,|, \end{aligned} \tag{4.39}$$

where $|\, \Phi_1\rangle = (c_I^\dagger c_I^\dagger + c_{II}^\dagger c_{II}^\dagger) |\, \mathrm{vac}\rangle /2$, $|\, \Phi_2\rangle = (d_I^\dagger d_I^\dagger + d_{II}^\dagger d_{II}^\dagger) |\, \mathrm{vac}\rangle /2$, $|\, \Phi_3\rangle = (c_I^\dagger d_I^\dagger + c_{II}^\dagger d_{II}^\dagger) |\, \mathrm{vac}\rangle /\sqrt{2}$ are states with double occupancy in one row and an empty site in the other row while $|\, \Phi_4\rangle = (c_I^\dagger d_{II}^\dagger - c_{II}^\dagger d_I^\dagger) |\, \mathrm{vac}\rangle /\sqrt{2}$ is a state with a singly occupied site in each row. Hence, after the BS we will find a doubly occupied site with probability $1 - \lambda_1\lambda_2 = P_+$ while two singly occupied sites result with probability $\lambda_1\lambda_2 = P_-$.

However, in practice it is impossible to completely turn off the interaction U which may result in a symmetric state failing to bunch. Let $|\, \Psi_s\rangle$ be any symmetric state. Because $H_{BS} + H_U$ acts only on the row indices, not the internal (qubit) states, and is symmetric between the two rows, the only

possible non-bunched outcome is $|\,\Psi_s\rangle$ itself, so the probability q_{bs} of failure to bunch is given by

$$\begin{aligned} q_{bs} &= |\,\langle\Psi_s\,|\,e^{i(H_{BS}+H_U)t}\,|\,\Psi_s\rangle\,|^2 \\ &= \frac{16J^2}{16J^2+U^2}\cos^2\left(\sqrt{16J^2+U^2}\frac{t_{bs}}{2}\right)+\frac{U^2}{16J^2+U^2}. \end{aligned} \tag{4.40}$$

The optimal choice for the BS time is $t_{bs}=\pi/\sqrt{16J^2+U^2}$ for which $q_{bs}=U^2/(16J^2+U^2)$. If the hopping term is not controlled perfectly accurately but fluctuates by δJ around a mean J we set $t_{bs}=\pi/\sqrt{16J^2+U^2}$ and obtain Eq. (4.16).

Chapter 5

Quantum Hall effect: review

In this chapter we review the fractional quantum Hall (FQH) effect, as observed for electrons in semiconductors, and as predicted for atoms in a rotating ultracold gas.

The fractional quantum Hall effect occurs in two-dimensional systems of interacting particles subjected to a strong perpendicular magnetic field, or a mathematical equivalent such as the Coriolis "force" from rotation, at simple rational values of the ratio of particles to flux quanta, $\nu \equiv \rho h/eB$ where ρ is the 2D number density and B the magnetic field strength. It has interparticle interaction as an essential component, which distinguishes it from the integer quantum Hall effect, which occurs at integer ν in fermions. Its ground state is strongly correlated, with an energy gap to its excitations, which have fractional particle number and fractional (anyonic) statistics. It is observed as plateaus in the Hall (transverse) conductivity, with quantised values $\nu e^2/h$, with the longitudinal conductivity simultaneously vanishing.

5.1 Physical realisations

5.1.1 Semiconductor system

The first [132], and so far the only, system in which the FQH effect has been experimentally observed is the depletion layer at a semiconductor surface, usually a GaAs/AlGaAs junction. The difference in Fermi energy between the two materials creates a narrow potential well at the surface, which makes the electron system effectively 2 dimensional as the quantum of excitation energy in the third dimension is much larger than the typical energy scale.

While this system has a crystal lattice, the lattice spacing is ~ 100 times smaller than the magnetic length scale $1/\sqrt{eB}$ on which the quantum Hall physics takes place, so a continuum description using the effective mass is adequate (this is considered more rigourously in [133]). In this approximation its Hamiltonian is (in $\hbar = 1$ units)

$$\begin{aligned} H = \int dxdy - \frac{1}{2m}\psi^\dagger(x,y)\left\{\left(-i\frac{\partial}{\partial x} - 2eBy\right)^2 + \frac{\partial^2}{\partial y^2}\right\}\psi(x,y) \\ +\psi^\dagger(x,y)(-eEy + V_{\text{noise}}(x,y))\psi(x,y) \\ + \int dXdY\psi^\dagger(x,y)\psi^\dagger(X,Y)\frac{e^2}{4\pi\epsilon r}\psi(x,y)\psi(X,Y), \end{aligned} \quad (5.1)$$

where $r = \sqrt{(X-x)^2 + (Y-y)^2}$, ψ is the electron field operator, the magnetic field is B along the z axis and the electric field E along the y axis. As with any electromagnetic system, we have a choice of gauge; we here use Landau gauge, which is convenient for current flow along the x axis as it makes the x translation symmetry explicit. m is the effective electron mass,

ϵ the permittivity of the semiconductor, and V_{noise} is a random noise term arising from the inevitable impurities and other imperfections in the crystal.

5.1.2 Rotating gas system

The fractional quantum Hall effect theoretically also occurs in a rotating ultracold atomic gas [58, 134], which has the Hamiltonian (also in $\hbar = 1$ units)

$$\begin{aligned} H &= \int dxdydz - \frac{1}{2m}\psi^\dagger(x,y,z)\left\{\left(-i\frac{\partial}{\partial x} - m\Omega_{\text{rot}}y\right)^2\right. \\ &\left. + \left(-i\frac{\partial}{\partial y} + m\Omega_{\text{rot}}x\right)^2 + \frac{\partial^2}{\partial z^2}\right\}\psi(x,y,z) \\ &+\psi^\dagger(x,y,z)\frac{1}{2}m\{(\omega_r^2 - \Omega_{\text{rot}}^2)(x^2+y^2) + \omega_z^2 z^2\}\psi(x,y,z) \\ &+g\psi^\dagger(x,y,z)\psi^\dagger(x,y,z)\psi(x,y,z)\psi(x,y,z), \end{aligned} \tag{5.2}$$

where $\psi(x,y,z)$ is the atomic field operator, Ω_{rot} the angular speed of rotation, ω_r and ω_z the radial and axial harmonic trapping frequencies, m the atomic mass and g the contact interaction strength. We here use symmetric gauge, which is convenient for an isotropic trap as it makes the rotational symmetry explicit, but here too we are free to change the gauge.

The Coriolis terms are equivalent to a magnetic field, as can be seen by substituting $m\Omega_{\text{rot}} = eB$. However, the rotation also produces a centrifugal term $-m\Omega_{\text{rot}}^2(x^2+y^2)/2$, which makes the net trapping frequency $\omega = \sqrt{\omega_r^2 - \Omega_{\text{rot}}^2}$ rather than ω_r. Lowering the density into the FQH regime $\nu \sim 1$ requires high ratios $\Omega_{\text{rot}}/\omega$, and hence precise balancing of Ω_{rot} and ω_r. The experiments [134] did not have such precise control available, and

hence were only able to reach the vortex lattice regime $1 \ll \nu \ll N$ (where N is the number of particles), and not the FQH regime. (The extra quartic potential used in some experiments [134] helps in that it prevents the atoms from escaping should ω^2 become negative, but does not remove the need for precise balancing of $\Omega_{\rm rot}$ and ω_r.)

The 2D confinement is also relatively weak in this system, with the third dimension not necessarily completely frozen out [134].

5.2 Single particle states: Landau levels

In this section, we solve the FQH Hamiltonian for the case of a single particle, obtaining the massively degenerate Landau levels. We consider

$$\begin{aligned} H &= \int dxdy - \frac{1}{2m}\psi^\dagger(x,y)\left\{\left(-i\frac{\partial}{\partial x} - 2m\Omega y\right)^2 + \frac{\partial^2}{\partial y^2}\right\}\psi(x,y) \\ &\quad + \psi^\dagger(x,y)\left(\frac{1}{2}m\omega^2 y^2 - eEy\right)\psi(x,y), \end{aligned} \tag{5.3}$$

that is an external potential with a linear part $-eEy$ (uniform electric field E for the electron system, acceleration or field gradient [44] for the rotating gas system) and/or a harmonic part of frequency ω in the y direction only, in Landau gauge with $\Omega = eB/m$ or $\Omega_{\rm rot}$.

This has x translation invariance, so consider wavefunctions of definite x momentum $\phi \propto e^{iKx}$:

$$H\phi = \frac{1}{2m}\left((K - 2m\Omega y)^2\phi - \frac{\partial^2\phi}{\partial y^2}\right) + \frac{1}{2}m\omega^2 y^2\phi - eEy\phi$$

$$= -\frac{1}{2m}\frac{\partial^2\phi}{\partial y^2} + \frac{1}{2}m\Omega_{\rm eff}^2(y-y_c)^2\phi + \left(\frac{K^2}{2m} - \frac{1}{2}m\Omega_{\rm eff}^2 y_c^2\right)\phi. \quad (5.4)$$

The first two terms form a harmonic oscillator of frequency $\Omega_{\rm eff} \equiv (4\Omega^2 + \omega^2)^{1/2}$ and centre $y_c \equiv (2K\Omega + eE)/m\Omega_{\rm eff}^2$, while the rest is (at fixed K) constant, so the energies are

$$E_n = \left(n+\frac{1}{2}\right)\Omega_{\rm eff} + \frac{K^2}{2m} - \frac{1}{2}m\Omega_{\rm eff}^2 y_c^2 = \left(n+\frac{1}{2}\right)\Omega_{\rm eff} + \frac{K^2\omega^2 - 4K\Omega eE - e^2E^2}{8m\Omega^2 + 2m\omega^2}, \quad (5.5)$$

where $n \geq 0$ is the oscillator level, called a Landau level [34].

The states within a Landau level are hence degenerate in the absence of trapping and electric field ($\omega = E = 0$), and nearly degenerate when these are weak compared to the magnetic field ($\omega, (e^2E^2/m)^{1/3} \ll \Omega$). This massive degeneracy allows strongly correlated states to form even if the interaction is weak compared to Ω; we will consider the nature of these states in the next section.

In a system of length L with periodic boundary conditions, the allowed K values are integer multiples of $2\pi/L$, so the spacing between state centres $y_c = K/2m\Omega$ is $\pi/m\Omega L$ and the number of states per Landau level per unit area is $m\Omega/\pi$. The filling factor $\nu \equiv \rho\pi/m\Omega$ is hence also the ratio of particles to states per Landau level. For fermions, when all states of a Landau level are occupied there is an energy gap Ω to the next Landau level, the *integer quantum Hall* gap. (For electrons, because of the two spin

states, $\nu = 2, 4, 6, \ldots$ are full Landau levels with single particle gap Ω, while $\nu = 1, 3, 5, \ldots$ fill only one spin state so their single particle gap is the Zeeman splitting, which in GaAs is considerably smaller.) For bosons, there is no limit to the number in the lowest Landau level and hence no integer quantum Hall effect, though occupation of higher levels can occur if the interaction is strong enough to make it energetically more favourable than putting more particles in the lowest level.

The expected x velocity of these states is

$$\langle v_x \rangle = \langle -i\frac{1}{m}\frac{\partial}{\partial x} - 2\Omega y \rangle = \frac{K}{m} - 2\Omega y_c = \frac{K\omega^2 - 2eE\Omega}{m(4\Omega^2 + \omega^2)}, \tag{5.6}$$

which in the $\omega = E = 0$ case is zero for all K: while these states have nonzero x wavevector K, they are not moving. With an electric field E only, it is equal to $-eE/2m\Omega$ for all K, giving the Hall current $I_x = \rho e^2 EW/2m\Omega = \nu e^2 V_y/2\pi$ (where W is the width of the sample and $V_y = EW$ the Hall voltage) and Hall conductance $I_x/V_y = \nu e^2/2\pi$. Note that in a disorder-free system this is true for all values of ν, and is exact even in the presence of interaction because the electric field is zero in a reference frame moving with this velocity [34]; the observed Hall plateaus *require* disorder.

With the harmonic trap present,

$$\begin{aligned} \frac{1}{2m\Omega}\frac{\partial}{\partial y}\left(\frac{1}{2}m\omega^2 y^2 - eEy\right)\Big|_{y=y_c} &= \frac{1}{2m\Omega}\left(m\omega^2\frac{2K\Omega + eE}{m\Omega_{\text{eff}}^2} - eE\right) \\ &= \frac{1}{2m\Omega}\frac{2K\omega^2\Omega - 4eE\Omega^2}{\Omega_{\text{eff}}^2} \\ &= \langle v_x \rangle, \end{aligned} \tag{5.7}$$

that is the local velocity is proportional to the local electric field, with the same constant of proportionality as for a uniform field. This is in fact approximately the case for general slowly varying potentials [34, 133], with the states lying along equipotentials. Exact solution is also possible for an isotropic harmonic trap $\frac{1}{2}m\omega^2(x^2+y^2)$, most easily in symmetric gauge; in this case each state has definite angular momentum and is peaked along a circular equipotential.

5.3 Many-particle states

The general form of an N particle lowest Landau level state in symmetric gauge is [34]

$$\phi(z_1,\ldots,z_N) = f(z_1,\ldots,z_N)\exp\left(-\sum_i |z_i|^2/4\right), \tag{5.8}$$

where f is any totally antisymmetric (fermions) or symmetric (bosons) analytic function of the dimensionless particle positions $z_j = 2(x_j+iy_j)/r_0$ and $r_0 = (m\Omega)^{-1/2}$. In the absence of interaction and external potential, all these states are degenerate; if these are present but weak compared to Ω, it is reasonable to approximate the ground state by minimising their energy within the lowest Landau level. We will now consider some states which attempt to do this.

5.3.1 Laughlin states

Inserting $(z_i - z_j)$ factors in f prevents those pairs of particles from coming together, reducing their interaction energy. The simplest way to satisfy (anti)symmetry is to have a single term containing M such factors for every pair of atoms,

$$\phi_L(z_1, \ldots, z_N) = \prod_{i>j} (z_i - z_j)^M \exp\left(-\sum_i \frac{|z_i|^2}{4}\right), \tag{5.9}$$

where M must be odd for fermions and even for bosons. These are called the *Laughlin states* [135]. For contact interaction this state has exactly zero interaction energy for any $M > 0$, so $M = 2, 4, 6, \ldots$ are all degenerate *exact* ground states for bosons in the absence of a trap, and the presence of any trap, however weak, will favour $M = 2$ over the less dense higher M. For Coulomb interaction it is not an exact eigenstate, but $M = 3$ and $M = 5$ are very close to the numerically calculated ground states of small systems.

To determine the physical properties of this state, we use the *plasma analogy* [34]: defining

$$\beta H_{\rm cl} \equiv -\log|\phi_L|^2 = -\sum_{i>j} 2M \log|z_i - z_j| + \frac{1}{2}\sum_i |z_i|^2, \tag{5.10}$$

the probability distribution (including all correlations) $|\phi_L|^2$ of the particle positions in a Laughlin state is the same as the probability distribution $e^{-\beta H_{\rm cl}}$ in thermal equilibrium of the classical system described by the Hamiltonian $H_{\rm cl}$, which is a 2D one component plasma with 2D Coulomb interactions and a uniformly charged background. This plasma had previously been the-

oretically studied; like a normal plasma it seeks to be electrically neutral, which makes the density of the Laughlin state a uniform $\nu = 1/M$, and in the relevant parameter regime it is not crystalline, so neither is the Laughlin state.

The Laughlin state is a liquid: its density is fixed but its shape can change. ϕ_L is circular; multiplying by $\exp\{\sum_i f(z_i)\}$, where $f(z)$ is any analytic function, gives it the shape of a contour of $f(z)+|z|^2/4$. For contact interaction, only the trap potential energy depends on the shape, so the ground state shape will follow a contour of the trap.

The Laughlin state can also be adapted to topologies other than the disk; edgeless topologies such as the sphere or torus, while impractical to physically implement (impossible in the semiconductor system, as they require magnetic monopoles), are useful for numerical studies [136, 137] as the absence of edges reduces some finite size effects. The Laughlin state on a sphere is [136]

$$\phi_{L,\mathrm{sph}}(z_1,\ldots,z_N) = \prod_{i>j}(z_i - z_j)^M \prod_{i=1}^{N}\left(1 - \frac{|z_i|^2}{4R^2}\right)^{-(1+N_\phi/2)}, \qquad (5.11)$$

where R is the radius of the sphere, the z_i are stereographic projection coordinates ($|z_i| = 2R$ at the equator), and $N_\phi = M(N-1)$ is the number of magnetic flux quanta.

5.3.2 Read-Rezayi states

If the number N of atoms in a trapped rotating gas is increased while keeping the trap strength fixed, at some point the Laughlin state must cease to be the ground state, as the trap potential energy cost of adding a particle to the

edge of the Laughlin state will eventually exceed the interaction energy cost of adding it "on top of" the Laughlin state in the centre of the trap. The N at which this happens can be estimated by comparing the approximate energy cost $N\omega^2/\Omega$ to add another particle to the Laughlin state and the approximate energy cost $um\Omega/\pi$ to add the particle in the single-particle ground state. This gives $N \lesssim um\Omega^2/\pi\omega^2$ if the Laughlin state is to be the ground state. Above this value of N, denser states are more energetically favourable than the Laughlin state.

The density can be increased above $\nu = 1/2$ either by using the next Landau level (costing kinetic energy 2Ω per particle) or by allowing particles to come together (costing interaction energy $\sim um\Omega$ per particle); if the interaction is weak ($um \ll 1$) the latter is more energetically favourable. It is believed [138] that there is then a series of incompressible states with half-integer filling factors $\nu = 1, 3/2, 2, \ldots$ reasonably approximated by the Read-Rezayi (RR) states [136]. For weak traps and large N the local density approximation can be made, leading to a stepped density profile including several such states [138], analogous to the Mott insulator density profile.

The RR state of filling factor $\nu = k/2$ is the symmetrized product of k $M = 2$ Laughlin states [139],

$$\phi_{\mathrm{RR}}(z_1, \ldots, z_N) = \mathrm{Symm}\left(\prod_{i>j}\prod_{l=1}^{k}(z_{ki+l} - z_{kj+l})^2\right)\exp\left(-\sum_m \frac{|z_m|^2}{4}\right), \tag{5.12}$$

where $i, j = 0, \ldots, N/k - 1$ and Symm denotes bosonic symmetrization, but

can also be written as [136]

$$\phi_{\mathrm{RR}}(z_1,\ldots,z_N) = \mathrm{Symm}\left(\prod_{i>j}\prod_{l=1}^{k}(z_{ki+l}-z_{kj+l})(z_{ki+l}-z_{kj+(l+_k1)})\right) \times \exp\left(-\sum_m \frac{|z_m|^2}{4}\right), \tag{5.13}$$

where $l+_k1$ wraps around modulo k ($k+_k1=1$), which divides the particles into clusters of size k, with i,j labelling the clusters and k the particles within a cluster, with no restriction on particles from the same cluster coming together. $k=1$ is the Laughlin state.

These wave functions allow up to k particles to come together at a point, but become zero if $k+1$ particles do so. They are also the densest states that do this, so are the exact zero energy ground states of $k+1$ body contact interactions [136]. Implementing such 3- and 4-body interactions may be possible using Feshbach molecules [140], but this is beyond the scope of this thesis; we consider the RR states only as approximate eigenstates of 2-body interactions.

There are also fermionic RR states given by $\prod_{i>j}(z_i-z_j)\phi_{\mathrm{RR}}(z_1,\ldots,z_N)$ at $\nu=k/(k+2)=1/2,3/5,\ldots$ [136], and the $\nu=5/2,12/5$ states observed in the FQH of electrons are conjectured to be such states of holes in the second Landau level [136, 33, 39]. The $k=2$ RR state is also called the Pfaffian or Moore-Read state.

5.3.3 Vortex lattice state

At even higher filling factors, bosons can form a condensate within the lowest Landau level

$$\phi(z_1, \ldots, z_N) = \prod_{i=1}^{N} \prod_{j=1}^{N_V} (z_i - w_j) \exp\left(- \sum_i |z_i|^2/4 \right), \qquad (5.14)$$

with N_V vortices at the positions w_j. This is gapless and compressible, and can have any ν, so is not an FQH state; it is called a mean field quantum Hall state. In the absence of trapping the energy is minimised by placing the vortices in a triangular (Abrikosov) lattice; in a trap this lattice is slightly distorted to more closely match the density profile to the trap [141]. The transition from Read-Rezayi states to vortex lattice had been thought to happen at $\nu \approx 6$ [138], but a recent numerical study [137] suggests it may happen for ν as low as 2.

5.3.4 Two component states

We now consider FQH states where the particles occupy two distinct internal states. In the case of electrons, while it is possible to use the two spin states [142], this is often energetically unfavourable because of the Zeeman energy splitting and the ferromagnetic interaction between spins. Bilayer devices (two close but separate quantum Hall layers) offer more control [35]. In the rotating gas system, two hyperfine states could be used.

The analogue of the Laughlin state is the mnr state [143],

$$\phi_{mnr}(\{z_i\},\{w_i\}) = \left(\prod_{i>j}(z_i-z_j)^m(w_i-w_j)^n\right)\left(\prod_{i,j}(z_i-w_j)^r\right) \times \exp\left(-\sum_i \frac{|z_i|^2+|w_i|^2}{4}\right), \quad (5.15)$$

where there are N_1 particles in one internal state at positions z_i, and N_2 in the other at positions w_i. The exponents m and n must be even for bosons or odd for fermions, but there is no symmetry restriction on r, because the two internal states are distinguishable. In particular, the 221 state is an allowed state for bosons, and is the densest (total $\nu = 2/3$) with zero contact interaction energy.

The analogue of the Read-Rezayi state is the non-Abelian spin singlet (NASS) state [144], which for bosons is similarly constructed by taking symmetrized products of 221 states.

The vortex lattice state has two types of vortices, one for each internal state, and the shape of the lattice cell depends on the ratio of interspecies to intraspecies interaction strength [145, 146].

5.4 Anyonic excitations and topological computation

In this section we describe the anyonic excitations of fractional quantum Hall states, and their potential usefulness for quantum computation.

Anyons are defined as particles whose exchange statistics are neither

bosonic nor fermionic. Any phase factor $\psi(x_1, x_2) \rightarrow e^{\pi i s}\psi(x_2, x_1)$ on interchange satisfies the requirement that interchange of identical particles not alter probabilities. In 3D two successive interchanges give the identity operation so $s = 0$ (bosons) or 1 (fermions), but there is no such restriction in 2D because interchanges there have a well-defined sense (clockwise or anticlockwise) and only two interchanges of opposite sense have to equal the identity. Two interchanges in the same sense are equivalent to taking one particle in a loop around the other, which is a topologically nontrivial operation in 2D. Particles with $s \neq 0, \pi$ are hence allowed in 2D, and are called *Abelian anyons* of statistics s [31].

In systems with multiple degenerate states for given particle positions, such as the excitations of Read-Rezayi states [147], there is an even more exotic possibility: the exchange operator may act as a non-trivial matrix on these states. Such particles are called *non-Abelian anyons*. In some cases, including the Fibonacci anyon [41], these exchange (braiding) matrices form a computationally universal gate set. This allows these systems to be used for universal *topological quantum computation*, where gates are performed by moving anyons around each other [32, 31]. The exchange matrices depend only on the topology of the path and not its actual shape, and the states are a global topological property of the set of anyons that cannot be distinguished by measuring each anyon separately so are immune to local decoherence [32], so this form of quantum computation could be practically error-free if the computational anyons are kept well apart and the temperature is low compared to the anyon pair production gap [33].

The elementary excitations of a $\nu = 1/M$ Laughlin state are quasiholes

[34], given by

$$\phi_{\mathrm{L,qh}}(z_1,\ldots,z_N)=\prod_i(z_i-w)\prod_{i>j}(z_i-z_j)^M\exp\left(-\sum_i\frac{|z_i|^2}{4}\right), \qquad (5.16)$$

where w is the dimensionless position of the quasihole, and quasiparticles, which have no such simple form. These have fractional particle number $\mp 1/M$ (in the case of the quasihole, this can be found from the plasma analogy), which has been measured as a reduced current shot noise [36], and are also Abelian anyons of statistics $1/M$ [37, 38]. mnr two-component states have two types of quasihole, one in each component, which are again Abelian anyons.

The Read-Rezayi and NASS states have non-Abelian anyon quasiholes (in both their bosonic and fermionic forms), and the possibility of using these for computation is one motivation for studying them. For the $k=2$ RR state, these quasiholes occur in pairs, with wavefunction

$$\begin{aligned}\phi_{\mathrm{RR,2qh}}(\{z_i\}) =&\mathrm{Symm}\left[\prod_i\{(z_{2i+1}-w_1)(z_{2i+2}-w_2)\right.\\ &+(z_{2i+1}-w_2)(z_{2i+2}-w_1)\}\exp\left(-\sum_m\frac{|z_m|^2}{4}\right)\\ &\left.\times\prod_{i>j}\prod_{l=1}^{2}(z_{2i+l}-z_{2j+l})(z_{2i+l}-z_{2j+(l+_21)})\right], \qquad (5.17)\end{aligned}$$

where w_1, w_2 are the dimensionless quasihole positions [147]. With 4 quasi-

holes,

$$\begin{aligned}\phi_{\mathrm{RR,4qh}}(\{z_i\}) =& \mathrm{Symm}\left[\prod_i \{(z_{2i+1}-w_1)(z_{2i+2}-w_2)(z_{2i+1}-w_3)(z_{2i+2}-w_4)\right.\\ &+(z_{2i+1}-w_2)(z_{2i+2}-w_1)(z_{2i+1}-w_4)(z_{2i+2}-w_3)\}\\ &\times\prod_{i>j}\prod_{l=1}^{2}(z_{2i+l}-z_{2j+l})(z_{2i+l}-z_{2j+(l+_21)})\\ &\left.\times\exp\left(-\sum_m\frac{|z_m|^2}{4}\right)\right], \end{aligned} \tag{5.18}$$

and the exchange $w_3 \leftrightarrow w_4$ gives a *different* state even after symmetrization: these two states form a topological qubit, and adding more quasiholes gives more qubits [147]. These qubits do not support purely topological universal computation [147], but could be used as a topologically protected quantum memory [33], or together with noisy (as much as $\sim 10\%$ error) non-topological gates for computation [147].

For the $\nu = 3/2$ Read-Rezayi state [39] and the $\nu = 4/3$ NASS state [40], the quasihole statistics include a Fibonacci anyon (called ϵ in [39], ρ in [40]), and these states hence do support universal topological quantum computation [41].

Chapter 6

Optical lattice quantum Hall effect

6.1 The Hamiltonian

In this section we introduce the Hamiltonian we will study and describe how it might be realised experimentally in an optical lattice.

We consider an optical lattice with J_z negligibly small, giving the effective 2-dimensionality. To obtain the FQH effect we also require "magnetic" terms in the Hamiltonian, which can be produced in at least four ways: rotating the lattice (along with the coordinate system and trapping potential) [58, 42], an EIT laser carrying orbital angular momentum [43], laser-induced hopping [44, 59], or an oscillating quadrupole potential [45]. Since all these methods give the same Hamiltonian, our results are equally applicable to all of them. We also add a potential term $V(p, q)$ (defined to include any potential arising as a by-product of the "magnetic" field, such as the anti-trapping (centrifugal)

term produced by rotation or EIT, as well as the explicit trapping potential), making our total Hamiltonian [42]

$$\begin{aligned} H &= \sum_{p,q} -J(e^{2\pi i\alpha q}a^\dagger_{p,q}a_{p-1,q} + e^{-2\pi i\alpha q}a^\dagger_{p,q}a_{p+1,q} + a^\dagger_{p,q}a_{p,q-1} \\ &\quad + a^\dagger_{p,q}a_{p,q+1}) + V(p,q)a^\dagger_{p,q}a_{p,q} + \frac{U}{2}a^\dagger_{p,q}a^\dagger_{p,q}a_{p,q}a_{p,q}, \end{aligned} \tag{6.1}$$

where the "magnetic" field strength is parameterised by the number of flux quanta per lattice cell α. The phase shift from hopping around one lattice cell is $2\pi\alpha$, and α is only defined mod 1 so we may restrict to $-1/2 < \alpha \leq 1/2$ or $0 \leq \alpha < 1$. This system has a gauge symmetry as long as α stays constant; we are here using the Landau gauge, as its translational symmetry is more convenient for our purposes than the rotational symmetry of the symmetric gauge (where all four hopping terms carry a phase).

6.2 Small α limit: continuum approximation

In this section we consider the case of small α (large magnetic length compared to the lattice spacing) and weak trapping, in which the lattice can be approximated by a continuum, and verify that in this case the system does reduce to a bosonic quantum Hall system.

First consider a one particle state $|\psi\rangle = \sum_{p,q} \psi(p,q)a^\dagger_{p,q}|0\rangle$, with normali-

sation condition $\sum_{p,q} |\psi(p,q)|^2 = 1$:

$$\begin{aligned} H|\psi\rangle &= \sum_{p,q} \psi(p,q)(-J_x(e^{2\pi i\alpha q}a^\dagger_{p+1,q} + e^{-2\pi i\alpha q}a^\dagger_{p-1,q}) \\ &\quad -J_y(a^\dagger_{p,q+1} + a^\dagger_{p,q-1}) + V(p,q)a^\dagger_{p,q})|0\rangle \\ &= \sum_{p,q} -J_x(e^{2\pi i\alpha q}\psi(p-1,q) + e^{-2\pi i\alpha q}\psi(p+1,q)) \\ &\quad -J_y(\psi(p,q-1) + \psi(p,q+1)) + V(p,q)\psi(p,q))a^\dagger_{p,q}|0\rangle. \end{aligned} \tag{6.2}$$

If the lattice spacing is small compared to the lengthscale on which ψ varies (which requires that $|\alpha| \ll 1$ and the trap is similarly weak) we can approximate the discrete space wavefunction ψ by a continuous space wavefunction $\phi(x,y)$ where $\psi(p,q) = d^2\phi(pd,qd)$, d is the lattice spacing and $\int \phi(x,y)dxdy = 1$. The first quantised Hamiltonian in this approximation is

$$\begin{aligned} H\phi &\approx H_0\phi \equiv -J_x\left(\left(2 - \frac{4\pi^2\alpha^2y^2}{d^2}\right)\phi - 4\pi i\alpha y\frac{\partial\phi}{\partial x} + d^2\frac{\partial^2\phi}{\partial x^2}\right) \\ &\quad -J_y\left(2\phi + d^2\frac{\partial^2\phi}{\partial y^2}\right) + V(x,y)\phi. \end{aligned} \tag{6.3}$$

Defining the (possibly anisotropic) effective mass $(m_x, m_y) = 1/2(J_x, J_y)d^2$ and the cyclotron frequency $\Omega = \pi\alpha/\sqrt{m_xm_y}d^2$, and discarding the constant zero point energy term $-2(J_x + J_y)\phi$, we then have

$$\begin{aligned} H_0\phi &= -\frac{1}{2m_x}\left(-4m_xm_y\Omega^2y^2\phi - 4i\sqrt{m_xm_y}\Omega y\frac{\partial\phi}{\partial x} + \frac{\partial^2\phi}{\partial x^2}\right) \\ &\quad -\frac{1}{2m_y}\frac{\partial^2\phi}{\partial y^2} + V(x,y)\phi \\ &= \frac{1}{2m_x}\left(-i\frac{\partial}{\partial x} - 2\sqrt{m_xm_y}\Omega y\right)^2\phi - \frac{1}{2m_y}\frac{\partial^2\phi}{\partial y^2} + V(x,y)\phi, \end{aligned} \tag{6.4}$$

which is exactly the usual single particle quantum Hall Hamiltonian with V being the "electric" potential, and hence has the usual Landau level solutions. The anisotropic effective mass simply becomes an anisotropic magnetic length, making the dimensionless coordinate $z = x/r_x + iy/r_y$.

For interacting particles, the continuum approximation is

$$H \approx \sum_i H_0(x_i, y_i) + \sum_{i \neq j} u\delta(x_i - x_j)\delta(y_i - y_j)/2, \tag{6.5}$$

where (x_i, y_i) are the coordinates of particle i and $u = Ud^2$, and the typical interparticle spacing must also be large compared to the lattice spacing (particle density $\rho \ll 1/d^2$). By analogy with the solid state FQH we define the filling factor $\nu = \rho\pi/m\Omega = \rho d^2/\alpha$.

In this limit we will hence find the same states as in a continuum bosonic quantum Hall system, that is $\nu = 1/2$ Laughlin, $\nu = 1, 3/2, \ldots$ Read-Rezayi, and vortex lattice.

Anyonic quasiholes could be created and moved using focused lasers [58], but for the Read-Rezayi (non-Abelian anyon) states to appear the interaction must be weak compared to the field ($um \lesssim 1$), which also reduces the quasiparticle-quasihole pair creation gap ($\sim um\Omega$). As thermally created anyons moving around the computational anyons are a source of error, such computation would hence require very low temperatures, such as might be reached by the methods of [148]. Alternatively, it has been suggested that non-Abelian field QH [10, 149] may offer non-Abelian excitations in the lowest density state, allowing a strong interaction to be used to increase the gap to $\sim \Omega$, but this has yet to be confirmed.

System	Electrons (GaAs)	Rotating gas (Rb)	Lattice (Rb)
Particles	Electrons	Atoms	Atoms
Statistics	Fermi	Bose	Bose
Interaction potential	$1/r$	$\delta(r)$	$\delta(r)$
Confinement	Sharp edges	Smooth trap	Smooth trap
Physical parameters			
System diameter	$\sim 10^{-2}$m	$10^{-5} - 10^{-4}$m	$10^{-5} - 10^{-4}$m
Number of particles N	$\sim 10^{11}$	$10^5 - 10^6$	$\sim 10^4$
2D number density ρ	$1 - 2 \times 10^{15}\text{m}^{-2}$	$\sim 10^{12}\text{m}^{-2}$	$10^{10} - 10^{11}\text{m}^{-2}$
Field strength Ω	$\sim 10^{14}$Hz	$10^2 - 10^3$Hz	$\sim 10^3$Hz
Free mass m_0	9×10^{-31}kg	1.5×10^{-25}kg	1.5×10^{-25}kg
Effective mass m	6×10^{-32}kg	1.5×10^{-25}kg	$10^{-24} - 10^{-23}$kg
Lattice spacing d	2×10^{-10}m	n/a	$\sim 10^{-6}$m
Temperature T	$0.1 - 0.3$K	$\sim 10^{-8}$K	$\sim 10^{-8}$K
Dimensionless parameters			
α (lattice/field)	10^{-4}	n/a	$0.1 - 0.5$
ν (density/field)	$0.2 - 10$	$10^3 - 10^4$	$1 - 10$
$\rho u/\Omega$ (interaction/field)		$0.1 - 1$	~ 0.1
$k_B T/\Omega$ (temperature/field)	10^{-3}	$1 - 10$	~ 1
Internal states	spin or bilayer	hyperfine	hyperfine
Tunability			
Ω, ρ, T	yes	yes	yes
um	no	yes	yes
m_x/m_y	no	no	yes

Table 6.1: Comparison of FQH systems. The FQH regime is $\nu \sim 1$, $\Omega \gg \rho u \gg k_B T$. Values for the BEC are from current experiments [134], which are still some way from this regime. Values for the lattice are for a single plane; if hopping between planes is negligible, the FQH effect occurs independently in each plane, so multiple planes can be used to increase the signal strength without increasing ν out of the FQH range.

6.2.1 Comparison to other realisations

In this section and Table 6.1 we compare our optical lattice system to the original solid state FQH system, and also to another possible QH system, a rotating ultracold atomic gas without a lattice.

In comparison to the original solid state semiconductor (Si or GaAs) FQH system, where $\alpha = eBd^2/\pi$ is very small ($\sim 10^{-4}$) at available magnetic fields B, our system has the advantages that the effective mass and effective interaction strength can be easily varied by changing the laser intensity, and that the $\alpha \sim 1$ regime is attainable without resorting to complicated superlattices. The optical lattice is also free from the lattice defects and impurities which are inevitable in a real crystal. While the original has fermions with a $1/r$ Coulomb interaction, our system has bosons with a $\delta(r)$ contact interaction; we consider the effect of this in the next subsection. (While it is possible to load fermionic atoms into an optical lattice, there are no fractional QH states for contact interacting fermions, only the $\nu = 1, 2, 3, \ldots$ integer QH states.)

In comparison to the rotating gas system, the lattice has tighter 2D confinement and a lower particle number per plane, and can avoid the centrifugal balancing problem by using laser-induced hopping or oscillating quadrupole, making it more feasible to lower ν into the FQH regime. Rotation and EIT however do produce a centrifugal term, which is actually made *worse* if they are used with a lattice, as the magnetic term Ω scales with the free/effective mass ratio and the centrifugal term does not.

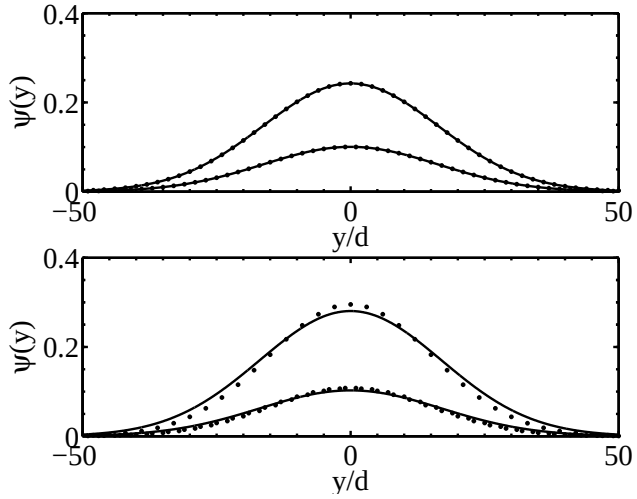


Figure 6.1: Wavefunction for (a) $\alpha = 1/2$ and (b) $\alpha = 1/3$, in linear geometry with trap $V(y) = m\omega^2 y^2/2$ and $\omega = 10^{-3}\pi/md^2$. The dots show the numerical wavefunction and the solid curves the analytic approximations for $y/d \equiv 0 \mod n$ (upper curve) and $y/d \neq 0 \mod n$ (lower curve).

6.3 Near simple rational α: multi-component wavefunctions

In this section we consider $\alpha \approx l/n$, where l, n are small integers, first for a single particle then for many particles.

6.3.1 Single particle states

Numerically calculated single particle ground state wavefunctions (Fig. 6.1) for $\alpha \approx l/n$ (where n is a small integer) and weak potentials V have an n-site periodic pattern superposed on a smooth large-scale variation, suggesting the representation $\psi(np+i, nq+j) = \sum_k \chi_k((np+i)d, (nq+j)d)v_{ij}^{(k)}d^2$ where χ_k is a continuous function and $\mathbf{v}^{(k)}$ an $n \times n$ matrix. We find by expansion about $\alpha_c \equiv l/n$ (see Sec. 6.7) that there are n degenerate $\mathbf{v}^{(k)}$, of the form

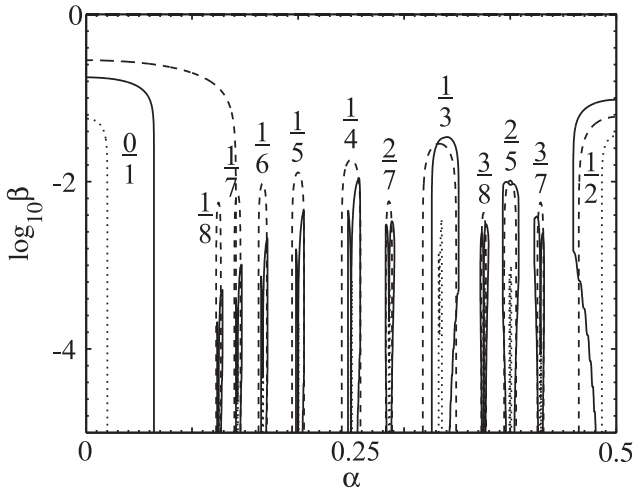


Figure 6.2: Areas of validity of the theory of Sec. 6.3.1 for the α_c indicated, for a single particle in a one-dimensional harmonic trap $V(x,y) = \frac{1}{2}m\omega^2 y^2$ of dimensionless strength $\beta \equiv md^2\omega/\pi$. The areas enclosed by the solid (dashed) lines satisfy $|\langle \psi_{\rm theory} | \psi_{\rm numeric} \rangle| > 0.99$ (0.999), $|E_{\rm theory} - E_{\rm numeric}| < 0.01/(md^2)$ $(0.001/(md^2))$. The dotted lines are the theoretical areas of validity obtained by taking "$a \gg b$" in Eq. (6.8) to mean $a > 50b$.

$v_{IJ}^{(k)} = e^{2\pi i k I l/n} v_{J-k}$ where $\mathbf{v}$ is a fixed n component vector for each l, n and the subscript $J-k$ wraps around mod n, and that the $\chi_k(x,y)$ obey

$$-\frac{C}{2m}\frac{\partial^2 \chi_k}{\partial y^2} + \frac{C}{2m}\left(2m\tilde{\Omega}y - i\frac{\partial}{\partial x}\right)^2 \chi_k + V(x,y)\chi_k = \left(E - \frac{E_0}{md^2}\right)\chi_k \qquad (6.6)$$

where $\tilde{\Omega} \equiv (\alpha - \alpha_c)\pi/(md^2)$ and C, E_0 depend only on l, n. This formula reduces to Eq. (6.4) for $\alpha_c = 0/1$, and agrees well with numerical calculations (Figs. 6.1, 6.2) near other simple α_c, especially $1/2$.

For this procedure to be consistent, the lengthscale on which χ_k varies, which for a harmonic trap $V(x,y) = \frac{1}{2}m\omega^2 y^2$ is $(C/(4Cm^2\tilde{\Omega}^2 + m^2\omega^2))^{1/4}$, must be large compared to the "small scale" periodicity nd, but small enough

that $m\tilde{\Omega}yd \ll 1$, that is

$$\frac{1}{n^4 d^4} \gg \frac{1}{C}(4Cm^2\tilde{\Omega}^2 + m^2\omega^2) \gg m^4 d^4 \tilde{\Omega}^4 \tag{6.7}$$

or equivalently

$$\frac{1}{n^4} \gg \frac{1}{C}(4C(\alpha - \alpha_c)^2 + \beta^2) \gg (\alpha - \alpha_c)^4 \tag{6.8}$$

where $\beta \equiv md^2\omega/\pi$ is the dimensionless trap strength. Fig. 6.2 compares this criterion with numerical results for the wavefunctions. Fractions α_c with larger denominator appear over narrower ranges of α, requiring more accurate parameter control, and are destroyed by weaker external potentials V, so would be more difficult to see experimentally.

6.3.2 Interacting particles

Eq. (6.6) can be extended to the many-particle case as

$$\begin{aligned} H \approx & \int dxdy \sum_k \chi_k^\dagger(x,y) \left\{ -\frac{C}{2m}\frac{\partial^2}{\partial y^2} \right. \\ & \left. + \frac{C}{2m}\left(2m\tilde{\Omega}y - i\frac{\partial}{\partial x}\right)^2 + V(x,y) \right\} \chi_k(x,y) + \frac{E_0}{md^2} \\ & + \sum_{k_1,k_2,k_3,k_4} u G_{k_1,k_2,k_3,k_4} \chi_{k_1}^\dagger(x,y)\chi_{k_2}^\dagger(x,y)\chi_{k_3}(x,y)\chi_{k_4}(x,y), \end{aligned} \tag{6.9}$$

where $G_{k_1,k_2,k_3,k_4} \equiv \sum_j v_{j+k_1} v_{j+k_2} v_{j+k_3} v_{j+k_4}/n$ if $k_1 + k_2 \equiv k_3 + k_4 \bmod n$ and 0 otherwise. (The conservation mod n is due to the x quasimomentum $2\pi k/nd$ carried by $\mathbf{v}^{(k)}$.) For example, for $\alpha_c = 1/2$, $G_{1111} = G_{2222} = 3/2$

and $G_{1212} = G_{2121} = G_{1122} = G_{2211} = 1/2$: particles with the same k interact more strongly because their $\mathbf{v}^{(k)}$ are peaked on the same sites.

In the case $\alpha_c = 1/2$, a change of basis from $\chi_{1,2}$ to $\chi_\pm = \chi_1 \pm i\chi_2$ makes this effective Hamiltonian analogous to a bilayer FQH system, with $\chi_\pm$ being the two "layers"; however, the interaction ratio is 1:2 with the inter"layer" interaction being the stronger one, while it is equal or weaker in most other realisations of multicomponent FQH states.

The highest density zero interaction energy LLL state of such a system is still the 221 state defined by

$$\phi_{221}(\{z_i\},\{w_i\}) = \left(\prod_{i>j}(z_i - z_j)^2(w_i - w_j)^2\right)\left(\prod_{i,j}(z_i - w_j)\right) \times \exp\left(-\sum_i |z_i|^2/4 + |w_i|^2/4\right), \tag{6.10}$$

where there are $N/2$ particles in the $+$ "layer" with coordinates $z = 2(x + iy)/r_0$ and $N/2$ in the $-$ "layer" with coordinates $w = 2(x + iy)/r_0$, and $r_0 = (m^2\tilde{\Omega}^2 + m^2\omega^2)^{-1/4}$. This state has filling factor $\tilde{\nu} \equiv \rho\pi/m\tilde{\Omega} = 2/3$ (and can be extended to general $\alpha_c = l/n$ with $\tilde{\nu} = n/(n+1)$) with respect to $\tilde{\Omega}$, and as it has exactly zero interaction energy, it would be the lowest step of the density profile in a slowly varying external potential. The next higher state might be either a $\tilde{\nu} = 4/3$ NASS state, or a $\tilde{\nu} = 3/2$ Read-Rezayi state in a single "layer", the other being empty.

At high $\tilde{\nu}$ a two-component vortex lattice [145, 146] would form; the Lindemann criterion [150] suggests that this lattice would melt at similar $\tilde{\nu}$ to the single component ($\alpha \ll 1$) lattice. We have numerically simulated

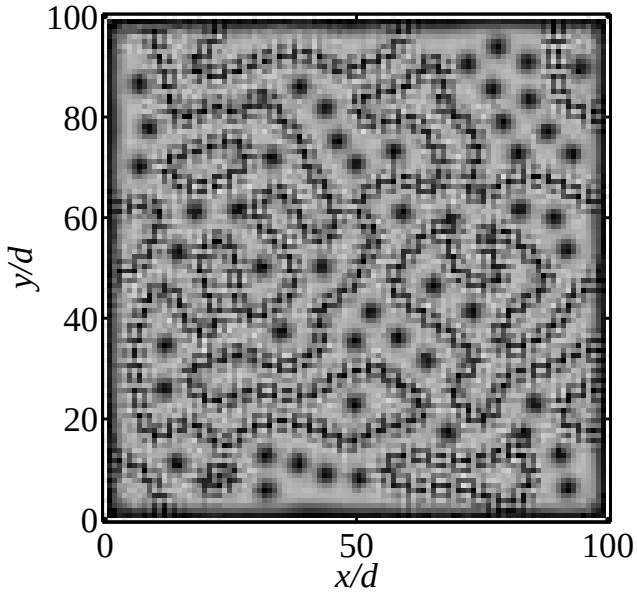


Figure 6.3: Numerical approximation to the ground state of the $\alpha_c = 1/2$ vortex lattice phase, calculated using imaginary time propagation of a Gutzwiller ansatz. The parameters are $\alpha = 0.48$, $U = 0.1J$.

this vortex lattice phase using imaginary time propagation of the Gutzwiller ansatz [54],

$$|\,\psi\rangle = \prod_{i,j} \sum_{n_i=0}^{n_{\max}} \alpha_{i,j,n_i} \left(a_{i,j}^{\dagger}\right)^{n_i} |\,\mathrm{vac}\rangle\,, \tag{6.11}$$

where the state is specified by the complex numbers α_{i,j,n_i}; this can describe both superfluid vortex lattice and Mott insulator states, but not off-site correlated states such as FQH states. We found it to form alternating stripes of the two components (Fig. 6.3), as found in a continuum two-component system [145, 146], confirming that at least in this regime the two-component description is meaningful. The stripes straighten out only very slowly with increasing imaginary time (decreasing temperature), as in [146], and there is a slight tendency to phase separation; the perfectly straight stripes of [145]

exist only in the zero temperature limit. At exactly $\alpha = \alpha_c$, $\tilde{\nu} = \infty$ and one has an n component superfluid with no vortices, which is analogous to frustration [42]. This may be the possible superfluid phase found at $\alpha = 1/3, 1/2$ in the exact diagonalisations of [45].

In a sufficiently weak trap for the local density approximation to apply, each incompressible state gives a constant density step ($d\rho/dx = d\rho/d\mu dV/dx = 0$). FQH states for which Eq. (6.9) is valid occur at fixed $\tilde{\nu}$ and hence $\rho \propto |\alpha - \alpha_c|$, while ordinary ($\alpha \ll 1$) FQH states occur at fixed ν and Mott insulator states at fixed ρd^2. An in-trap density profile measurement could hence distinguish these possibilities by comparing measurements at different Ω, as well as measuring the $\tilde{\nu}$ at which incompressible states occur, but we will see in the next section that a time of flight expansion measurement gives a more clear-cut distinction, as well as being easier.

6.4 Time of flight expansion

Time of flight expansion, where the lattice and trap are switched off and the atomic cloud allowed to expand freely for a time before measuring its density distribution, is a standard measurement technique for ultracold atomic systems [52, 56]; in this section we consider applying it to our system.

If interaction during the expansion can be neglected, which is reasonable as each optical lattice site rapidly expands from its tight initial confinement, and the expansion is to many times the cloud's initial size, the result of this

process is

$$\rho_m(\mathbf{X}) = \tilde{w}(\mathbf{X}m_0/t) \sum_{\mathbf{x}_1,\mathbf{x}_2} \rho_1(\mathbf{x}_1;\mathbf{x}_2) e^{i\mathbf{X}\cdot(\mathbf{x}_1-\mathbf{x}_2)m_0/t} \tag{6.12}$$

where $\tilde{w}$ is the Fourier transform of the Wannier function, ρ_1 is the 1-particle density matrix of the state, the $\mathbf{x}_i$ are summed over all lattice sites, $\rho_m(\mathbf{X})$ is the measured density at position $\mathbf{X}$ and time t after release, and m_0 is the free mass.

The "momentum" measured by this process is the wavevector (free space momentum) $-i\nabla$, not the momentum $(-i\partial_x - 2m\Omega y, -i\partial_y)$ of the system Hamiltonian. This is *not* gauge invariant (it does not have to be because the sudden switch-off of the "magnetic" field does not obey Maxwell's equations). ρ_1 must be in the natural gauge of the particular experimental method being used: symmetric gauge for rotation or EIT, Landau gauge for the laser-induced hopping scheme of [44].

For constant density lowest Landau level states, which include the Laughlin, RR, 221 and NASS states, ρ_1 is as given in [151] in symmetric gauge for low α states, and a similar form with a $\sum_k \mathbf{v}^{(k)*}\mathbf{v}^{(k)}$ factor from the small scale structure for high α states, giving

$$\begin{aligned}\rho_m(\mathbf{X}) &= \tilde{w}(\mathbf{X}m_0/t) \sum_{\mathbf{x}_1,\mathbf{x}_2} \sum_k \mathbf{v}'^{(k)*}(\mathbf{x}_1)\mathbf{v}'^{(k)}(\mathbf{x}_2)\frac{\tilde{\nu}}{2\pi k} \\ &\quad \times \exp\left\{-\frac{(\mathbf{x}_1-\mathbf{x}_2)^2}{4r_0^2} + i\left(\frac{Xm_0}{t} + \frac{y_1+y_2}{4r_0^2}\right)(x_1-x_2)\right. \\ &\quad \left. +i\left(\frac{Ym_0}{t} - \frac{x_1+x_2}{4r_0^2}\right)(y_1-y_2)\right\}, \end{aligned} \tag{6.13}$$

where the prime indicates the $\mathbf{v}^{(k)}$ are also in symmetric gauge (which doubles their period to $2n$).

Summing first over $\mathbf{x}_1 - \mathbf{x}_2$ and approximating this by an integral, we see that each $\mathbf{x}_1 + \mathbf{x}_2$ contributes an approximate Gaussian centered on $(-y_1 - y_2, x_1 + x_2)t/4m_0r_0^2$, and then summing over $\mathbf{x}_1 + \mathbf{x}_2$ we get the in-trap density profile smeared out on a scale r_0, rotated through a right angle and scaled by $t/4m_0r_0^2$. Physically this happens because lowest Landau level wavefunctions are as close to rigid body rotation as a quantum state can be, and once released from the field the wavevector becomes the physical momentum so they fly apart as if they were rotating. Because the sum is in fact a discrete one, the pattern repeats every reciprocal lattice cell (size $2\pi t/dm_0$) with a decaying envelope $\tilde{w}$, and high α states can have multiple peaks per reciprocal lattice cell from the small scale structure.

Fig. 6.4 shows some numerically calculated examples; the pattern repeats every reciprocal lattice cell with a slow decay given by $\tilde{w}$ [56]. As expected from the above, FQH states have stepped peaks, further distinguishing them from the featureless $\tilde{w}$ of a Mott insulator [49, 56], while vortex lattice states have Thomas-Fermi (inverted parabola) peaks. Low α states have one peak per reciprocal lattice cell while $\alpha \approx 1/2$ states have 4. The extra peaks (previously described for the vortex lattice in [42]) confirm the existence of small scale structure; they do not however show whether one or both "layers" are occupied.

As time of flight expansion only measures single particle properties, it cannot detect correlations, so different FQH states are distinguished only by their density. We will now consider an enhancement of this method that can

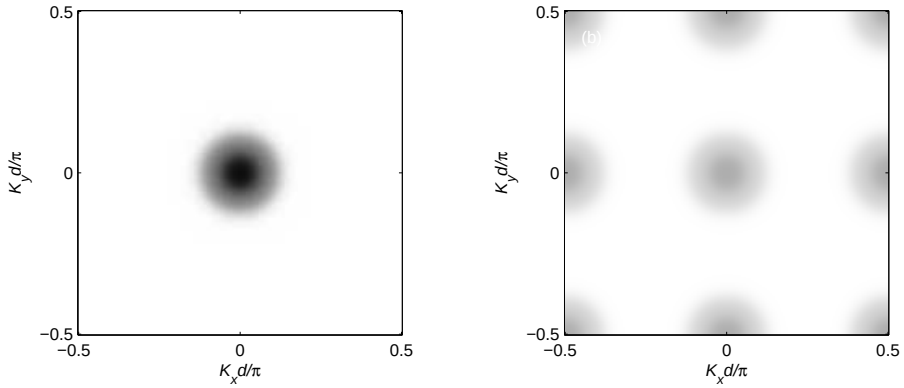


Figure 6.4: Numerically calculated time of flight expansions in symmetric gauge of (a) Laughlin (outer ring) and RR (centre circle) state ($\nu = 1/2, 1$, $\alpha = 0.01$), (b) 221 and NASS state ($\tilde{\nu} = 2/3, 4/3$, $\alpha = 0.51$). The initial states are circular with diameter 100 lattice sites for the outer ring and 50 for the inner one. Area shown is one reciprocal lattice cell; the pattern repeats each cell with a slow decay given by $\tilde{w}$, which is not included here as its speed is implementation dependent. White is no particles, both are to the same brightness scale.

measure their correlations.

6.5 Correlation measurement

Two-particle correlations in a state lead to correlations in the fluctuations (shot noise) of the density [48, 152], which were recently measured for the Mott insulator state [49]. At time t after release from an optical lattice these correlations are given by [48]

$$G(\mathbf{r}, \mathbf{r}') \propto t^{-6} \sum_{ii'jj'} e^{i\mathbf{R}_{ii'}\cdot\mathbf{Q}(\mathbf{r})+i\mathbf{R}_{jj'}\cdot\mathbf{Q}(\mathbf{r}')} \langle a_i^\dagger a_j^\dagger a_{j'} a_{i'} \rangle - \langle n(\mathbf{r}) \rangle \langle n(\mathbf{r}') \rangle, \qquad (6.14)$$

where i, j, i', j' run over lattice sites, $\mathbf{R}_{ii'}$ is the displacement vector from site i to site i' and $\mathbf{Q}(\mathbf{r}) = m_0\mathbf{r}/t$ where m_0 is the free mass. For states described

by a continuum wavefunction $\langle a_i^\dagger a_j^\dagger a_{j'} a_{i'}\rangle = d^2\rho_2(z_i, z_j; z_j', z_i')$ where ρ_2 is the continuum 2-particle density matrix, which for lowest Landau level constant density states is of the form [151]

$$\rho_2(z_i, z_j; z_i', z_j') = \exp\left\{-\frac{1}{4r_0^2}\left(|z_i|^2 + |z_{i'}|^2 + |z_j|^2 + |z_{j'}|^2 - 2z_i^* z_{i'} - 2z_j^* z_{j'}\right)\right\} \times \left(\frac{\nu}{2\pi}\right)^2 g((z_i - z_j)^*(z_{i'} - z_{j'})), \tag{6.15}$$

where $g(|z_i - z_j|^2)$ is the two-point correlation function and $g(z)$ is then defined for arbitrary complex z by analytic continuation.

For the $\alpha \approx 1/2$ two component states, ρ_2 is replaced by

$$\sum_{k_i, k_j} \mathbf{v}^{(k_i)*}(i)\mathbf{v}^{(k)}(i')\mathbf{v}^{(k)*}(j)\mathbf{v}^{(k)}(j')\rho_2^{(k_i,k_j)}(z_i, z_j; z_i', z_j'), \tag{6.16}$$

where $\rho_2^{(11)} = \rho_2^{(22)}$ is the continuum density matrix for two particles of the same type and $\rho_2^{(12)} = \rho_2^{(21)}$ for two particles of opposite type.

To obtain g we fit the series

$$g_{aa}(|z|^2) = 1 + e^{-|z|^2/2} + \sum_{m\geq 0 \text{ even}} \frac{2c_m}{m!}\left(\frac{|z|^2}{4}\right)^m e^{-|z|^2/4}, \tag{6.17}$$

$$g_{ab}(|z|^2) = 1 + \sum_{m\geq 0} \frac{2\tilde{c}_m}{m!}\left(\frac{|z|^2}{4}\right)^m e^{-|z|^2/4}, \tag{6.18}$$

which works for any lowest Landau level state ([153], with a sign change because our particles are bosons), to Monte Carlo data for the state. The Laughlin and 221 states have $g(0) = 0$ (Fig. 6.5), meaning that particles cannot come together and the interaction energy is hence zero, while the RR

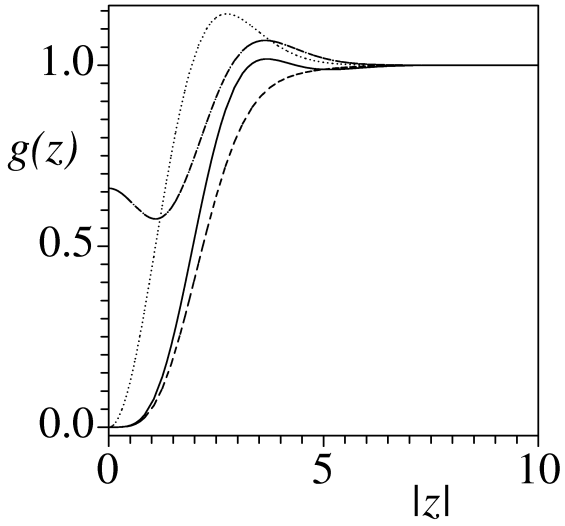


Figure 6.5: Two-point functions: $\nu = 1/2$ Laughlin state (solid), $\tilde{\nu} = 2/3$ 221 state $g_{11} = g_{22}$ (dashed) and $g_{12} = g_{21}$ (dotted), and $\nu = 1$ RR state (dash-dotted).

and NASS states have $g(0) > 0$ and hence nonzero interaction energy. The data for the RR and NASS states is very limited because only 8-12 particles were used, due to the exponential number of terms in their wavefunctions after symmetrization, and is hence not sufficient to determine whether $\tilde{\nu} = 4/3$ NASS or $\tilde{\nu} = 3/2$ RR has the lower variational energy.

Eq. (6.14) involves a sum over 4 complex variables, which makes its direct numerical evaluation computationally intensive. To simplify this problem, we integrate over $\mathbf{r} + \mathbf{r}'$, which gives a delta function setting $z_i + z_j - z_i' - z_j' = 0$, and removes all explicit dependence on $z_i + z_j + z_i' + z_j'$. The resulting correlation, which (ignoring the t^{-6} prefactor) is a function of momentum difference $\Delta\mathbf{K} \equiv Q(\mathbf{r}) - Q(\mathbf{r}')$, can hence be evaluated for an infinite size state by summing over just 2 complex variables, $z_i - z_j$ and $z_i' - z_j'$. However,

this does not work for a finite size state because the ranges of $z_i - z_j$ and $z'_i - z'_j$ then do depend on $z_i + z_j + z'_i + z'_j$, and assuming an infinite size state while necessarily summing over a finite range introduces the possibility of numerical artefacts.

Fig. 6.6 shows some numerically calculated examples; again one reciprocal lattice cell is shown and the pattern repeats. Fully Bose condensed states, including ideal vortex lattices, have zero correlation. The Laughlin and 221 states are found to show near 100% anticorrelation at small ΔK (note that as this measurement works in Fourier space, this is not the same thing as full real-space anticorrelation: the Mott insulator shows positive correlation [49]). The 221 state shows 8 additional anticorrelation dips at $\Delta K = \pm\pi d/2$; in Fig. 6.6 these are of 50% strength, but we suspect that this is an artefact and that they are really 100%. Higher density FQH states also show anticorrelation but of reduced strength. Our data suggests that RR states have a ringed pattern with their strongest anticorrelation ($\approx 50\%$ for $\nu = 1$ and $\approx 35\%$ for $\nu = 3/2$) at a nonzero ΔK, while the $\tilde{\nu} = 4/3$ NASS state has $\approx 40\%$ anticorrelation at zero ΔK and no ring, but is insufficient to determine whether the presence or absence of such rings conclusively distinguishes RR from NASS states.

6.6 Hall current and disorder

In this section we consider the dynamics of the system, in particular its Hall current, and the effect of adding disorder to the lattice.

When a linear potential $V(x, y) = may$ is applied to a continuum FQH

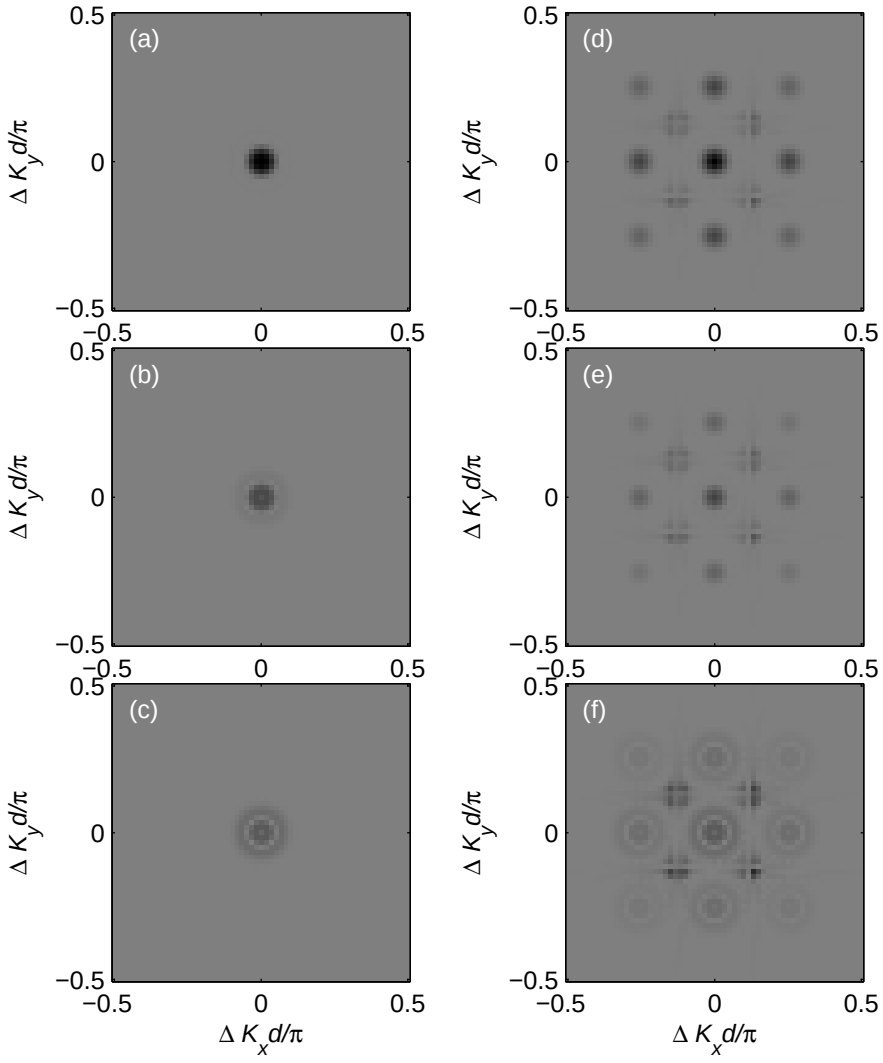


Figure 6.6: Numerically calculated shot noise correlations for infinite system in symmetric gauge, (a) Laughlin (b) $\nu = 1$ RR (c) $\nu = 3/2$ RR (d) 221 (e) $\tilde{\nu} = 4/3$ NASS (f) $\tilde{\nu} = 3/2$ RR. $\alpha = 0.02$ in (a)-(c), $\alpha = 0.52$ in (d)-(f). Gray is no correlation, black 100% anticorrelation. The four extra dips at $\Delta K = (\pm\pi d/4, \pm\pi d/4)$ in (d)-(f) are probably artefacts of the necessary approximations.

system, all states acquire a velocity $a/(2\Omega)$ at right angles to the potential gradient: this is the Hall current. In a perfect continuum system this is an exact result, unaffected by interaction, because such an acceleration term is exactly cancelled out by Galilean-transforming Eq. (6.5) to a reference frame moving with this velocity. In a lattice system it is valid at sufficiently low α for the continuum approximation to be valid; at higher α the lattice, which defines a rest frame, becomes important and a different velocity can occur. In particular, near simple rational α where Eq. (6.9) is valid, the velocity is $a/(2\tilde{\Omega})$, which can be very different: for $\alpha < \alpha_c$ it even has the opposite sign.

For nonlinear potentials of large lengthscale compared to the magnetic length $(m\tilde{\Omega})^{-1/2}$, the single particle eigenstates lie along the equipotentials and Hall current flows along equipotentials at the velocity given by the local potential gradient. This motion is not visible in equilibrium as the steps in the density profile lie along equipotentials, but it can be made visible by putting the system out of equilibrium, for example by suddenly changing the trapping potential. Relaxation to equilibrium will be slow because non-forward scattering is energetically forbidden in the FQH system, making the Hall current a supercurrent [133, 34].

When sufficiently mild disorder is added to an FQH system, some of the particles become localised and cannot carry current, but those which remain free move faster and the average velocity is still $a/(2\tilde{\Omega})$ [34, 133]. For example, for smooth disorder ($V(x, y) = may$+random potential of lengthscale $\gg r_0$), $v_x = (\partial V/\partial y)/(2m\tilde{\Omega})$ remains valid, so particles on closed equipotentials are localised, but the random part of v_x averages to zero so the average velocity remains $a/(2\tilde{\Omega})$ in the x direction. The current is hence determined by the

width over which each extended level is occupied. A simple model of this is to describe the disorder by a density of states $\rho_d(E)$ =number of LLL states per unit energy interval per unit area at energy E, $\int \rho_d(E)\mathrm{d}E = m\tilde{\Omega}/\pi$; for smooth disorder $\rho_d(E)$ is proportional to the probability distribution of the noise potential. For a linear geometry, we then have

$$N = L\int \mathrm{d}y \int^{\mu-V_1(y)} \mathrm{d}E \sum_{j\geq 0}(\nu_j - \nu_{j-1})\rho_d(E-E_j) \tag{6.19}$$

$$I = \frac{m}{2\pi}\int \mathrm{d}y \frac{dV_2}{dy} \int^{\mu-V_1(y)} \mathrm{d}E \sum_{j\geq 0}(\nu_j - \nu_{j-1})\delta(E-E_j) \tag{6.20}$$

where L is the length of the system along the x-axis, I is the net current (in the x direction), N the number of particles and μ the chemical potential, the FQH states are at filling factors ν_j and energies per particle E_j, and V is suddenly changed from $V_1(y)$ to $V_2(y)$. For $\alpha \approx 0$ (Read-Rezayi states), $\nu_j = (j+1)/2$ and $E_j \approx (um\Omega/2\pi)j$ [138]. This equation is valid for weak trapping potentials ($dV/dy \ll$ disorder); stronger potentials can break weakly localised states free, replacing the $\delta(E-E_j)$ density of extended states in I by a finite width distribution.

In a square-well potential (as in a solid state system) the localised states create a finite range of filling factor over which a given number of FQH extended state levels are completely full, giving rise to the almost perfectly flat FQH plateaus. In a harmonic trap there will not be FQH plateaus, only corners each time a new extended level begins to fill (Fig. 6.7), but unlike the square-well case, it is possible to obtain the complete distribution $\rho_d(E)$ by measuring I against N (or Ω).

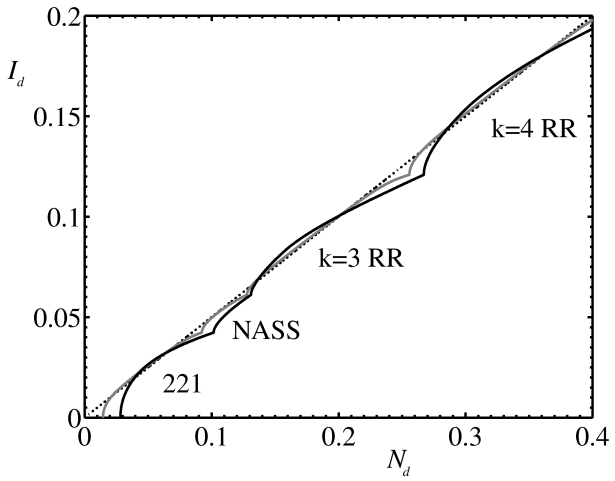


Figure 6.7: Dimensionless Hall current $I_d \equiv I/\left\{(a/\omega)\sqrt{u/2\pi\tilde{\Omega}}\right\}$ against dimensionless number of atoms per unit length $N_d \equiv N/\left\{L(\tilde{\Omega}/\pi)^{3/2}m\sqrt{u}/\omega\right\}$, where L is the length of the system, in a 1D harmonic trap $V(x,y) = \frac{1}{2}m\omega^2y^2 + may$ at $\alpha \approx 1/2$. The linear term may is turned on after the atoms have come to equilibrium in the trap, and the curves are for no disorder (dotted straight line), maximal disorder (constant density of states) (black curve), and Lorentzian disorder of width $\frac{1}{5}\frac{um\tilde{\Omega}}{2\pi}$ (grey curve). The named states are the highest occupied; the corresponding plot for small α is qualitatively similar, but with more evenly spaced dips as Laughlin and $k = 2$ RR replace 221 and NASS. Note that this graph is based on very rough estimates of the energy per particle E_j of each state; the actual positions of the dips would be different, and the $\tilde{\nu} = 1$ RR state might appear instead of or as well as the $\tilde{\nu} = 4/3$ NASS state.

6.7 Derivation of high α states

In this section we describe in detail the derivation of the $\alpha \approx l/n$ single particle states introduced in Sec. 6.3.1.

We take $V = \frac{1}{2}m\omega^2 y^2$ and, since numerical wavefunctions (Fig. 6.1) show an n site periodicity superimposed on slow variation, consider a state $\psi(np+i, nq+j) = d^2\phi_j((nq+j)d)e^{iK(np+i)d}$ where the $\phi_j(y)$ are slowly varying compared to the lattice spacing. Since H is independent of x if V is, the x quasimomentum K is conserved exactly for this choice of V; let $K = 2\pi kl/nd + \tilde{K}$, where k is an integer and $\tilde{K} \ll 1/n$ to give an n site periodicity plus slow variation in the x direction.

$$
\begin{aligned}
H\phi_j &= -\frac{1}{md^2}\cos\left(\frac{2\pi jl}{n} + 2m\tilde{\Omega}yd - Kd\right)\phi_j + \frac{1}{2}m\omega^2 y^2\phi_j \\
&\quad -\frac{1}{2m}\left(\frac{\phi_{j+1}}{d^2} + \frac{1}{d}\frac{\partial\phi_{j+1}}{\partial y} + \frac{1}{2}\frac{\partial^2\phi_{j+1}}{\partial y^2}\right. \\
&\quad \left. +\frac{\phi_{j-1}}{d^2} - \frac{1}{d}\frac{\partial\phi_{j-1}}{\partial y} + \frac{1}{2}\frac{\partial^2\phi_{j-1}}{\partial y^2}\right) + O(d) \\
&= -\frac{1}{2md^2}\left(\phi_{j+1} + 2\cos\left(\frac{2\pi(j-k)l}{n}\right)\phi_j + \phi_{j-1}\right) \\
&\quad -\frac{1}{2md}\left((\tilde{K} - 2m\tilde{\Omega}y)\sin\left(\frac{2\pi(j-k)l}{n}\right)\phi_j + \frac{\partial\phi_{j+1}}{\partial y} - \frac{\partial\phi_{j-1}}{\partial y}\right) \\
&\quad -\frac{1}{2m}\left(-(\tilde{K} - 2m\tilde{\Omega}y)^2\cos\left(\frac{2\pi(j-k)l}{n}\right)\phi_j\right. \\
&\quad \left. -m^2\omega^2 y^2\phi_j + \frac{1}{2}\frac{\partial^2\phi_{j+1}}{\partial y^2} + \frac{1}{2}\frac{\partial^2\phi_{j-1}}{\partial y^2}\right) + O(d). \qquad (6.21)
\end{aligned}
$$

Note that for $n = 1$ or 2 the odd powers cancel by symmetry and we get an expansion in d^2, but that for larger n the expansion is in d. Define

$\phi = (\phi_1 \dots \phi_n)^T$ and expand in powers of d: $\phi = \phi^{(0)} + d\phi^{(1)} + d^2\phi^{(2)} + O(d^3)$. Similarly expand the energy $E = E_0/d^2 + E_1/d + E_2 + O(d)$ and define

$$\mathbf{A}_0 = \begin{pmatrix} 2\cos 2\pi(1-k)\frac{l}{n} & 1 & 0 & \cdots & 1 \\ 1 & 2\cos 2\pi(2-k)\frac{l}{n} & 1 & & 0 \\ 0 & 1 & \ddots & \ddots & \vdots \\ \vdots & & & \ddots & 0 \\ 0 & & \ddots & & 1 \\ 1 & 0 & \cdots & 1 & 2\cos 2\pi(n-k)\frac{l}{n} \end{pmatrix} \tag{6.22}$$

The $O(1/d^2)$ terms then become $\mathbf{A}_0\phi^{(0)} = -2mE_0\phi^{(0)}$, so $\phi^{(0)}(y)$ is an eigenvector of $\mathbf{A}_0$, with the ground state having the largest eigenvalue. Assuming non-degenerate eigenvalues, $\phi^{(0)}(y)$ is hence proportional to the same eigenvector $\mathbf{v}^{(k)}$ at all y, so can depend on y only in overall magnitude $\phi^{(0)}(y) = \chi(y)\mathbf{v}^{(k)}$.

Since changing k is equivalent to changing the origin of j, the eigenvalues are the same for all k, with ground state eigenvectors $v_j^{(k)} = v_{j-k}$, where $\mathbf{v}$ is the normalised ground state eigenvector for $k = 0$ and the subscript $j - k$ wraps around mod n. This gives n degenerate ground states $k = 0, \dots, n-1$, which are orthogonal because of their different K values. For simplicity we take $k = 0$ in the remainder of this derivation.

For the $O(1/d)$ terms, define

$$\mathbf{A}_1 = \begin{pmatrix} 0 & 1 & 0 & \cdots & -1 \\ -1 & 0 & 1 & & \vdots \\ 0 & -1 & 0 & \ddots & 0 \\ \vdots & & \ddots & \ddots & 1 \\ 1 & \cdots & 0 & -1 & 0 \end{pmatrix} \tag{6.23}$$

$$\mathbf{A}_2 = \begin{pmatrix} \sin 2\pi l/n & 0 & \cdots & 0 \\ 0 & \sin 4\pi l/n & \ddots & \vdots \\ \vdots & \ddots & \ddots & 0 \\ 0 & \cdots & 0 & \sin 2n\pi l/n \end{pmatrix} \tag{6.24}$$

and $\mathbf{w}_1 = \mathbf{A}_1\mathbf{v}$, $\mathbf{w}_2 = \mathbf{A}_2\mathbf{v}$ giving

$$\begin{aligned} (\mathbf{A}_0 + 2mE_0)\phi^{(1)}(y) &= 2mE_1\chi(y)\mathbf{v} + \frac{d\chi}{dy}\mathbf{w}_1 \\ &\quad +(K - 2m\tilde{\Omega}y)\chi(y)\mathbf{w}_2 \end{aligned} \tag{6.25}$$

The left hand side of (6.25) is orthogonal to $\mathbf{v}$ because $\mathbf{A}_0+2mE_0$ annihilates $\mathbf{v}$ and is Hermitian, while $\mathbf{w}_1$ is orthogonal to $\mathbf{v}$ because $\mathbf{A}_1$ is antisymmetric and hence so is $\mathbf{v}^T\mathbf{A}_1\mathbf{v}$, but the latter is 1×1 so can only be antisymmetric if it is zero. Hence a solution can only exist if $\mathbf{w}_2$ is also orthogonal to $\mathbf{v}$ (and $E_1 = 0$); this is the case for all α_c in Fig. 6.2 to within numerical accuracy, but we have not been able to prove that it is always the case.

For the $O(1)$ terms define

$$\mathbf{A}_3 = \begin{pmatrix} 0 & 1 & 0 & \cdots & 1 \\ 1 & 0 & 1 & & \vdots \\ 0 & 1 & 0 & \ddots & 0 \\ \vdots & & \ddots & \ddots & 1 \\ 1 & \cdots & 0 & 1 & 0 \end{pmatrix} \tag{6.26}$$

$$\mathbf{A}_4 = \begin{pmatrix} \cos 2\pi l/n & 0 & \cdots & 0 \\ 0 & \cos 4\pi l/n & \ddots & \vdots \\ \vdots & \ddots & \ddots & 0 \\ 0 & \cdots & 0 & \cos 2n\pi l/n \end{pmatrix} \tag{6.27}$$

giving

$$\begin{aligned} (2mE_2 - m^2\omega^2 y^2)\chi(y)\mathbf{v} - (2m\tilde{\Omega}y - K)^2\chi(y)\mathbf{A}_4\mathbf{v} \\ + \frac{1}{2}\frac{d^2\chi}{dy^2}\mathbf{A}_3\mathbf{v} \\ + \left((K - 2m\tilde{\Omega}y)\mathbf{A}_2 + \frac{d}{dy}\mathbf{A}_1\right)(\mathbf{A}_0 + 2mE_0)^{-1} \\ \times \left(2mE_1\chi(y)\mathbf{v} + \frac{d\chi}{dy}\mathbf{w}_1 + (K - 2m\tilde{\Omega}y)\chi(y)\mathbf{w}_2\right) \\ + (\mathbf{A}_0 + 2mE_0)\phi^{(2)} = \mathbf{0} \end{aligned} \tag{6.28}$$

Taking the dot product of this with $\mathbf{v}$ gives a harmonic oscillator equation

for $\chi(y)$:

$$-\frac{C_1}{2m}\frac{\partial^2\chi}{\partial y^2}+\frac{C_2}{2m}(2m\tilde{\Omega}y-i\frac{\partial}{\partial x})^2\chi+V(x,y)\chi \\ =(E-\frac{E_0}{md^2})\chi \tag{6.29}$$

where the dimensionless constants $C_1=\mathbf{v}^T\mathbf{A}_3\mathbf{v}/2-\mathbf{w}_1^T(\mathbf{A}_0+2mE_0)^{-1}\mathbf{w}_1$ and $C_2=\mathbf{v}^T\mathbf{A}_4\mathbf{v}-\mathbf{w}_2^T(\mathbf{A}_0+2mE_0)^{-1}\mathbf{w}_2$ depend only on p and n. This oscillator has mass m/C_1, frequency $\omega_{\rm eff}=(4C_1C_2\tilde{\Omega}^2+C_1\omega^2)^{1/2}$, centre $y_c=2C_2K\tilde{\Omega}/(4C_2m\tilde{\Omega}^2+m\omega^2)$ and ground state energy $E_0/d^2+\omega_{\rm eff}/2+C_2\omega^2K^2/(8C_2m\tilde{\Omega}^2+2m\omega^2)$.

Since the magnetic field terms are (after a change of gauge) symmetric in x and y, $C_1=C_2\equiv C$. For general slowly varying V, K is no longer exactly conserved, but the expansion works if $\chi(y)e^{i\tilde{K}x}$ is replaced by $\chi(x,y)$ and $\tilde{K}$ by $-i\partial\chi/\partial x$, giving Eq. (6.6).

Chapter 7

Conclusions

7.1 Purity-based entanglement detection

We considered possible methods for the experimental implementation of the purity-based entanglement detection scheme introduced in [29], and how its performance would be affected by the limitations of those methods. In particular, we described a possible implementation in optical lattices using a period 2 superlattice beamsplitter followed by 2 atom loss.

We proved that counting the antisymmetric pairs without any spatial resolution was sufficient to detect all pure entangled states, and in many cases such as the cat and cluster states to do so using a number of state copies independent of the number of qubits. This compares favourably to existing entanglement detection methods using witness operators or state tomography.

We also considered the effect of imperfections in the beamsplitter, loss and detection processes, finding that these types of error can be corrected,

in a reasonable number of additional experimental runs for error rates $\lesssim 1/k$ for purities of k atoms. If single atom counting is not available or the error rate is too high for full entanglement detection, the scheme can still be useful for state parameter estimation.

7.2 Fractional quantum Hall effect

We considered an optical lattice realisation of the fractional quantum Hall system. This would allow access to the high field regime $\alpha \sim 1$ where lattice effects are important, which is very difficult to reach in solid state systems. We have constructed an approximate analytic theory valid near simple rationals $\alpha \approx \alpha_c \equiv l/n$ in the presence of a weak trapping potential, which predicts that the particles behave as if they had n internal states and were in an effective field $\alpha - \alpha_c$, observable as densities and Hall currents proportional to $\alpha - \alpha_c$ rather than α.

Under standard time of flight expansion we predict a stepped profile, similar to the in-trap density profile. This would clearly distinguish fractional quantum Hall states from superfluid vortex lattice or Mott insulator states. Measuring the density of each step would test the above prediction of effective field $\alpha - \alpha_c$, and would give the filling factor of each state, partially identifying it. The expected strong atom-atom correlations could be probed using shot noise correlation.

Some of the states we expect, at both low α and $\alpha \approx 1/2$, have non-Abelian anyon excitations suitable for universal topological quantum computation. However, the weak interaction required for these states to exist also

gives them a small gap, possibly too small to prevent excessive thermal anyon pair production; the more robust Laughlin and 221 states have only Abelian anyons. It has been hypothesised that non-Abelian field QH [149] might have states that are both robust and suitable for topological computation; testing this could be a subject for future research.

Bibliography

[1] M.A. Nielsen and I.L. Chuang, *Quantum Computation and Quantum Information* (Cambridge University Press, Cambridge, 2000); A.M. Steane, Rept. Prog. Phys. **61** 117 (1998) (quant-ph/9708022).

[2] P.W. Shor, in *Proc. 35th Annual Symp. on Foundations of Computer Science*, Santa Fe (IEEE Computer Society Press, 1994); P.W. Shor, SIAM J. Sci. Statist. Comput. **26**, 1484 (1997).

[3] B.M. Boghosian and W. Taylor, Physica **D120**, 30 (1998); D.S. Abrams and S. Lloyd, Phys. Rev. Lett. **83**, 5162 (1999).

[4] A.M. Steane, in *Decoherence and its implications in quantum computation and information transfer*, Gonis and Turchi, eds, pp. 284-298 (IOS Press, Amsterdam, 2001) (quant-ph/0304016).

[5] A.M. Steane, Phys. Rev. A **68**, 042322 (2003).

[6] C.A. Sackett *et al.*, Nature **404**, 256 (2000); J. Chiaverini *et al.*, Nature **432**, 602 (2004).

[7] C. Ramanathan, N. Boulant, Z. Chen, D.G. Cory, I. Chuang, and M. Steffen, quant-ph/0408166.

[8] D. Jaksch and P. Zoller, Annals of Physics **315**, 52 (2005).

[9] D. Jaksch, Contemporary Physics **45**, 367 (2004).

[10] M. Lewenstein, A. Sanpera, V. Ahufinger, B. Damski, A. Sen De, and U. Sen, Advances in Physics **56**, 243 (2007).

[11] E. Jané, G. Vidal, W. Dür, P. Zoller, and J.I. Cirac, Quant. Inf. Comp. **3**, 15 (2003).

[12] O. Mandel, M. Greiner, A. Widera, T. Rom, T.W. Hänsch, and I. Bloch, Nature **425**, 937 (2003).

[13] R. Scheunemann, F.S. Cataliotti, T.W. Hänsch, and M. Weitz, Phys. Rev. A **62**, 051801 (2000).

[14] R. Franzosi, M. Cristiani, C. Sias, and E. Arimondo, Phys. Rev. A **74**, 013403 (2006).

[15] J. Joo, Y.L. Lim, A. Beige, and P.L. Knight, Phys. Rev. A **74**, 042344 (2006); C. Zhang, S.L. Rolston, and S. Das Sarma, Phys. Rev. A **74**, 042316 (2006).

[16] J. Cho, Phys. Rev. Lett. **99**, 020502 (2007).

[17] R. Horodecki, P. Horodecki, M. Horodecki, and K. Horodecki, quant-ph/0702225.

[18] C.H. Bennett, G. Brassard, C. Crepeau, R. Jozsa, A. Peres, and W.K. Wootters, Phys. Rev. Lett. **70**, 1895 (1993).

[19] P.W. Shor, in *37th Symposium on Foundations of Computing* (IEEE Computer Society Press, 1996), pp. 56-65 (quant-ph/9605011).

[20] A.M. Steane, Phys. Rev. Lett. **78**, 2252 (1997).

[21] R. Raussendorf, H.-J Briegel, Phys. Rev. Lett. **86**, 910 (2001); R. Raussendorf, H.-J Briegel, Phys. Rev. Lett. **86**, 5188 (2001).

[22] P. Walther, K.J. Resch, T. Rudolph, E. Schenck, H. Weinfurter, V. Vedral, M. Aspelmeyer, A. Zeilinger, Nature **434**, 169 (2005).

[23] M. Bourennane *et al.*, Phys. Rev. Lett. **92**, 087902 (2004).

[24] D.F.V. James, P.G. Kwiat, W.J. Munro, and A.G. White, Phys. Rev. A **64**, 052312 (2001).

[25] S.E. Sklarz, I. Friedler, D.J. Tannor, Y.B. Band, C.J. Williams, Phys. Rev. A **66**, 053620 (2002); S. Peil *et al.*, Phys. Rev. A **67**, 051603(R) (2003); W.K. Hensinger *et al.*, Nature **412**, 52 (2001).

[26] G. Tóth, O. Gühne, Phys. Rev. Lett. **94**, 060501 (2005).

[27] L. Chen and Y.-X. Chen, quant-ph/0705.2665.

[28] Y.-C. Wu and G.-C. Guo, Phys. Rev. A **75**, 052333 (2007).

[29] C. Moura Alves and D. Jaksch, Phys. Rev. Lett. **93**, 110501 (2004).

[30] M. Horodecki, P. Horodecki, and R. Horodecki, Phys. Lett. A **210**, 377 (1996).

[31] J. Preskill, *Lecture Notes for Physics 219: Quantum Computation, Chapter 9: Topological Quantum Computation* (http://www.theory.caltech.edu/ preskill/ph219/topological.pdf).

[32] A.Yu. Kitaev, Annals of Physics **303**, 2 (2003).

[33] S. Das Sarma, M. Freedman, and C. Nayak, Phys. Rev. Lett. **94**, 166802 (2005).

[34] R.E. Prange and S.M. Girvin, Eds., *The Quantum Hall Effect* (Springer-Verlag, New York, 1990).

[35] Z.F. Ezawa, *Quantum Hall effects: field theoretical approach and related topics* (World Scientific, 2000).

[36] L. Saminadayar, D.C. Glatti, Y. Jin, and B. Etienne, Phys. Rev. Lett. **79**, 2526 (1997); R. de Picciotto, M. Reznikov, M. Heiblum, V. Umansky, G. Bunin, and D. Makalu, Nature **389**, 162 (1997).

[37] D. Arovas, J.R. Schrieffer and F. Wilczek, Phys. Rev. Lett. **53**, 722 (1984).

[38] F.E. Camino, W. Zhou, and V.J. Goldman, cond-mat/0606742.

[39] S.B. Chung and M. Stone, Phys. Rev. B **73**, 245311 (2006).

[40] E. Ardonne, cond-mat/0110108; E. Ardonne and K. Schoutens, cond-mat/0606217.

[41] N.E. Bonesteel, L. Hormozi, G. Zikos, and S.H. Simon, Phys. Rev. Lett. **95**, 140503 (2005).

[42] M. Polini, R. Fazio, M.P. Tosi, J. Sinova, A.H. MacDonald, Laser Physics **14**, 603 (2004); M. Polini, R. Fazio, A.H. MacDonald, and M.P. Tosi, Phys. Rev. Lett. **95**, 010401 (2005).

[43] G. Juzeliūnas and P. Öhberg, Phys. Rev. Lett. **93**, 033602 (2004); G. Juzeliūnas, P. Öhberg, J. Ruseckas, and A. Klein, Phys. Rev. A **71**, 053614 (2005).

[44] D. Jaksch and P. Zoller, New J. Phys. **5**, 56 (2003).

[45] A.S. Sørensen, E. Demler, and M.D. Lukin, Phys. Rev. Lett. **94**, 086803 (2005).

[46] D.R. Hofstadter, Phys. Rev. B **14**, 2239 (1976).

[47] C. Albrecht, J.H. Smet, K. von Klitzing, D. Weiss, V. Umansky, and H. Schweizer, Phys. Rev. Lett. **86**, 147 (2001).

[48] E. Altman, E. Demler, and M.D. Lukin, Phys. Rev. A **70**, 013603 (2004).

[49] S. Fölling, F. Gerbier, A. Widera, O. Mandel, T. Gericke and I. Bloch, Nature **434**, 481 (2005).

[50] I. Bloch, Physics World, **17**, 25 (2004).

[51] M.P.A. Fisher, P.B. Weichman, G. Grinstein, and D.S. Fisher, Phys. Rev. B **40**, 546 (1989).

[52] For a review of continuum (non-lattice) BECs, see C.J. Pethick and H. Smith, *Bose-Einstein condensation in dilute gases* (Cambridge University Press, 2001), or A.J. Leggett, Rev. Mod. Phys. **73**, 307 (2001).

[53] D. Jaksch, C. Bruder, J.I. Cirac, C.W. Gardiner, and P. Zoller, Phys. Rev. Lett. **81**, 3108 (1998).

[54] W. Krauth, M. Caffarel, J.-P. Bouchaud, Phys. Rev. B **45**, 3137 (1992).

[55] M. Capello, F. Becca, M. Fabrizio, and S. Sorella, Phys. Rev. Lett. **99**, 056402 (2007).

[56] M. Greiner, O. Mandel, T. Esslinger, T.W. Haensch, and I. Bloch, Nature **415**, 39 (2002).

[57] T. Stöferle, H. Moritz, C. Schori, M. Köhl, and T. Esslinger, Phys. Rev. Lett. **92**, 130403 (2004).

[58] B. Paredes, P. Fedichev, J.I. Cirac, and P. Zoller, Phys. Rev. Lett. **87**, 010402 (2001).

[59] E.J. Mueller, Phys. Rev. A **70**, 041603(R).

[60] V.W. Scarola and S. Das Sarma, Phys. Rev. A **73**, 041609 (2006).

[61] B. Damski, J. Zakrzewski, L. Santos, P. Zoller, and M. Lewenstein, Phys. Rev. Lett. **91**, 080403 (2003).

[62] U. Gavish and Y. Castin, Phys. Rev. Lett. **95**, 020401 (2005).

[63] D. Jaksch, H.-J. Briegel, J.I. Cirac, C.W. Gardiner, P. Zoller, Phys. Rev. Lett. **82**, 1975 (1999).

[64] S. Peil, J.V. Porto, B. Laburthe Tolra, J.M. Obrecht, B.E. King, M. Subbotin, S.L. Rolston, and W.D. Phillips, Phys. Rev. A **67**, 051603 (2003).

[65] A. Kay and J.K. Pachos, New J. Phys. **6**, 126 (2004); A. Kay, J.K. Pachos, and C.S. Adams, Phys. Rev. A **73**, 022310 (2006).

[66] A. Bririd, S.C. Benjamin, and A. Kay, quant-ph/0308113.

[67] M. Horodecki, P. Horodecki and R. Horodecki, in *Quantum Information: An Introduction to Basic Theoretical Concepts and Experiments* (Springer, 2001) (quant-ph/0109124).

[68] R.F. Werner, Phys. Rev. A **40**, 4277 (1989).

[69] P. Horodecki, Phys. Lett. A **232**, 333 (1997).

[70] G. Aubrun and S.J. Szarek, Phys. Rev. A **73**, 022109 (2006).

[71] M.D. Barrett *et al.*, Nature **429**, 737 (2004).

[72] J.S. Bell, Physics **1** 195, 1964; A. Aspect, P. Grangier, G. Roger, Phys. Rev. Lett. **49**, 91 (1982).

[73] C.M. Dawson, H.L. Haselgrove, and M.A. Nielsen, Phys. Rev. A **73**, 052306 (2006).

[74] C.H. Bennett, S. Popescu, D. Rohrlich, J.A. Smolin, and A.V. Thapliyal, Phys. Rev. A **63**, 012307 (2000).

[75] C.H. Bennett, H.J. Bernstein, S. Popescu, and B. Schumacher, Phys. Rev. A **53**, 2046 (1996).

[76] P.M. Hayden, M. Horodecki, and B.M. Terhal, J. Phys. A **34**, 6891 (2001).

[77] D. Yang, M. Horodecki, R. Horodecki, and B. Synak-Radtke, Phys. Rev. Lett. **95**, 190501 (2005).

[78] C.H. Bennett, G. Brassard, S. Popescu, B. Schumacher, J.A. Smolin, and W.K. Wootters, Phys. Rev. Lett **76**, 722 (1996).

[79] W. Dür, H.-J. Briegel, J.I. Cirac, and P. Zoller, Phys. Rev. A **59**, 169 (1999).

[80] C.H. Bennett, D.P. DiVincenzo, J.A. Smolin, and W.K. Wootters, Phys. Rev. A **54**, 3824 (1996).

[81] P.W. Shor and J. Preskill, Phys. Rev. Lett. **85**, 441 (2000).

[82] B. Groisman, N. Linden, and S. Popescu, Phys. Rev. A **72**, 062322 (2005).

[83] A.W. Harrow and M.A. Nielsen, Phys. Rev. A **68**, 012308 (2003).

[84] R. Jozsa and N. Linden, Proc. R. Soc. Lond. A **459**, 2011 (2003).

[85] G. Vidal, Phys. Rev. Lett. **91**, 147902 (2003).

[86] A. Datta and G. Vidal, Phys. Rev. A **75**, 042310 (2007).

[87] D.A. Meyer, Phys. Rev. Lett. **85**, 2014 (2000); D. Kenigsberg, T. Mor, and G. Ratsaby, Quant. Inf. Comp. **6**, 606 (2006).

[88] N.A. Gershenfeld and I.L. Chuang, Science **275**, 350 (1997).

[89] R. Hildebrand, Phys. Rev. A **75**, 062330 (2007).

[90] L. Gurvits and H. Barnum, Phys. Rev. A **66**, 062311 (2002).

[91] E. Knill and R. Laflamme, Phys. Rev. Lett. **81**, 5672 (1998).

[92] A. Ambainis, L.J. Schulman, and U.V. Vazirani, *Proceedings of the 32nd STOC*, edited by F. Yao (ACM, New York, 2000), pp. 705-714 (quant-ph/0003136).

[93] D. Poulin, R. Blume-Kohout, R. Laflamme, and H. Ollivier, Phys. Rev. Lett. **92**, 177906 (2004).

[94] A. Datta, S.T. Flammia, and C.M. Caves, Phys. Rev. A **72**, 042316 (2005).

[95] A. Peres, Phys. Rev. Lett. **77**, 1413 (1996).

[96] M. Horodecki, P. Horodecki, and R. Horodecki, Phys. Lett. A **223**, 1 (1996).

[97] C.H. Bennett, D.P. DiVincenzo, T. Mor, P.W. Shor, J.A. Smolin, and B.M. Terhal, Phys. Rev. Lett. **82**, 5385 (1999).

[98] M. Horodecki, P. Horodecki and R. Horodecki, Phys. Rev. Lett. **80**, 5239 (1998).

[99] R. Augusiak and P. Horodecki, Phys. Rev. A **74**, 010305R (2006).

[100] M.A. Nielsen and J. Kempe, Phys. Rev. Lett. **86**, 5184 (2001).

[101] L. Gurvits, in *Proceedings of the 35th ACM Symposium on the Theory of Computing* (ACM Press, New York, 2003), pp. 10-19.

[102] F. Hulpke and D. Bruß, J. Phys. A **38**, 5573 (2005).

[103] L.M. Ioannou, B.C. Travaglione, D. Cheung, and A.K. Ekert, Phys. Rev. A **70**, 060303(R) (2004).

[104] B. Terhal, Phys. Lett. A **271**, 319 (2000).

[105] P. Horodecki and A. Ekert, Phys. Rev. Lett. **89**, 127902 (2002).

[106] P. Horodecki, R. Augusiak, and M. Demianowicz, Phys. Rev. A **74**, 052323 (2006).

[107] F.G.S.L. Brandão and R.O. Vianna, Phys. Rev. A **70**, 062309 (2004).

[108] O. Gühne *et al.*, Phys. Rev. A **66**, 062305 (2002); O. Gühne and P. Hyllus, Int. J. Theor. Phys. **42**, 1001 (2003).

[109] M. Lewenstein, B. Kraus, J.I. Cirac, P. Horodecki, Phys. Rev. A **62**, 052310 (2000).

[110] A. Peres, Found. Phys. **29**, 589 (1999).

[111] R.F. Werner and M.M. Wolf, Phys. Rev. A **64**, 032112 (2001); M. Żukowski and Č. Brukner, quant-ph/0102039.

[112] N.D. Mermin, Phys. Rev. Lett **65**, 1838 (1990).

[113] L. Masanes, Phys. Rev. Lett. **97**, 050503 (2006).

[114] R.D. Somma, J. Chiaverini, and D.J. Berkeland, Phys. Rev. A **74**, 052302 (2006).

[115] A.M. Steane and B. Ibinson, Phys. Rev. A **72**, 052335 (2005).

[116] R.T. Thew, K. Nemoto, A.G. White, and W.J. Munro, Phys. Rev. A **66**, 012303.

[117] Z. Hradil, Phys. Rev. A **55**, R1561 (1997); Z. Hradil, J. Summhammer, and H. Rauch, Physics Letters A **261**, 20 (1999).

[118] J. Řeháček, Z. Hradil, and M. Ježek, Phys. Rev. A **63**, 040303R (2001).

[119] A.I. Lvovsky, J. Opt. B: Quantum Semiclass. Opt. **6** S556 (2004).

[120] Z. Hradil, D. Mogilevtsev, and J. Řeháček, Phys. Rev. Lett. **96**, 230401 (2006); D. Mogilevtsev, J. Řeháček, and Z. Hradil, Phys. Rev. A **75**, 012112 (2007).

[121] J. Řeháček, Z. Hradil, E. Knill, and A.I. Lvovsky, Phys. Rev. A **75**, 042108 (2007).

[122] C.K. Hong, Z.Y. Ou, L. Mandel, Phys. Rev. Lett. **59**, 2044 (1987); K. Mattle, H. Weinfurter, P.G. Kwiat, A. Zeilinger, Phys. Rev. Lett. **76**, 4656 (1996).

[123] M. Hendrych, M. Dusek, R. Filip, J. Fiurasek, Phys. Lett. A **310**, 95 (2003).

[124] A.K. Ekert *et al.*, Phys. Rev. Lett. **88**, 217901 (2002); C. Moura Alves, D.K.L. Oi, P. Horodecki, A.K. Ekert, and L.C. Kwek, Phys. Rev. A **68**, 032306 (2003).

[125] F.A. Bovino, G. Castagnoli, A. Ekert, P. Horodecki, C. Moura Alves, and A.V. Sergienko, Phys. Rev. Lett. **95**, 240407 (2005).

[126] J.I. Cirac, M. Lewenstein, K. Molmer, and P. Zoller, Phys. Rev. A **57**, 1208 (1998).

[127] C.H. van der Wal *et al.*, Science **290**, 773 (2000); J.R. Friedman, V. Patel, W. Chen, S.K. Tolpygo, and J.E. Lukens, Nature **406**, 43 (2000).

[128] W. Dür, C. Simon, and J.I. Cirac, Phys. Rev. Lett. **89**, 210402 (2002).

[129] A. Widera *et al.*, Phys. Rev. Lett. **92**, 160406 (2004).

[130] M. Trupke, J. Goldwin, B. Darquié, G. Dutier, S. Eriksson, J. Ashmore, and E.A. Hinds, Phys. Rev. Lett. **99**, 063601 (2007).

[131] M.S. Tame, M. Paternostro, M.S. Kim, V. Vedral, quant-ph/0502081.

[132] D.C. Tsui, H.L. Störmer, and A.C. Gossard, Phys. Rev. Lett. **48**, 1559 (1982), Phys. Rev. B **25**, 1405 (1982).

[133] D.R. Yennie, Rev. Mod. Phys. **59**, 781 (1987).

[134] V. Bretin, S. Stock, Y. Seurin, and J. Dalibard, Phys. Rev. Lett. **92**, 050403 (2004); V. Schweikhard, I. Coddington, P. Engels, V.P. Mogendorff, and E.A. Cornell, Phys. Rev. Lett. **92**, 040404 (2004).

[135] R.B. Laughlin, Phys. Rev. Lett. **50**, 1395 (1983), Phys. Rev. B **27**, 3383 (1983).

[136] N. Read and E. Rezayi, Phys. Rev. B **59**, 8084 (1999).

[137] N.R. Cooper and E.H. Rezayi, Phys. Rev. A **75**, 013627 (2007).

[138] N.R. Cooper, F.J.M. van Lankvelt, J.W. Reijnders, and K. Schoutens, Phys. Rev. A **72**, 063622 (2005).

[139] A. Cappelli, L.S. Georgiev, and I.T. Todorov, Nucl. Phys. **B599**, 499 (2001).

[140] N.R. Cooper, Phys. Rev. Lett. **92**, 220405 (2004).

[141] A. Aftalion, X. Blanc, and J. Dalibard, Phys. Rev. A **71**, 023611 (2005).

[142] H. Cho, J.B. Young, W. Kang, K.L. Campman, A.C. Gossard, M. Bichler, and W. Wegscheider, Phys. Rev. Lett. **81**, 2522 (1998).

[143] B. Halperin, Helv. Phys. Acta **56**, 75 (1983).

[144] E. Ardonne, K. Schoutens, Phys. Rev. Lett. **82**, 5096 (1999).

[145] E.J. Mueller and T.-L. Ho, Phys. Rev. Lett. **88**, 180403 (2002).

[146] K. Kasamatsu, M. Tsubota, and M. Ueda, Phys. Rev. Lett. **91**, 150406 (2003).

[147] M. Freedman, C. Nayak, and K. Walker, Phys. Rev. B **73**, 245307 (2006).

[148] M. Popp, J.-J. Garcia-Ripoll, K.G. Vollbrecht, and J.I. Cirac, Phys. Rev. A **74**, 013622 (2006); M. Popp, J.-J. Garcia-Ripoll, K.G.H. Vollbrecht, and J.I. Cirac, New J. Phys. **8**, 164 (2006).

[149] K. Osterloh, M. Baig, L. Santos, P. Zoller, and M. Lewenstein, Phys. Rev. Lett. **95**, 010403 (2005); L.-H. Lu and Y.-Q. Li, cond-mat/0701481.

[150] A. Rozhkov and D. Stroud, Phys. Rev. B **54**, R12697 (1996); J. Sinova, C.B. Hanna and A.H. MacDonald, Phys. Rev. Lett. **89**, 030403 (2002).

[151] A.H. MacDonald and S.M. Girvin, Phys. Rev. B **38**, 6295 (1988).

[152] N. Read and N.R. Cooper, Phys. Rev. A **68**, 035601 (2003).

[153] S.M. Girvin, Phys. Rev. B **30**, 558 (1984); S.M. Girvin, A.H. MacDonald, and P.M. Platzman, Phys. Rev. B **33**, 2481 (1986).